Title
The Er3+ : Y2O3 Ceramic System

Author
Joshi, Abhijeet

Publication Date
2012

Peer reviewed|Thesis/dissertation

University of California
Los Angeles

The $Er^{3+} : Y_2O_3$ Ceramic System

A dissertation submitted in partial satisfaction
of the requirements for the degree
Doctor of Philosophy in Electrical Engineering

by

Abhijeet Joshi

2012

The dissertation of Abhijeet Joshi is approved.

Warren G. Grundfest

Jane P. Chang

Chandrashekhar J. Joshi

Oscar M. Stafsudd, Committee Chair

University of California, Los Angeles

2012

89. ....It (logical investigation) takes its rise, not from an interest in the facts of nature, nor from a need to grasp causal connexions: but from an urge to understand the basis, or essence, of everything empirical. Not, however, as if to this end we had to hunt out new facts; it is, rather, of the essence of our investigation that we do not seek to learn anything <u>new</u> by it. We want to <u>understand</u> something that is already in plain view. For <u>this</u> is what we seem in some sense not to understand.

Ludwig Wittgenstein

Philosophical Investigations

Table of Contents

List of Figures

List of Tables

Acknowledgments

Prof. O. M. Stafsudd has been more than just an academic advisor to me - he has been my guide, philosopher and friend. This raconteur of unparalleled genius has trained me to be a scientist. His hands-on approach has taught me much and yet there is still a lot to learn. It is to him offer my first gratitude, hearty thanks and cheers to the years of collaboration to come.

This was perhaps the best time of my life thus far - the memories of these years will be dearly cherished.

Science, and experimental work in particular, is a team-effort and as such it would be a crime to ignore the collaborators that helped make this research possible:

- Dr. W. Cochran of San Luis Obispo, CA.
- Dr. Ramesh Shori of the Naval Air Warfare Center, China Lake, CA.
- Prof. John Ballato from Clemson University, SC.
- Dr. David Zelmon from the Wright-Patterson Air Force Base, OH.
- Dr. David Bennett and Prof. Warren Grundfest from the Bio-Medical Engineering Department at UCLA.
- Dr. Robert Schwartz of the Electrical Engineering and Chemistry Department.

I would also like to thank the many people with whom I've had very good conversations on the topic of rare-earth materials, amongst those were Vladan Jankovich and James Dorman formerly from Prof. J. P. Chang's lab.

I would also like to thank Professors J. P. Chang, W. Grundfest and C. Joshi for agreeing to be part of my PhD Defense Committee and also for their suggestions in improving this work.

I must also thank Jacquie Stafsudd for valiantly braving bad writing and editing most of these chapters to publishable standards. The exercise also whipped my editing skills into shape.

Finally, I offer my cheers to my labmates and friends who tolerated my jokes and larking all these years. They famously include: Jere H, Suneel K, Amir T, Daniel S, Joel S and too many others to note in this limited space - I'm afraid they'll have to deal with me for a few more years.

Publications

I've contributed significantly (device design or other material contribution or experimentation and data analysis), and in many cases exclusively, for all the publications below.

Conference Papers

→ *Localized/Selective Ge & SiGe Formation By Liquid Phase Epitaxy (LPE) Using Ge-Plasma Ion Implantation And Laser Melt Annealing.*

John Borland, Shu Qin, Peter Oesterlin, Karim Huet, Walt Johnson, Lauren Klein, Gary Goodman, Alan Wan, Steven Novak, *Abhijeet Joshi*, Si Prussin. 13th International Workshop on Junction Technology 2013, 6-7 June 2013, Kyoto, Japan.

→ *Effect of Implant Temperature and Millisecond annealing on Dopant Activation and Diffusion.*

E. J. H. Collart, P. M. Kopalidis, Michael Hou, S. McCoy, P. J. Tilmans, *A. Joshi* and S. Prussin. Proceedings of 19^{th} International Conference on Ion Implantation Technology, 25-29 June 2012, Valladolid, Spain.

→ *High Efficiency Rare Earth Doped Core-Shell Nanophosphors for Energy Applications.*

James Dorman, Gregory Kuzmanich, *Abhijeet Joshi*, Ju H. Choi and Jane P. Chang. American Institute of Chemical Engineers (AIChE) Annual Meeting 2011. Minneapolis, MN.

→ *Experimental Validation of Cooperative Environmental Boundary Tracking with On-board Sensors.*

Abhijeet Joshi, Trevor Ashley, Yuan R. Huang and Andrea L. Bertozzi. Proceed-

ings of 2009 American Control Conference, St. Louis, MO.

→ *A second generation micro-vehicle testbed for cooperative control and sensing strategies.*

Kevin Ka Kei Leung, Chung Hua Hsieh, Yuan (Rick) Huang, *Abhijeet Joshi*, Vlad Voroninski, Andrea L.Bertozzi. Proceedings of the 2007 American Control Conference, New York City, NY.

→ *Robotic path planning and visibility with limited sensor data.*

Yanina Landa, David Galkowski, Yuan (Rick) Huang, *Abhijeet Joshi*, Christine Lee, Kevin Ka Kei Leung, Gitendra Malla, Jennifer Treanor, Vlad Voroninski, Andrea L.Bertozzi, Yen Hsi Richard Tsai. Proceedings of the 2007 American Control Conference, New York City, NY.

→ *Implementations of control laws for motion camouflage in a pursuit-evasion system.*

Carmeliza Navasca, Ani Asatrya, Vatche Attarian, Yuan (Rick) Huang, Kevin Ka Kei Leung, *Abhijeet Joshi*, Vlad Voroninski, Meghdi Aboulian, Krystle McBride. Proceedings of the 2007 American Control Conference, New York City, NY.

Journal Papers

→ *Template-Free Routes to Macroporous Monoliths of Nickel and Iron Oxides: Toward Porous Metals and Conformally Coated Pore Walls.*

Eric Toberer, *Abhijeet Joshi*, Ram Seshadri. Chemistry of Materials (2005), vol. 17 (8) (pgs 2142-2147).

→ *Multiphonon-based comparison of erbium-doped yttria in large, fine grain polycrystalline ceramics and precursor forms.*

Abhijeet Joshi, Oscar Stafsudd, Karn Serivalsatit and John Ballato. Optical Materials. Optical Materials, Vol. 34, Issue 1, pgs: 95-98, November 2011.

→ *Refractive Indices and Thermo-optic coefficients of Er^{3+} doped ceramic Y_2O_3.*
Abhijeet Joshi, Ramesh Shori, Oscar Stafsudd, David E. Zelmon and Nicholas Hayes. Optics Express, Vol. 20, Issue 4, pgs: 4428-4435 (2012).

→ *Surface-micromachined magnetic undulator with period length between 10 μm and 1 mm for advanced light sources.*
J Harrison, *A Joshi*, J Lake, R Candler, P Musumeci. Physical Review Special Topics-Accelerators and Beams 15 (7), 070703.

→ *Stress-optic law for $Er^{3+} : Y_2O_3$ ceramics.*
Abhijeet Joshi and Oscar M. Stafsudd. Accepted Nov 2013 to Optical Materials. Short length article.

→ *Study of Energy Transfer and Upconversion in $Er^{3+} : Y_2O_3$ ceramics.*
Abhijeet Joshi and Oscar M. Stafsudd. Pending revision Nov 2013 to Optical Materials. Full length article.

→ *Small-signal gain measurements for highly doped and co-doped Er^{3+}:YAG at 2.936 μm.*
Abhijeet Joshi, Mario Furtado, Ramesh Shori and Oscar M. Stafsudd, The Journal of Optics and Laser Technology. Vol.56, March 2014, pgs: 58-64.

→ *Multi-phonon based comparison of erbium-doped sesquioxide ceramics.*
Abhijeet Joshi and Oscar M. Stafsudd. Pending revision Nov 2013 to Optical Materials. Full length article.

In Progress

→ *Concentration dependent study of upconversion phenomena from $^4I_{13/2}$ and $^4I_{11/2}$ energy levels in erbium doped ceramics.*
Abhijeet Joshi and Oscar M. Stafsudd. *In progess, estimated submission Dec 2013. Full length article.*

$\rightarrow$ *The* $3\mu m$ Er^{3+}:YAG *radiation as a corneal hydration measurement tool.* *Abhijeet Joshi*, David Bennett, Warren Grundfest and Oscar M. Stafsudd. *In progess, estimated submission Nov 2013. Short Article.*

Vita

2006	B.S. (Electrical Engineering), University of California, Los Angeles.
2007	Staff Research Associate, Applied Math Laboratory, University of California, Los Angeles. PI: Professor Andrea Bertozzi.
2007-2008	Research Engineer, Systems and Unmanned Vehicle Division, Applied Research Laboratory, Pennsylvania State University, PA.
2008-2009	M.S. (Electrical Engineering), University of California, Los Angeles.
2010-	Research and Development, Differential Hall Effect - Continuous Anodic Oxidation Technique. Silicon dopant carrier concentration, mobility and, resistivity profiling with Angstrom level resolution. Group lead by Dr. Simon Prussin.
2011-2012	Teaching Assistant, Electrical Engineering Department, UCLA. Taught sections of Electrical Engineering 110L (circuits lab course) under direction of Professor Hassan Babaie and Professor Mesghali.
2008-2012	Graduate Student Researcher, Quantum Electronics Laboratory, Electrical Engineering Department, UCLA. Advisor: Professor Oscar M. Stafsudd
2012-2013	Graduate Student Researcher, Sensor and Technology Laboratory, Electrical Engineering Department, UCLA.

Abstract of the Dissertation

The $Er^{3+} : Y_2O_3$ Ceramic System

by

Abhijeet Joshi

Doctor of Philosophy in Electrical Engineering

University of California, Los Angeles, 2012

Professor Oscar M. Stafsudd, Chair

This thesis reports the experimental study of a new, promising class of solid-state laser gain media, namely erbium doped ceramic yttria. Optical quality ceramics have numerous advantages over single-crystal hosts and glass hosts, such as general mechanical robustness in extreme conditions ,the ability to engineer doping profiles and tailor the laser gain media, and depending on the material system chosen, higher thermal conductivity these materials demand greater attention of researchers in the field. Ceramic gain media can also be made in large volumes much like glass, leveraging cheap flash-pumping methods to generate very high powers for military and scientific purposes.

The work reported here spans many areas that when taken together present a full evaluation of a future laser host. We have experimentally ascertained thus far the refractive indices of varying doping levels of active ion erbium in polycrystalline *yttria* and the materials stress-optic behavior. Spectroscopic data such as absorption and emission spectra in the near and mid infra-red regions, and the calculated cross-sections are also included. Multiphonon studies were also completed, the data provides vital information on the dominant phonon frequency and the radiative lifetimes. Energy transfer amongst the erbium ions and up-

conversion behavior is also analyzed. The theoretical work provided included an up-to-date Judd-Ofelt analysis of the ion-host system.

The multiphonon analysis above was expanded to include some other oxide host materials and differing forms of the same material. Some new upconversion pathways were also discovered in a novel two-pump experiment. Comparisons have been drawn to the current standard *Er:YAG* system where necessary.

CHAPTER 1

Introduction

The mid-IR region is often called the "molecular footprint" region. Since it is well known that vibrational and rotational characteristics of relatively small atmospheric molecules such as CO, CO_2 , NO_2 , etc., can be ascertained by spectroscopic analysis of suitable wavelengths in this region, the availability of laser sources for environmental studies in the range is a necessity.

Apart from spectroscopic studies of these atmospheric constituents, this region of the spectrum also shows promise for free-space communication [1], the eye-safe laser and various military applications. LIDAR and scores of medical applications - ranging from advanced non-contact surgical cutting tools to in-situ spectroscopy [2],[3] demand the existence of ready sources in this energy regime. Such lasers will also be of immense importance in fields where light-matter interaction is closely studied - for instance laser-induced damage, surface characterization, and advances in fundamental laser-matter interactions and mechanisms.

Crystalline lasers have played an important role in the history of lasers in general, and mid-IR lasers in particular. Schawlow and Townes in 1958 were the first to recognize the possibility of solid-state lasers operating in the infra-red [4]. With chromium as the active ion in Al_2O_3, Maiman soon demonstrated laser action in 1960 [5]. One of the first mid-IR lasers was also one of the first lasers - $U^{3+} : CaF_2$ which was shown to lase at $2.6\mu m$ by Sorokin and Stevenson [6]. Many more active ion solid-state lasers were to follow including $Dy^{3+} : CaF_2$ in

1960[7], $Sm^{2+} : CaF_2$ in 1961[8], $Dy^{2+} : CaF_2$ in 1962[7][9], and perhaps the industrially most important lasing of the Nd^{3+} ion emitting near $1\mu m$ [10]. The lanthanide and actinide series have been the most dominant activators responsible for stimulated laser action. Research using lanthanide and actinide activators for the mid-IR region thereafter slackened and gave way to other systems of some promise such as semiconductor optically pumped lasers, vibrionic lasers using transitional metals (iron and chromium doped zinc-selenide/sulphide), and more recently engineered quantum structured laser gain media made using the $III-V$, $II-VI$ and IV groups.

The creation of mid-IR lasers with high output powers was perhaps realized first by the industrial research and laser-activated plasma communities. The laser systems of choice generally are $Nd^{3+} : YAG/Glass$ lasers and $Yb^{3+} : YAG$ disk lasers. The $1.06\mu m$ radiation (from Nd doped systems) doubled and redoubled in frequency and chirp-pulsed amplified allowed them to generate astoundingly high intensity levels with which to probe, excite and accelerate plasmas in wakefield generators - a research area in which the UCLA engineering faculty is a pioneer [11][12].

Except the glass hosts mentioned above, almost all traditional solid-state laser hosts rely on single-crystal matrices doped with active ions. In general, these single-crystals are grown using a wide variety of techniques including Czchoralski, float-zone , Bridgeman-Stockbarger, laser-assisted pedestal growth, etc. Ceramic host matrices provide a way to move away from these single-crystal growth methods, all of whom are very time consuming and expensive. As we shall see, ceramic hosts have other critical advantages as well.

1.1 The argument for ceramic hosts

The importance of the active ions in the system of choice cannot be understated - in fact we would have no lasers if it weren't for these unique elements. But of no less importance is the composition and structure of the host in which to subtend the active ions. Different hosts have been known to provide different lasing wavelengths [13] by changing the symmetry of the active ion site and thereby allowing formerly forbidden electronic dipole transitions, an effect known as the crystal-field effect, the theoretical basis for such lasers.

Single crystal hosts such as YAG, YGG, Al_2O_3, inter alia have been studied and continue to be studied, but not as much effort has been expended on polycrystalline, and non-crystalline hosts - with the notable exception of the $Nd^{3+} : Glass$ system. The first ceramic laser gain media was made in 1964 - the $Dy^{2+} : CaF_2$ system followed by the $Nd^{3+} : Y_2O_3 - ThO_2$ system in 1970s [14]. Research on ceramic gain media virtually stopped after that with the next successful laser oscillations reported in 1995 with the $Nd^{3+} : YAG$ ceramic system [15].

And yet the limitations in the single crystal hosts are glaring - thermal lensing at high powers, clustering of active ions causing cross relaxation (this has been known to happen in the $Er^{3+} : YAG$ system with increase in concentration [16]). Poor thermal conduction in some hosts causes the unabated creation of optical phonons ruining pumping efficiency. Quenching of excited levels depend strongly on concentration and temperature. Single-crystal gain media are also difficult to make in large quantities with the methods noted above requiring considerable investments of time, talent and money. All these factors have contributed to the lack of very high powered devices from this set of active ion doped solid state crystal lasers.

Ceramic hosts, on the other hand have multiple advantages over their single crystal cousins, namely the ease of making ceramic by well-studied material science techniques such as hot-isostatic pressing [17], and using nanocrystallite technologies [18], etc. We are also ensured an efficient utilization of the optical pump power since the dopant ion can be homogeneously distributed throughout the host reducing cross-relaxation at high dopant concentrations. And there is also the ability to create engineering bulk media as may be used to couple directly to optical fibers [19].

Being refractory materials these ceramic hosts have a higher tolerance to heat and won't shatter during high-power operation. Furthermore, if constituents are chosen wisely one can even manage thermal effects to an extent. The use of ceramic methodologies also permit the use of various sesquioxides which are difficult to produce as single-crystals[19].

Some of the latest developments in this field include increase in lasing efficiency in the $Nd^{3+}:YAG$ system [20], Yb^{3+} in Y_2O_3 [21] and Sc_2O_3 [22] and the co-doped system - $Nd^{3+}, Cr^{3+}:YAG$ [23] (all ceramic systems). High powered operation has also been reported with the highest powers thus far reaching $\approx 100W$ in $Nd^{3+}:YAG$[18].

Ceramic hosts are not without their own problems: Random orientations of the scatterers makes creating transparent ceramics with minimal scattering one of the major problems. But still much progress has been made to reduce this scattering attenuation constant most notably in the $Nd^{3+}:YAG$ system using a silica based sintering aid to reduce porosity.

In this thesis, we address the experimental study of a novel ceramic host for rare-earth activated laser gain media. This experimental study consists of measurement of the group refractive index of the materials at varying doping levels,

near-IR absorption and emission measurements - critical for the determination of appropriate diode pump wavelength regions and source of the near-IR telecommunication wavelength $\sim 1.55\mu m$, mid-IR emission measurements - the source of the technologically important $\sim 3\mu m$ lasing region. Multi-phonon measurements for the determination of temperature effects on lifetime of the ${}^4I_{11/2} \rightarrow {}^4 I_{13/2}$ transition have also been made.

The existing $Er : YAG$ laser gain media is used a basis for comparison throughout the thesis.

The thesis is structured as follows: Chapters 2, 3, 6, 7, 8 and 9 are abstractions of publications (noted in the above publication list) either in print or going through the peer-review process as of date. Chapters 4 and 5 have data that will be put into publications planned for a later date.

References

[1] *Performance of an Optical Wireless Communication System as a Function of Wavelength*, Haim Manor and Shlomi Arnon, Applied Optics, Vol. 42, Issue 21, pgs. 4285-4294.

[2] *Experimental studies of the application of the Er:YAG laser on dental hard substances: I. Measurement of the ablation rate*, Dr. Raimund Hibst and Ulrich Keller, Lasers in Surgery and Medicine, Volume 9 Issue 4, pgs. 338 - 344.

[3] *Experimental studies of the application of the Er:YAG laser on dental hard substances: II. Light microscopic and SEM investigations*, Dr. Raimund Hibst and Ulrich Keller, Lasers in Surgery and Medicine, Volume 9 Issue 4, pgs. 345 - 351.

[4] *Infrared and Optical Masers*, Schawlow, A. L., and Townes, C. H., Physical Review, 112, 1940 (1958).

[5] *Stimulated optical radiation in ruby*, Theodore Maiman, Nature 187, 493-494 (1960).

[6] *Stimulated Infrared Emission from Trivalent Uranium*, Sorokin, P. P., and Stevenson, M. J., Physical Review Letters. 5, 557 - 559 (1960).

[7] *Pulsed and continuous optical maser action in* CaF_2*:*Dy^{2+}, Kiss Z. J., Duncan R. C., Proceeding of IRE 50, pgs 1531 -1532 (1962)

[8] *Fluorescence and Optical Maser Effects in* CaF_2*:*Sm^{2+},Kaiser W., Garrett C. G. B., and Wood D. L.,Physical Review 123, 766 - 776 (1961).

[9] *Continous operation of* CaF_2*:*Dy^{2+} *optical maser*, Yariv A., Proceedings of IRE 50, 1699 (1962).

[10] *Maser Oscillations at 0.9 and 1.35 Microns in* $CaWO_4$*:*Nd^{3+}, Johnson L. F. and Thomas R. A., Physical Review 131, pgs. 2038 - 2040 (1963).

[11] *Ultrahigh gradient particle acceleration by intense laser-driven plasma density waves.* Joshi, C., Mori, W.B., Katsouleas, T., Dawson, J.M., Kindel, J.M., Forslund, D.W., Nature Journal Volume: 311: 5986, Oct 1984.

[12] *Near-GeV-Energy Laser-Wakefield Acceleration of Self-Injected Electrons in a Centimeter-Scale Plasma Channel*, Tsung F. S., Narang Ritesh, Mori W. B, Joshi C., Fonseca R. A., and Silva L. O., Physical Review Letters 93, 185002 (2004).

[13] *Laser Crystals Their: Physics and Properties*, Kaminskii, A. A., Springer-Verlag, Vol 14, Second Edition.

[14] *Ceramic Laser Materials*, Ikesue A., Aung Y. L., Nature Photonics, Vol 2, December 2008.

[15] *Fabrication and Optical Properties of High-Performance Polycrystalline Nd : YAG Ceramics for Solid-State Lasers*, Akio Ikesue, Toshiyuki Kinoshita, Kiichiro Kamata, Kunio Yoshida, Journal of the American Ceramic Society, Volume 78 Issue 4, Pages 1033 - 1040.

[16] *Concentration effects of Er^{3+} ion in YAG : Er laser crystals*, Yu. Yaqin, Wu. Zhijian, and Zhang. Siyuan, Journal of Alloys and Compounds Volume 302, Issues 1-2, 28 April 2000, pg 204-208.

[17] *Polycrystalline Nd : YAG ceramic lasers*, Ikesue. A, Optical Materials Volume 19, Issue 1, February-March 2002, Pages 183-187.

[18] *Neodymium doped yttrium aluminum garnet ($Y_3Al_5O_{12}$) nanocrystalline ceramics - a new generation of solid state laser and optical materials*, Lu. Jianren, Ueda. Ken-ichi, Yagi. Hideki, Yanagitani. Takagimi, Akiyama, Yasuhiro and Kaminskii, A. A., Journal of Alloys and Compounds, Volume 341, Issues 1-2, 17 July 2002, Pages 220-225.

[19] *Fabrication and Optical Properties of High-Performance Polycrystalline Nd:YAG Ceramics for Solid-State Lasers*, Ikesue. A, Kinoshita. T ,Kamata. K, Yoshida. K, Journal of the American Ceramic Society Volume 78 Issue 4, Pages 1033 - 1040.

[20] *Highly efficient $2\%Nd$:yttrium aluminum garnet ceramic laser*,Lu. J, Prabhu. M, Xu. J, Ueda. K, Yagi. H, Yanagitani. T, Kaminskii, A. A., Appl. Phys. Lett. 77, 3707 (2000)

[21] *Diode-pumped mode-locked Yb^{3+} : $Y2O3$ ceramic laser*,A. Shirakawa, K. Takaichi, H. Yagi, J. Bisson, J. Lu, M. Musha, K. Ueda, T. Yanagitani, T. Petrov, and A. Kaminskii, Optics Express, Vol. 11, Issue 22, pp. 2911-2916.

[22] *Yb^{3+} : $Sc2O3$ ceramic laser*, Lu, J.; Bisson, J. F.; Takaichi, K.; Uematsu, T.; Shirakawa, A.; Musha, M.; Ueda, K.; Yagi, H.; Yanagitani, T.; Kaminskii, A. A., Applied Physics Letters, Volume 83, Issue 6, id. 1101 (2003).

[23] *Synthesis of Nd^{3+},Cr^{3+}-codoped YAG Ceramics for High-Efficiency Solid-State Lasers*, Akio Ikesue, Kiichiro Kamata, Kunio Yoshida, Journal of the American Ceramic Society Volume 78 Issue 9, Pages 2545 - 2547.

CHAPTER 2

Optical Properties

The refractive index n or more accurately the real part of the *complex, linear* index, is one of the first measures that are performed for any material claiming to be a new optical material. Here we measured the refractive index using the *minimum angle of deviation* method using specially made prisms for the purpose. Sellemeier coefficients have also been computed for the wavelength range that extends from visible part the spectrum to the mid-IR.

2.1 Theory

Physically in a lossless, non-magnetic material (not polarized by an external magnetic field), the electric permittivity ϵ_0 in a vacuum is replaced by the permittivity of the material, say ϵ. This change is the electric permittivity from a vacuum to a material is measured by the relative electric permittivity - ϵ/ϵ_0, which is called the dielectric constant of the medium. The propagation constant in the medium is then,

$$k = \omega\sqrt{\mu_0\epsilon} = \frac{n\omega}{c} \tag{2.1}$$

where,

$$n = \sqrt{\frac{\epsilon}{\epsilon_0}} \tag{2.2}$$

But, no real world material is lossless. In this case the permittivity is a complex quantity thus,

$$k^2 = \omega^2 \mu_0 \epsilon = \omega^2 \mu_0 (\epsilon' + i\epsilon'') \tag{2.3}$$

Subsequently, the index of refraction becomes complex as well,

$$n = \sqrt{\frac{\epsilon' + i\epsilon''}{\epsilon_0}} = n' + in'' \tag{2.4}$$

In the most general case of an anisotropic material ϵ is a second rank tensor

$$\begin{pmatrix} \epsilon_{11} & \epsilon_{12} & \epsilon_{13} \\ \epsilon_{21} & \epsilon_{22} & \epsilon_{23} \\ \epsilon_{31} & \epsilon_{32} & \epsilon_{33} \end{pmatrix}$$

With the constants such as ϵ_{ij} $(i \neq j)$, correspond to transfer of polarization and energy from the i^{th} direction in space to the j^{th} direction in the medium. That said, it usually should be possible to reduce the above matrix to a purely diagonal one, in the general case with the three permittivities ϵ_1, ϵ_2, and ϵ_3 differing. Evidently this is reflected in the refractive indices change in the different directions as well. [1]

Ceramic materials, such as Y_2O_3 or ceramic YAG, are made up of crystallites with particles with sizes ranging from $\sim 100nm$ to $\sim 10\mu m$. And although

individually the crystallites might have a purely anisotropic character, when in the random arrangement that defines this class of material, we may safely assume isotropy,

$$\epsilon_1 = \epsilon_2 = \epsilon_3 \Rightarrow n_1 = n_2 = n_3 \tag{2.5}$$

What follows is the measurement and mapping of the wavelength dependence of the real part of the refractive index for the region extending from the visible part of the spectrum to the the mid-IR region.

In general the refractive index is calculated using an empirical Sellemeier equation, which in turn is obtained by fitting wavelength dependent refractive index data to an equation derived from the Lorentz model of the refractive index,

$$n(\omega)^2 = 1 + \frac{Ne^2}{m\epsilon_0} \sum \frac{f_j}{\omega_{0,j}^2 - \omega^2 - i\gamma_j\omega} \tag{2.6}$$

Here n is the complex refractive index, ω is the optical frequency, $\omega_{0,j}$ is the resonant frequency of the jth oscillator, f_j is the oscillator strength. The complex terms i, γ_j and, ω in the denominator of the sum represent the losses in the Lorentz model. N, e^2, m, and ϵ_0 represent the number of oscillators, charges on the oscillators, their masses and the dielectric constant of vacuum. If one were to assume the losses to be negligible, and rewrite the above equation in terms of wavelength, the resulting equation would be known as *Sellemeier's formula*.

2.2 Experimental Details

The refractive index was calculated from the measured angle of minimum deviation of the ceramic samples. The samples available were equilateral prisms of pure Y_2O_3,
$(Er_{0.1}Y_{0.9})_2O_3$ and $(Er_{0.2}Y_{0.8})_2O_3$. The refractive index is calculated in two stages in the minimum angle of deviation method. One first measures the angle of minimum angle of deviation and then from it calculates the refractive index of the substance relative to the surrounding air using the formula,

$$n = \frac{sin((\alpha + \delta_{min})/2)}{sin(\alpha/2)} \tag{2.7}$$

where, α is the apex angle of the prism and δ_{min} is the minimum angle of deviation. The output from either a tunable multi-wavelength HeNe laser (visible spectrum) or a $Nd : VO_3$ laser ($1.064nm$) or a NIR HeNe ($3.39\mu m$ transition) was used to provide the discrete wavelengths used in the experiment. The refracted beams were projected on a screen after a circa 10m throw to amplify the effect to slight changes in angle.

Refracted beam spot was imaged by an assortment of detectors to cover each range.

Region	Detector	D^*
visible	naked eye	$\sim 10^{17}$ [2]
$1.06\mu m$	Newport IR viewer	Sensitivity $\sim 0.001mA/W$ [3]
$3.39\mu m$	Electrophysics PV320LZ pyro-camera	$\sim 10^8$

A goniometer (Gaertner Scientific Corp.) was used to obtain measurements of the prism apex angle and the angles of minimum deviation. It has a nominal

resolution of $20 arcsec$. The refracted beam was located after passing through the prism, the minimum-deviation angle was found by carefully rotating the goniometer stage until the beam reversed direction. The point of reversal marks the angle of minimum deviation. The refractive index was then calculated for each measured minimum deviation angle with the standard formula (2.7).

The system was calibrated by measuring the refractive index of single crystal *YAG*. These calibrated measurements were made at two HeNe wavelengths ($0.632\mu m$ and $0.543\mu m$). These measurements gave values that were within $\sim 0.65\%$ from known values in literature (relative error) [4].

The result of multiple measurements of the angle of minimum-deviation (δ_{min}) angle resulted in a standard deviations for the calculated refractive index to span the range $2.7 \times 10^{-5} \leftrightarrow 7.8 \times 10^{-4}$ over the whole range of wavelengths measured for all prisms considered. The temperature for all measurements was $21 - 22^{o}C$. The refractive index for air at that temperature is ~ 1.00027 for a wide range of wavelengths covering the wavelengths of interest here.

The apex angles were also measured using surface reflections and were found to have a relative error in the range of $0.24\% \leftrightarrow 1.1\%$ from the 60^{o} value.

2.3 Results

The refractive indices thus calculated were used to compute Sellemeier co-efficients valid in this region. We fit the data to a two oscillator equation with resonant frequencies located in the ultraviolet and the infra-red region. The Sellemeier equation chosen was the oscillator equation,

$$n^2 - 1 = \frac{A\lambda^2}{\lambda^2 - \lambda_A^2} + \frac{B\lambda^2}{\lambda^2 - \lambda_B^2} \tag{2.8}$$

Table 2.1: Sellemeier co-efficients for varyingly doped Y_2O_3.

	Pure Y_2O_3	$(Er_{0.1}Y_{0.9})_2O_3$	$(Er_{0.2}Y_{0.8})_2O_3$
A	2.5444	2.5574	2.5711
$\lambda_A(\mu m)$	0.1311	0.1331	0.1355
B	4.327	4.308	4.317
$\lambda_B(\mu m)$	22.85	22.86	22.89

where A and B are constants, proportional to the oscillator strengths f_j. And λ_A and λ_B are resonant wavelengths.

To obtain the fitting parameters A, B, λ_A and λ_B we used a non-linear fitting method derived from the Levenberg-Marquardt algorithm.

The algorithm was written in-house.

Given the above trend of the refractive index with varying concentrations of Er_2O_3 substitution units in the Y_2O_3 matrix, we can calculate the refractive index of the intermediate concentrations and also the refractive index of - Er_2O_3. This employs the use of the using the semi-empirical effective medium theory [5][6]. See figures (2.3, 2.4 and 2.5).

2.3.1 Effective Medium Theory

The theory due to Weiner[5], gives the limits for the dielectric function for compound materials. The two-phases of the compound material are assumed to be arbitrarily and homogeneously distributed [6] in the theory and this suits our situation quiet well. Essentially, the effective dielectric constant can be given by,

$$\epsilon_{eff} = f_a\epsilon_a + (1 - f_a)\epsilon_b \tag{2.9}$$

Table 2.2: Comparison of Refractive indices for pure Y_2O_3

$\lambda = 589.3nm$ [4]	$\lambda = 594nm$	at $\lambda = 589.3nm$ using Table(2.1)	% Error
1.9348 ± 0.0069	1.9162 ± 0.00046	1.9177	$\leq 0.9\%$

Table 2.3: Comparison of Refractive indices for Er_2O_3

$\lambda = 589.3nm$ [4]	$\lambda = 594nm$	at $\lambda = 589.3nm$ using Figure(2.4)	% Error
1.9227 ± 0.0174	1.9635 ± 0.00268	1.9626	$\sim 2.05\%$

Where, f_a is the volume fraction of material a and $\epsilon_{(eff/a/b)}$ is the real dielectric constant for *effective*, a and b material, as the case may be. The above equation along with (eqn.2.2) allows the calculation of the refractive index.

2.4 Discussion

As noted above Y_2O_3 is cubic sesquioxide as a single crystal, and the dielectric constants are isotropic (deduced from [4]). We believe it would be fair to assume the refractive indices should be very close to the single crystal version of the compound. And in fact the values tally quite well to the published reference for these materials ([4]). It must be noted the reference index values were measured at the sodium D-line of $\lambda = 589.3nm$.

With three known levels of substitutional dopings available, we were able to estimate the refractive index for Er_2O_3 ceramic figure(2.3).

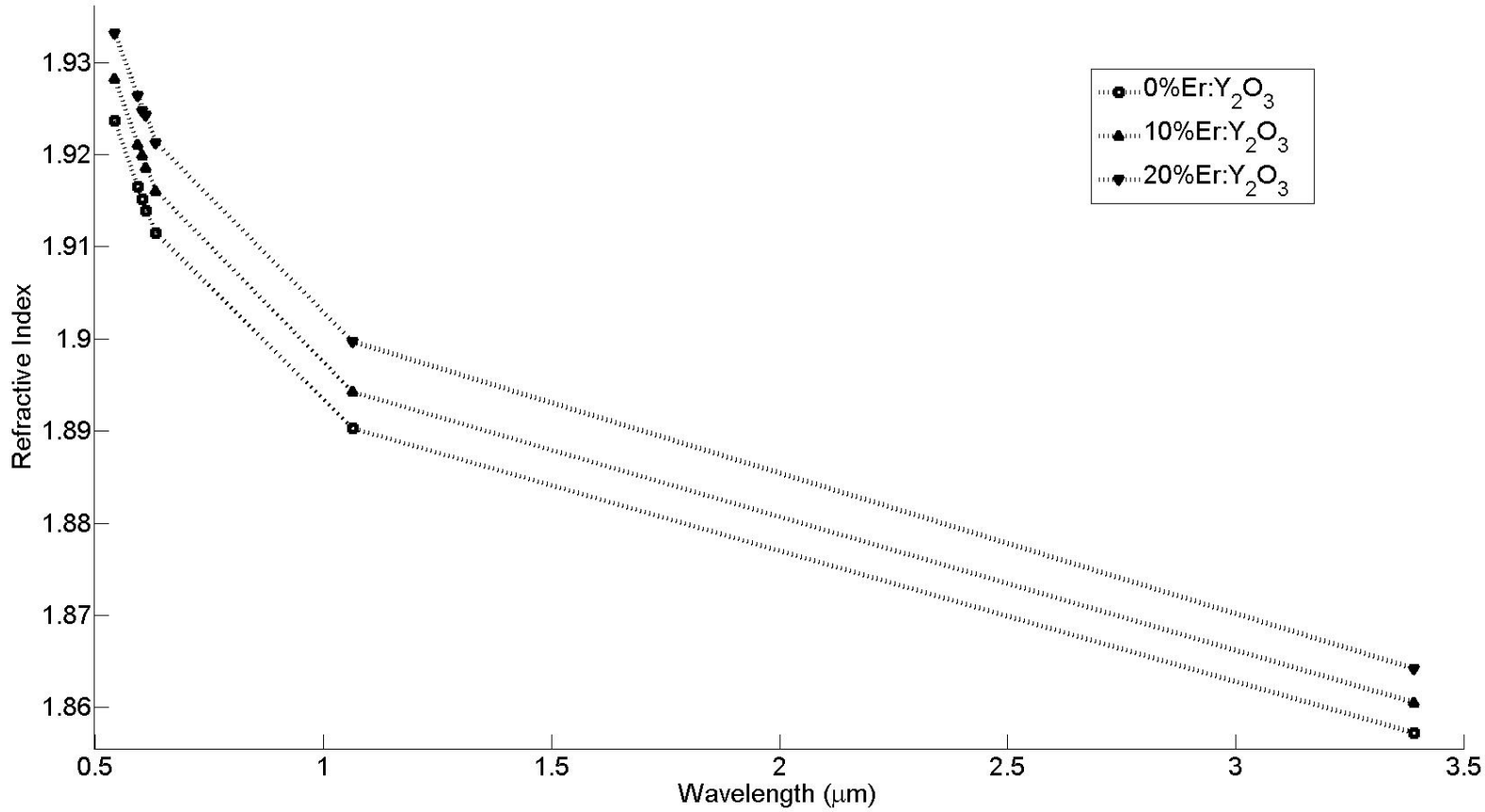

Figure 2.1: Trend of refractive indices.

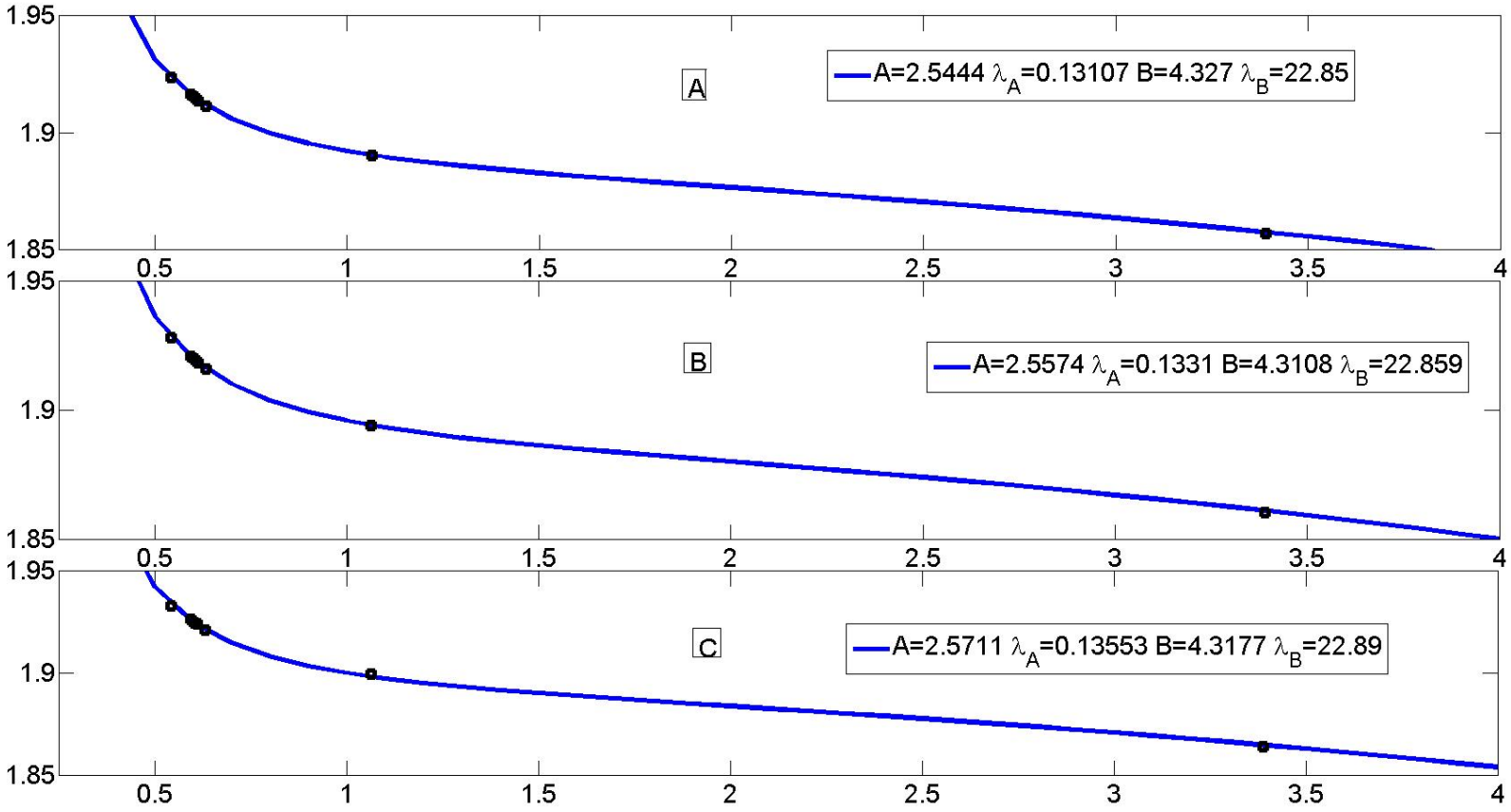

Figure 2.2: Two oscillator fit for pure Y_2O_3 ceramic - (A), $(Er_{0.1}Y_{0.9})_2O_3$ ceramic - (B), $(Er_{0.2}Y_{0.8})_2O_3$ ceramic - (C).

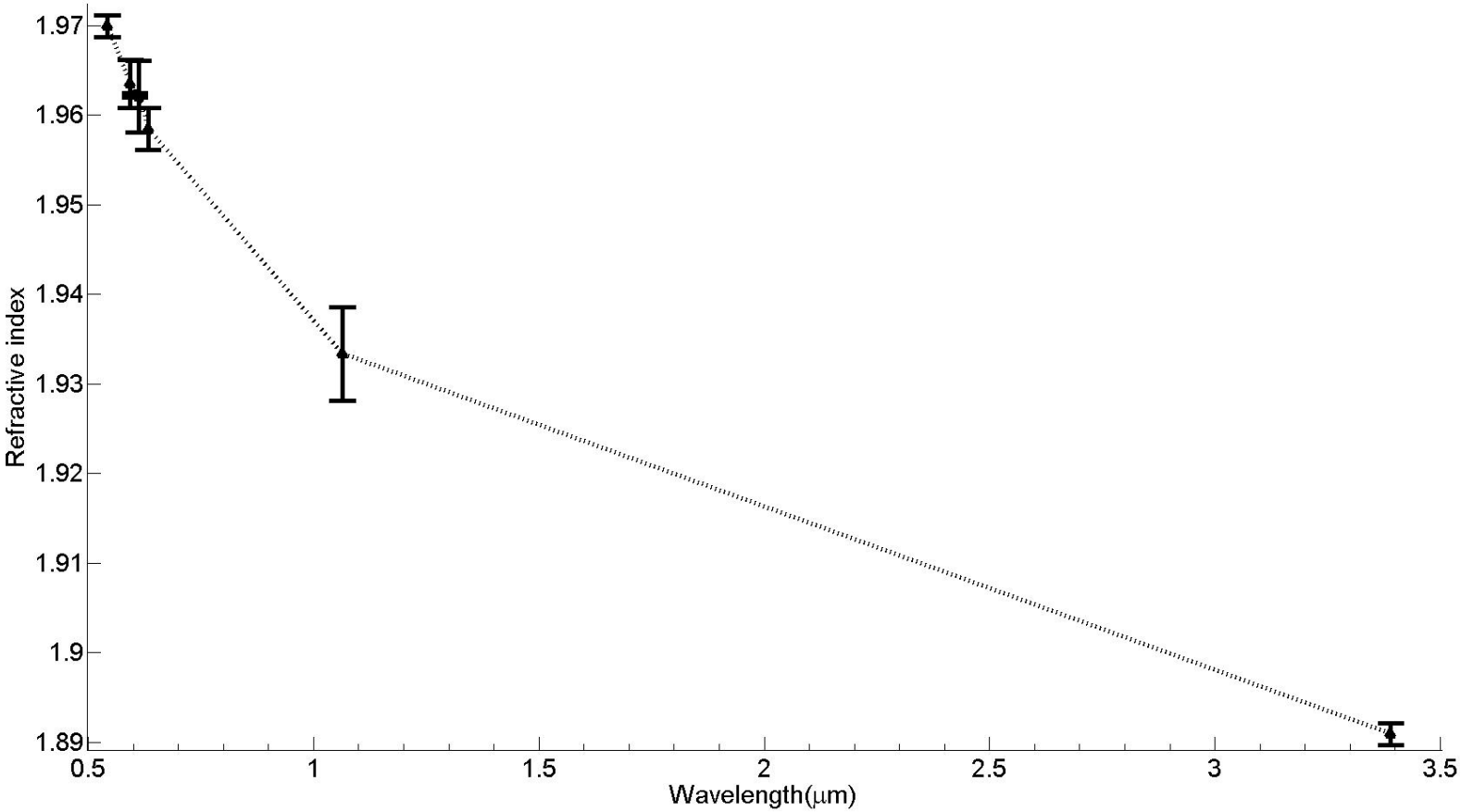

Figure 2.3: Refractive index of Er_2O_3.

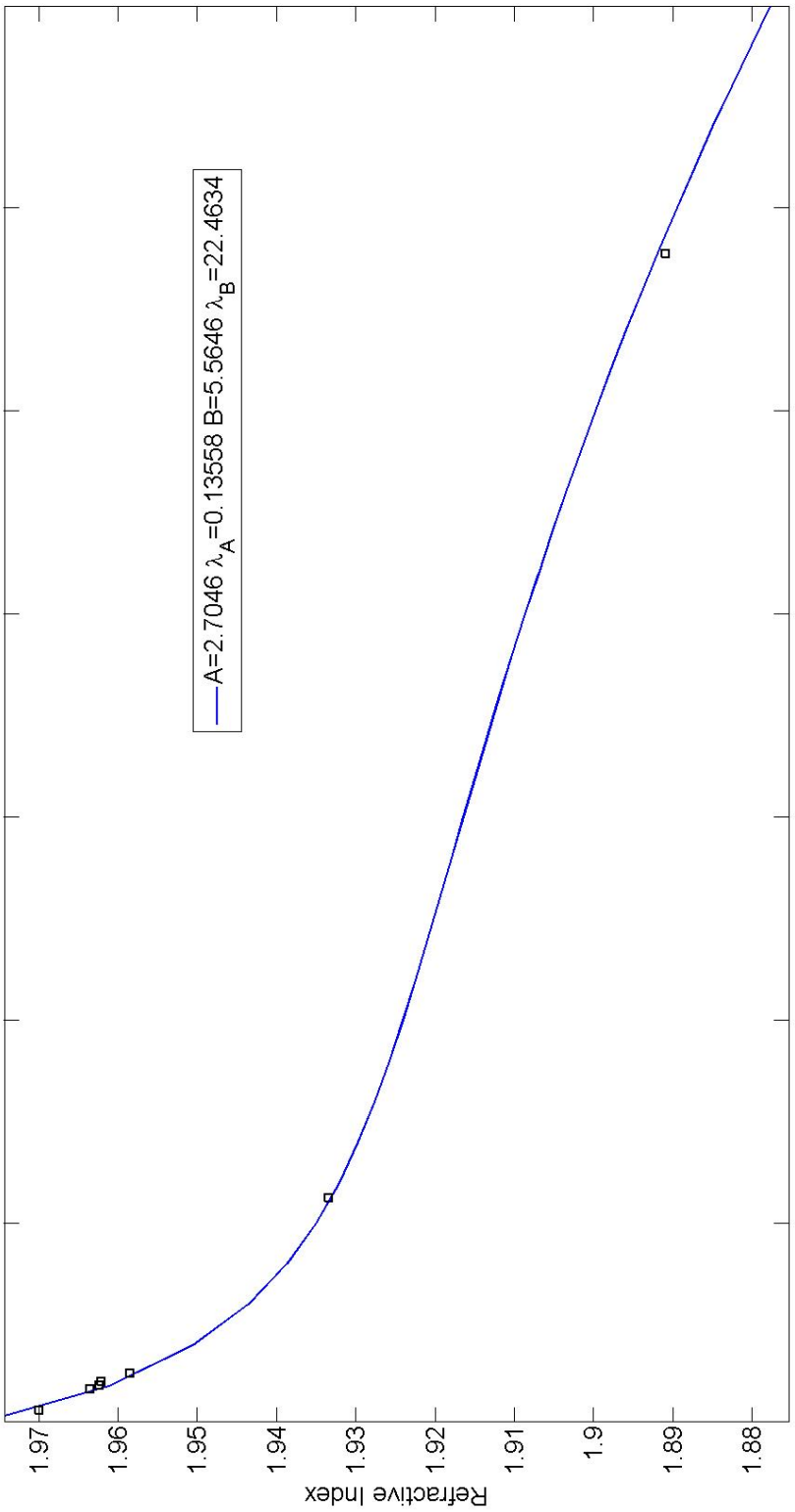

Figure 2.4: Two oscillator fit for Er_2O_3 ceramic.

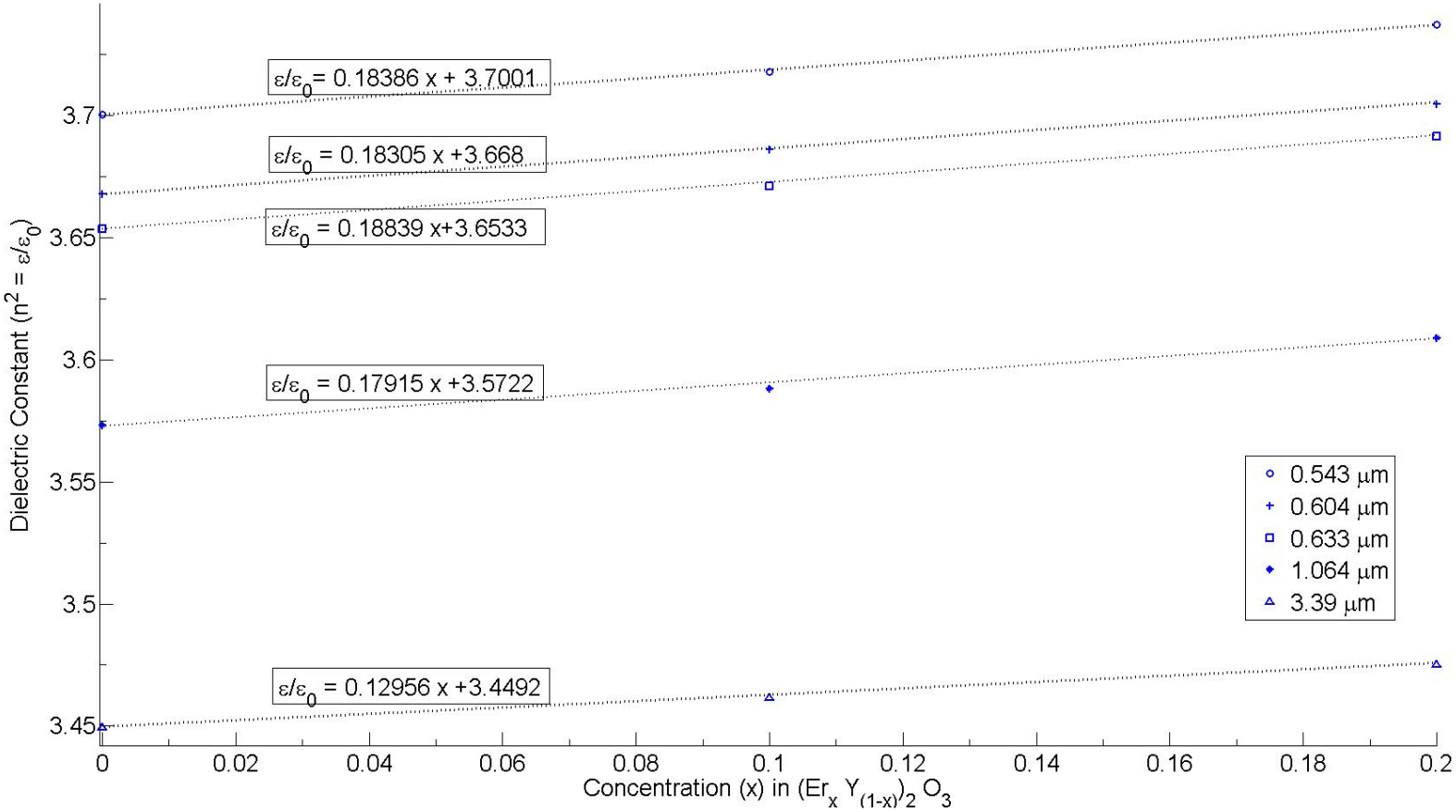

Figure 2.5: Dielectric Constant versus atomic % (x) substituted in $(Er_xY_{1-x})_2O_3$ for various wavelengths.

References

[1] *Material gleaned from Photonic Devices, delivered via lectures, notes*, Jia-Ming Liu, Cambridge University Press 2005.

[2] *Photodetectors, their performance and their limitations*, F. Stockmann, Applied Physics A: Materials Science and Processing, Vol. 7, No. 1, May 1975.

[3] *Catalogue information for IRV Series Infrared Viewers from Newport Corp.* http://www.newport.com/Infrared-IR-Viewer/316817/1033/catalog.aspx, Retrieved 23 Feb 2010.

[4] *Refractive Index and Dispersion of Flourides and Oxides*, Robert D. Shannon, Ruth C. Shannon, Olaf Medenbach and Reinhard X. Fischer, Journal of Physical Chemistry Reference Data, Vol. 31, No. 4, 2002.

[5] *Die Theorie des Mischkrpers fr das Feld der stationaren Strmg. Erste Abhandlung: Die Mittel wert stze fur Kraft, Polarisation und Energie* O Weiner. Abhandlungen der Mathematisch-Physischen Klasse der Koeniglichen Saechsischen Gesellschaft der Wissenschaften 32, pp. 509604.

[6] *Generalized approach to multiphase dielectric mixture theory* W. R. Tinga, W. A. G. Voss and D. F. Blossey, Journal of Applied Physics 44, 3897 (1973).

CHAPTER 3

Stress-optic Behavior

he stress-induced birefringence for erbium doped yttria ceramics were measured at room temperature. An ellipsometer was used to measure the retardation effect of static loading on a set of ceramic equilateral prisms and the stress-optic co-efficients were obtained. The samples measured were equilateral prisms of pure Y_2O_3, $(Er_{0.1}Y_{0.9})_2O_3$ and $(Er_{0.2}Y_{0.8})_2O_3$. The stress-optic co-efficients were found to be in the range $1.6 \leftrightarrow 2.5 \times 10^{-5}$[nm/cm]/Pa showing no dependence on erbium concentration.

3.1 Introduction

Ceramic yttria (Y_2O_3) has become a material of interest to make gain media for high-power solid-state lasers. The physical characterization of such a material is crucial for engineering laser devices. Data for the refractive index and temperature-dependent change in the refractive index for erbium doped ceramic yttria was provided previously [1]. Here we provide the stress-optic coefficients for the same material system.

Thermal optical distortion in laser materials stems from energy dissipated as heat in the material as the laser is pumped optically. The dissipating heat causes two physical effects on the index of refraction n of the solid-state laser material.

$$n = n_0 + \Delta n_{thermal} + \Delta n_{stress}$$

The first effect, $\Delta n_{thermal}$, is the change in refractive index of the material with the temperature of the material. This effect is characterized by calculating the thermo-optic coefficients of the material by direct measurement of the change in refractive index as a function of the temperature of the material ($\frac{dn}{dT}[\frac{1}{^oC}]$). The second effect, Δn_{stress}, is the change in polarizability of the medium with the application of constrictive stress, which is in turn due to the change of the material volume due to temperature. Applied stress causes a change in refractive index of the material in differing directions which gives rise to birefringence affecting the polarization of the transmitted light. The stress-optic coefficient $\frac{Retardation}{AppliedPressure}[\frac{nm/cm}{Pa}]$ characterizes this effect.

Considering the rod design routinely employed while building water-cooled solid-state lasers, the thermal flux from flash-lamps or diode pumps causes expansion of the clamped laser-rod. The effect is to squeeze the rod radially. This causes birefringence in the radial and tangential direction throughout the length of the rod. As a consequence, a linearly polarized beam propagating through the gain medium will experience phase retardation as a function of the length of the rod (See Figure (1)).

During operation, lasers are subjected to various mechanical forces including stresses within the laser-rod mount, thermally induced stresses generated from thermal gradients, pressure gradients, vibrations, etc. For design verification and inspection during operation, it is desirable to have a full aperture description of the effect of the stress field on light passing through the laser rod. These birefringence measurements fulfill these conditions.

Ceramic laser gain media are now gaining prominence due to the various

advantages ceramics have over single crystal hosts. A simple stress-optic law is most notably one of them. We have measured the stress-optic behavior of erbium-doped yttria at varying concentrations of the dopant using He-Ne laser illumination.

Ceramic materials, such as Y_2O_3 or ceramic YAG, are made up of crystallites with particles with sizes ranging from $\sim 100nm$ to $\sim 10\mu m$ [2]. And although individually the crystallites might be anisotropic in character, when in the random arrangement that defines this class of material, we may safely assume isotropy in bulk. Therefore, fine grained ceramics are expected to behave as amorphous or isotropic media with a stress-optic matrix described by,

$$\begin{pmatrix} \pi_{11} & \pi_{12} & \pi_{12} & 0 & 0 & 0 \\ \pi_{12} & \pi_{11} & \pi_{12} & 0 & 0 & 0 \\ \pi_{12} & \pi_{12} & \pi_{11} & 0 & 0 & 0 \\ 0 & 0 & 0 & \times & 0 & 0 \\ 0 & 0 & 0 & 0 & \times & 0 \\ 0 & 0 & 0 & 0 & 0 & \times \end{pmatrix}$$

where the $\times$ components are proportional to the difference between the non-zero π_{11} and π_{12} components. A stress in the X direction results in a uniaxial optical medium with the index for light properties in the Y-Z plane, *i.e.* perpendicular to the stress, having indices of refraction of,

$$n_Y = n_Z = n^0 - \tfrac{1}{2}(n^0)^3\pi_{12}\sigma$$

In the direction of the stress, the index of refraction is,

$$n_X = n^0 - \tfrac{1}{2}(n^0)^3\pi_{11}\sigma$$

In the isotropic case we have, n_Y=n_Z since the π components are equal. σ is the stress load applied [3].

The experiment performed directly gives us the birefringence in polarization when light passes through the media. The birefringence B can then be written as,

$$B[\tfrac{nm}{cm}] = \Delta n \times \tfrac{\lambda[nm]}{length[cm]} = \tfrac{\Delta\phi}{180^o} \times \tfrac{\lambda[nm]}{length[cm]},$$

3.2 Experimental

Retardation caused by static-loading was studied in a polaroscopic arrangement in which the angular phase change was measured for samples with varying concentrations of the rare-earth dopant.

A polarized beam from a He-Ne laser served as a probe. After static loading and the subsequent polarization phase shift, the probe light suffered depolarization and was partially transmitted by the analyzer.

The polaroscopic experiment was constructed around a high-accuracy ellipsometer (Rudolph Scientific, angular measurement accuracy of 0.001^o), with the sample stage modified to hold incremental static loads of up to 1×10^6 Pa ($\sigma_{max} = 1 \times 10^6$Pa) (see Figure (2) for the schematic of the setup).

The control sample was a fused silica prism, roughly of the same dimension as the ceramic prisms. The known stress-optic coefficient for fused quartz is $\sim 3.52 \times 10^{-5}$ $[\frac{nm/cm}{Pa}]$ [4]. It compares well with our value of 3.54×10^{-5} $[\frac{nm/cm}{Pa}]$ (see Figure (3)).

The samples were transparent ceramic equilateral prisms of pure Y_2O_3, $(Er_{0.1}Y_{0.9})_2O_3$ and $(Er_{0.2}Y_{0.8})_2O_3$. They were produced by hot-isostatic pressing

Table 3.1: Stress-Optic coefficients

Sample	SO co-eff. [nm/cm]/Pa
Undoped Y_2O_3	1.781×10^{-5}
5% Y_2O_3	1.928×10^{-5}
10% Y_2O_3	2.481×10^{-5}
20% Y_2O_3	1.627×10^{-5}

(HIP) using nanocrystalline precursors [5]. The samples were subsequently cut into prisms (approximately 2cm high and 1.5cm in length) and mirror polished.

All the measurements were at the minimum angle of deviation δ_{min}, ensuring minimum variation in the signal beam as it propagated through the prism due to minor disturbances of the setup during loading and unloading.

3.3 Results and Discussion

The stress-optic coefficients (Figure (4), Table 3.1) characterize the effect of mechanical stress applied to ceramic yttria doped to varying percentages of active rare-earth dopants.

There have not been, to the authors' knowledge, publicly available numbers for the thermal expansion coefficient for ceramic yttria or any sort of correlation to the presented stress-optic numbers. The closest system studied is yttria-stabilized zirconia (with an $\alpha \sim 10^{-5}$ range around 600-700 K [6]), which is significantly different from bulk ceramic yttria made up of crystallite particles. There has been a recent publication of refractive index data on the ceramic material, along with the change in the refractive index due to temperature [1].

We expect the results presented here will provide quantitative optical characterization of the erbium doped yttria system.

The results show retardation on the order of $1 \leftrightarrow 3 \times 10^{-5}$ nanometers per centimeter for every pascal of load the sample is placed under. The plots are also linear, indicating an application of loads well within the elastic region of deformation.

The results show no dependence on the increasing amount of the erbium ion. Other properties such as the refractive indices ([1]) and the unit cell size on the other hand do differ, even if very slightly. The unit cell sizes of the sesquioxide forms of Y_2O_3 and Er_2O_3 are noted to be $a = 10.605 \pm 0.001\mathring{A}$ (for yttria) and $a = 10.550 \pm 0.001\mathring{A}$ (for the erbium sesquioxide) [7].

3.4 Conclusion

The operation of liquid-cooled, high-powered lasers ($\geq$kW range) demand sharp constraints on the limits of physical deformation due to high heat loads. Ensuring a material can withstand the heat loads and, furthermore, that has a predictable change is a major concern. The above report adds to the amount of information regarding ceramic media that are now gaining interest as future high-powered gain media.

The rich infra-red lasing behavior shown by erbium in insulating hosts drove the decision to study this particular system.

We expect this information along with the thermal-effect on the refractive index of the similar ceramic samples previously reported [1] to be of value for the ceramic yttria laser material system.

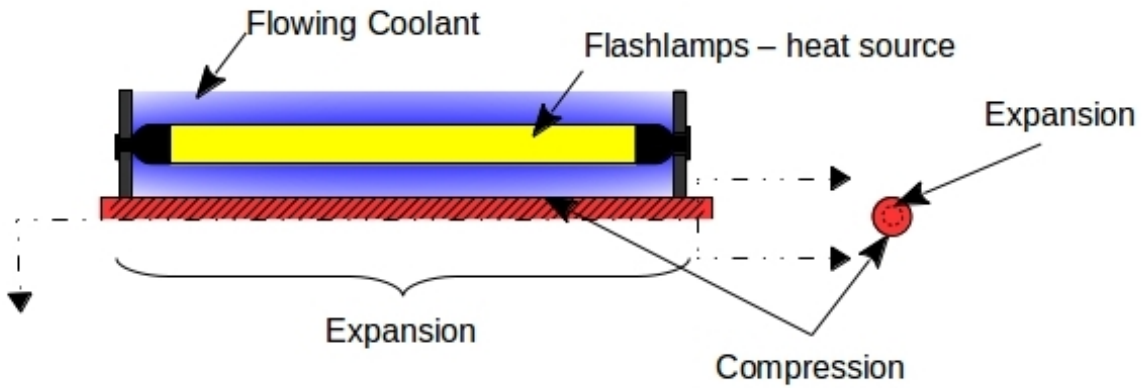

Figure 3.1: The compressed ends of the laser rod impose stress on the laser rod causing birefringence. This is also related to thermal-lensing.

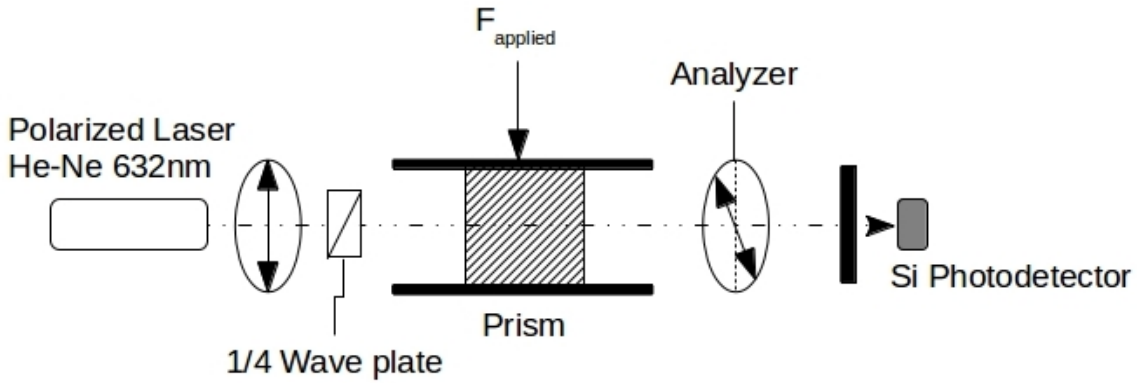

Figure 3.2: Schematic of the experimental set-up. The measurements were carried out at the angle of minimum deviation δ_{min}.

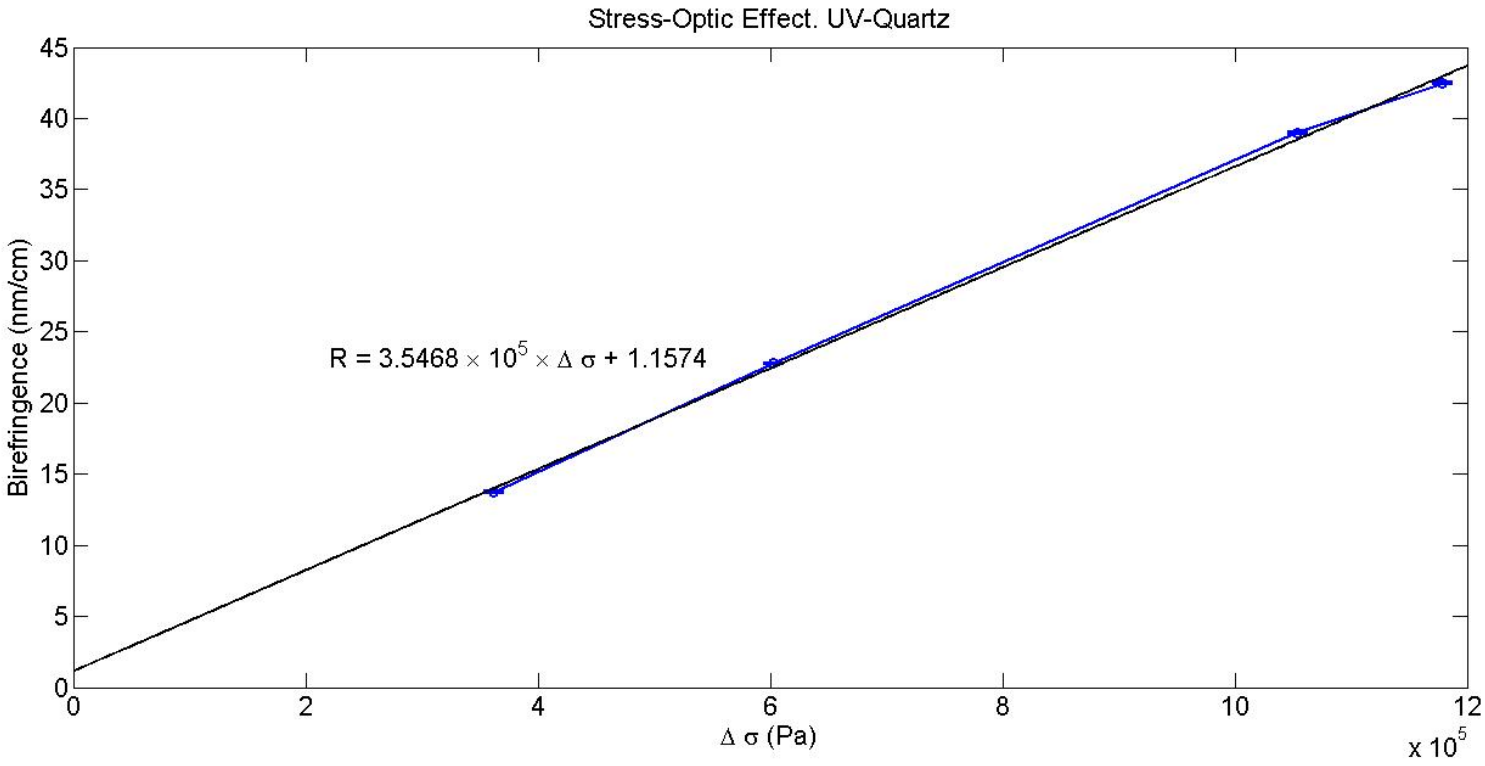

Figure 3.3: Stress-Optic behavior for the UV-quartz standard

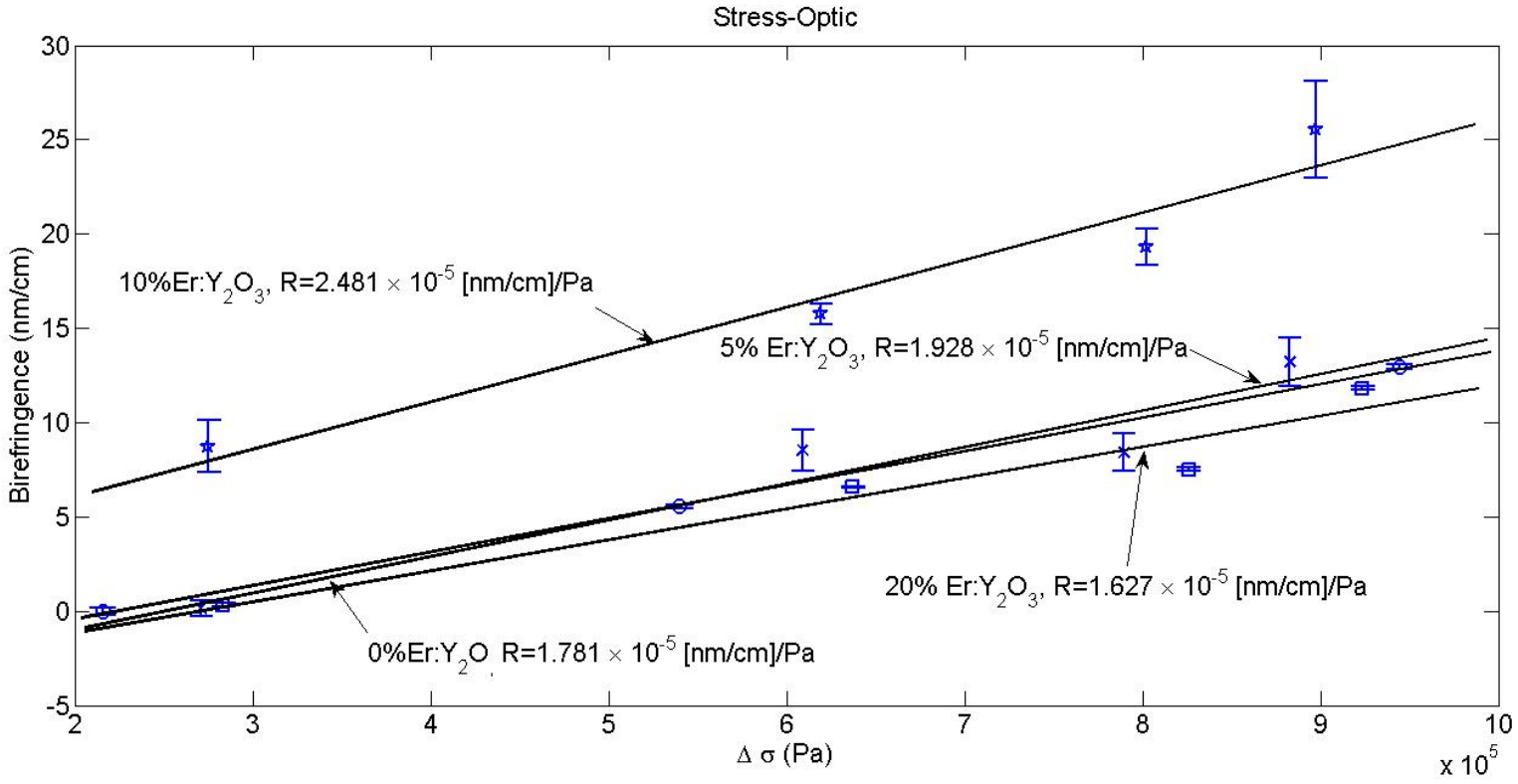

Figure 3.4: Stress-Optic behavior for the erbium doped yttria (0%, 5%, 10% and 20% at. wt.)

References

[1] *Impurity concentration and temperature dependence of the refractive indices of Er^{3+} doped ceramic Y_2O_3*, A. Joshi, N. D. Haynes, D. E. Zelmon, O. Stafsudd and R. Shori, Optics Express, Volume 20, Issue 4, Pages 4428-4435, 2012.

[2] *Multiphonon-based comparison of erbium-doped yttria in large, fine grain polycrystalline ceramics and precursor forms*, A. Joshi, O. M. Stafsudd, K. Serivalsatit, J. Ballato, Optical Materials, Volume 34, Issue 1, Pages 95-98, 2011.

[3] *Physical Properties of Crystals*, J. F. Nye, Oxford Science Publications, 1985.

[4] *Normalised dispersion of birefringence of quartz and stress optical coefficient of fused silica and plate glass*, N. K. Sinha, Physics and Chemistry of Glasses, Volume 19, Issue 4, August 1978.

[5] *Synthesis of transparent Nd-doped HfO_2-Y_2O_3 Ceramics Using HIP*, A. Ikesue, K. Kamata and K. Yoshida, Journal of the American Ceramic Society, Volume 79, Issue 2, Pages 359-364, 1996.

[6] *Thermal expansion coefficient of yttria stabilized zirconia for various yttria contents*, Hideko Hayashi, Tetsuya Saitou, Naotaka Maruyama, Hideaki Inaba, Katsuyuki Kawamura, Masashi Mori. Solid State Ionics, Volume 176, Issues 5-6, 14 February 2005, Pages 613-619.

[7] *Crystallographic Data. 144-147. Rare Earth Oxides. Yttrium Sesquioxide, Y2O3; Dysprosium Sesquioxide, Dy2O3; Erbium Sesquioxide, Er2O3; Ytterbium Sesquioxide, Yb2O3.*, E. Staritzky, Analytical Chemistry 28.12 (1956): 2023-2024.

CHAPTER 4

Concentration Dependent Spectroscopic data

Ceramic materials are being widely studied for many advantages that they have over single-crystal hosts including better thermal management, ease of manufacturing,manageable stress-optic behavior and the ability to customize doping profiles.

We have studied varying concentrations of erbium doped in ceramic yttria. In this manuscript we present concentration dependent spectroscopic and multiphonon behavior. The erbium ion has many important emission wavelengths in the near and mid IR region when doped in this insulating host matrix. We present absorption and emission characteristics for emissions in near-IR region ($\sim$ 980nm and $\sim$ 1550nm) and in the mid-IR region ($\sim 3\mu$).

The lifetimes of the higher-energy level ($^4I_{11/2}$) and the terminal level ($^4I_{13/2}$) of the mid-IR laser are presented. They show a concentration dependence that has never been seen before. The 'self-terminating' mid-IR laser transition $^4I_{11/2} \rightarrow {}^4I_{13/2}$ could potentially be overcome by tuning the doping level.

Concentration dependent multiphonon studies show the effect of high temperatures on the population in the mid-IR lasers higher energy level as well. Concentration dependent absorption and emission cross-sections are also provided for completeness.

4.1 Introduction

Crystals large enough to design high powered solid state laser systems are not easily made. Single crystal solid state media also have stringent limitations on their opto-mechanical, thermal properties and general mechanical robustness. This has given impetus to the development of ceramic solid state laser media. Ceramics are expected to have lower processing and fabricating temperatures and the ability to custom design multi-functional laser gain media. This would include spatially non-uniform doping and the mechanical advantages of ceramic media such as a lack of cleavage planes and enhanced toughness due to granular micro-structure. Ceramics are also expected to have the simpler stress-optic behavior of amorphous media as compared to single crystal versions of the same compounds.

4.2 Lifetimes of the $^4I_{11/2}$ and $^4I_{13/2}$ energy levels

With its rich variety of transitions and conveniently placed absorption bands, erbium has become an important ion to generate telecommunication wavelengths. Erbium doped in insulating hosts has well-known emissions at other wavelengths around $\sim 3\ \mu m$ (the $^4I_{11/2} \rightarrow^4 I_{13/2}$ transition). This emission line is important because the vibrational modes of the water molecule have energies very close to the energy of the mid-IR photon (2.936μm emission from the Er^{3+}:YAG system). This allows for high absorption of the radiation into the water molecule ($\alpha \sim 10^4 \text{cm}^1$). This method for injecting energy into dental tissue has been leveraged for use in dental surgery to great advantage [1].

As we shall see shortly, the lifetimes of the two transitions are inverted from what they ought to be, such that the upper transition is faster, at $\sim 100\mu s$, than the lower $^4I_{13/2}$ level lifetime, which is in the range of $\sim 6 - 7.5\mu s$ (measured in-

house). This fact alone virtually eliminates the possibility of lasing to occur, were it not for up-conversion processes that become dominant at high erbium concentrations. The 'self-saturation' problem, as it has been named, is overcome by the upconversion processes ${}^4I_{13/2} \rightarrow {}^4 I_{15/2} + {}^4 I_{13/2} \rightarrow {}^4 I_{9/2}$; these deplete the terminal level and feed the upper one via multi-phonon transitions (dotted arrows in figure(9.1)) [2]. This not the only upconversion process at play in this system others include: ${}^4I_{11/2} \rightarrow {}^4 I_{15/2} + {}^4I_{11/2} \rightarrow {}^4 F_{7/2}$, which also becomes important at high concentrations of erbium in the host. Cross-relaxation is another important process that takes place in this laser system that adds transitioning electrons to both the upper and lower lasing levels: ${}^4S_{3/2} \rightarrow {}^4 I_{9/2} + {}^4 I_{15/2} \rightarrow {}^4 I_{13/2}$. Continuous-wave laser action has, however, been obtained in straight (un-codoped) erbium YAG crystals; and the only way to explain such a laser is depopulation of the terminal level due to upconversion.

The situation in the system under consideration here (Er^{3+}:Y_2O_3) is qualitatively similar, though significantly more unfavorable. The upper level lifetime for the ${}^4I_{11/2}$ state in yttria is in the 3 5ms range and the lower level lifetime (${}^4I_{13/2}$) is in the 10 12ms range for a wide concentration range (Figure (4.2.2)).

The self-termination of the upper level in the $\sim 3\mu$m transition is now thought to be overcome by up-conversion processes[2].

The lifetime data 4.2.2 show a peculiar trend at low doping levels and at higher doping levels. Trends this stark have not been seen in other insulating hosts to the authors' knowledge.

4.2.1 Experimental

The experimental setup measured directly the decay lifetime from the ${}^4I_{11/2}$ and the ${}^4I_{13/2}$ energy-levels. The fluorescence was isolated from the pump radiation

by appropriate filters and detected via a *S-1* (Hamamatsu Electronics) (cutoff $\lambda = \sim 1.1\ \mu$m) surface photomultiplier or a Thorlabs pre-amplified InGaAs photodetector (PDA 10D, range : 1.2 μm $\leftrightarrow$ 2.5 μm).

The fluorescence decay was measured via a high-speed, high-bandwidth Tektronics (Digital Phosphorus) oscilloscope and transferred to a computer for analysis. The pump was a diode pumped neodymium orthophosphate laser (Coherent, DPSS laser) doubled to $532nm$. The laser was modulated by either a mechanical chopper or an acousto-optic beam diffractor. Sub-microsecond rise and fall times were available via the acousto-optic device (see Figure (4.4.2).

4.2.2 Results and Discussion

Two peculiarities may be readily noticed in the lifetime decay data
(see Figure4.2.2). Increasing the concentration from 0.1% at. wt. to about 5% at. wt. erbium in yttria monotonically increases the lifetime for both the measured decays: ${}^4I_{11/2} \rightarrow^4 I_{15/2}$ and ${}^4I_{13/2} \rightarrow^4 I_{15/2}$. The increase is dramatic for the ${}^4I_{13/2}$ energy-level.

The decay times decrease thereafter for both the transitions to levels we could not measure with our setup (sub-micro second levels). The lifetimes of the ${}^4I_{11/2}$ energy-level is larger than the ${}^4I_{13/2}$ energy-level when the concentration of the activated ion reaches about $\sim$24% at. wt. (see Figure4.2.2).

It is unclear why there is such a unusual dependence of lifetime with concentration of the active ion. Our data is most closely matched by concentration dependence of Nd^{3+} in LaF_3 and $LaCl_3$ [3]. A similar change is seen Nd^{3+}:LaF_3 but not in $LaCl_3$.

Such a dependence is not seen with change in erbium concentration in YAG [4]. The most likely explanation would be the varying quenching mechanism from

material to material. The actual mechanism appears to depend upon the details of the electronic energy levels, the lattice phonon structure, the electron-lattice interaction and the interaction between impurity ions. The authors [3] note that in LaF_3 pair cross relaxation may be the dominant relaxation mechanism as concentration exceeds 1%.

4.3 Near-IR Absorption and Emission Spectra

The erbium ion offers multiple wavelengths in the near and mid IR region that are technologically significant.

In the near IR region the erbium ion has electronic dipole transitions that provide $\sim 1\mu m$ ($^4I_{11/2} \rightarrow^4 I_{13/2}$) and $\sim 1.55\mu m$ ($^4I_{13/2} \rightarrow^4 I_{15/2}$) radiation. Of which, the latter wavelength lies in the fiber optical telecommunication window - so determined by low optical losses in silica fibers. The *C-band* extends from $1.53\mu m$ to $1.56\mu m$ covering the erbium emission lines. This wavelength region has been well-studied due to its commercial significance and won't be the focus of this section. Rather the erbium emission near the water absorption band around $\sim 3\mu$ is of technological importance and will be studied instead. The upper lasing level for the $\sim 1.55\mu m$ ($^4I_{13/2}$) radiation does in fact come into play automatically, since it is the lower lasing level for the $3\mu m$ transition.

4.3.1 Experimental

The absorption spectra was directly measured using a calibrated spectrometer with a nominal resolution of 1-2 nm resolution for the $^4I_{15/2} \rightarrow {}^4I_{11/2}$ transition and the $^4I_{15/2} \rightarrow {}^4I_{13/2}$ transition.

The automated spectrometer was a Ocean Optics device (HR2000) tuned to

operate in wavelength region starting at $\sim 800nm$ and extending to $\sim 1700nm$. A white light source provided the baseline transmission and the broadband source required for such an experiment.

The near-IR emission spectra were got by pumping the Er^{3+} ions with a light emitting diode operating at $589nm \pm 10nm$.

The data frames were averaged for more than one second, with a collection time of $10ms$ for each frame, to ensure clean datasets and substantial reduction in noise variance.

All the samples were of the same thickness that permits direct comparison.

The absorption and emission cross-sections were calculated from directly measured absorption and emission spectra and the above noted room-temperature lifetimes using the Fuchtbauer-Landenberg formulation. The absorption cross-section plots are given in figures (4.3.1 $\rightarrow$ 4.3.1).

The emission cross-section plots are given in figures (4.3.1 $\rightarrow$ 4.3.1).

4.3.2 Mid-IR Absorption and Emission Spectra

For mid-IR lasers to be of significance to the medical world, they must be at wavelengths that allow precise removal of tissue with minimal thermal damage to the surrounding region. Since water is the major constituent ($\sim 70 - 80\%$) in virtually all types of soft tissue, it behooves laser engineers to create devices where the absorption of mid-IR radiation by water is high. The $3\mu m$ region is where the main vibrational resonances lie when one considers the H_2O molecule. The absorption coefficient is noted to be in the vicinity of $\sim 10^4 cm^{-1}$ [1]. The erbium laser, first reported in 1975 [5], works on the transition ${}^4I_{11/2} \rightarrow {}^4 I_{13/2}$.

4.3.3 Experimental Details

The mid-IR emission spectra involved the use of a $1mtr$ Jarrell-Ash Czerny Turner Spectrometer. It has a $4in$ grating peaked at $\lambda = 2\mu m$ and a nominal resolution exceeding $5\mathring{A}$. The pump for this experiment was a fiber-coupled laser-diode operating at $\sim 0.97\mu m$. This is a device provided by Sheaumann Inc. and is branded as the *MIR-PAC* laser diode. The emission light after dispersion by the grating was collected with a cooled, $1mm^2$ PbS detector. When cooled to $\sim 243K(30^oC)$, as in this case, the specific detectivity (D^*) hovers well above $10^{11} Jones$ for detectors of this type. The small area was chosen to reduce noise.

The signal was routed to a lock-in amplifier, where the integration times varied from $300ms$ to $1sec$, depending upon the quality of the data and the rate of scan.

The signal was thereafter digitized and plotted.

4.3.4 Discussion: mid-IR region

Figures (4.12, 4.13 and 4.14)

The wavelengths of most technological interest lie in the water absorption bands near $3\mu m$ emitted by the active ion erbium. The plots include the fullscale values for the measurements so a s to provide

The lower plots provide a broader view of the emission spectrum, and one sees the expected peaks at in the $\sim 2.6\mu m - 2.85\mu m$, the presence of the $\sim 2.936\mu m$ peak is not even perceptible compared to the emission in this range. Yttria as a mid-IR host shows promise because of the large emission cross-section when compared to *YAG*. Since the emission cross-section is proportional to the emission signal, it's evident that erbium has a cross-section in Y_2O_3 roughly five times that in *YAG* in the $\sim 2.6\mu m - 2.85\mu m$ range. However, in the important water absorption region near $3\mu m$ the emission have similar absolute values.

Thus, making lasers at $2.936\mu m$ demand that oscillation at the other stronger emission bands in the $\sim 2.6\mu m - 2.85\mu m$ be eliminated.

4.4 Multiphonon Studies of the $^4I_{11/2} \rightarrow ^4 I_{15/2}$ transition

4.4.1 Theoretical

Quantification of the non-radiative component of the excited state decay is of importance. Along with two-ion energy (cross-relaxation, impurity quenching, etc.) transfer processes, phonon de-excitation is the most significant mechanism of loss of energy in excited solid state systems. It is also the limiting quenching process that reduces radiative efficiency. Direct energy transfer between two-excited ions, or one excited ion and another un-excited ion is not expected in

lightly doped samples since it requires the active ions to be physically close to each other. However, non-radiative emission can be experimentally studied using the multiphonon relaxation theory first developed by Kiel [6] and subsequently extended by Riseberg and Moos [7], [8].

We use the general formulation by Riseberg and Moos [7] [8] for calculating the probability of multiphonon non-radiative transitions between the Stark groups (J multiplets) of the ${}^4I_N$ states of trivalent erbium ions in hosts. The fluorescence decay rate of a level is then the sum of the radiative decay and multiphonon relaxation rates. These rates are determined primarily by the order of the process and the strength of the interaction. In the multiphonon decay theory, one assumes the emission of p_i equal energy phonons corresponding to the i^{th} phonon mode. The population of the modes occurs due to thermal excitation. The rate of decay of excited atoms due to both radiative and non-radiative effects (Ω) can be given by,

$$\Omega(T) = \Omega_0(n_i + 1)^{p_i} \tag{4.1}$$

where n_i is the average phonon occupancy number given by the Bose-Einstein formula,

$$n_i = \frac{1}{e^{\frac{E_p}{kT}} - 1} \tag{4.2}$$

Here, E_p is the characteristic phonon energy of the host matrix. Combining the above formulae we obtain,

$$\Omega(T) = \Omega_0 \left(\frac{e^{\frac{E_p}{kT}}}{e^{\frac{E_p}{kT}} - 1} \right)^{p_i} \tag{4.3}$$

As $T \to 0K$ we should get the radiative transition rate corresponding to the Einstein *"A"* co-efficient.

4.4.2 Experimental

Polycrystalline (ceramic) samples were placed in a heated brass chamber. Two holes at ninety degrees from each other allowed pump-light to enter and the fluorescence emission be observed at 90 degrees from the pump. The temperature was measured using a iron-konstantine thermocouple. The lifetime measurement setup was the same as the lifetime experimental details above (see Figure 4.4.2).

4.4.3 Experimental Results

In this study the ${}^4I_{11/2}$ fluorescent level of erbium was studied in $0.1\%, 1\%, 2\%$ and $10\%(at.)Er^{3+}$ in ceramic yttria .

The experimentally determined fluorescent lifetimes versus temperature were fit to the multiphonon model (eqn 4.3). The results are summarized in Table 7.1.

It should be noted that the simple multiphonon model yields a $0K$ lifetime for both the ceramic and crystalline forms within the admittedly large error-range from Weber's calculations. Using Judd-Ofelt analysis Weber reported a value of $\sim 6810 \pm 2470 \mu s$.

Parameter fitting on the data yields results as shown in Table 7.1. The plots of fluorescence rates versus temperature are given in Figures 4.17, 4.18, 4.19 and

Er^{3+} at. concentration	$E_p\ cm^{-1}$	p_i number of phonons	τ_{0^oK} (ms)
$0.1\%Er^{3+}:Y_2O_3$	556	5.6	3.707
$1\%Er^{3+}:Y_2O_3$	549.5	5.7	4.167
$2\%Er^{3+}:Y_2O_3$	528.2	5.4	4.444
$10\%Er^{3+}:Y_2O_3$	486.5	7.4	6.667

Table 4.1: Multiphonon fit parameters pursuant of equation (4.3)

4.20.

4.4.4 Results and Discussion

The multiphonon theory describes the effects of direct coupling between the active ion and the host lattice (see Figure4.16). We show elsewhere in the thesis, that the energy transferred in this manner appears to be related to the bond strength of the host material. Other oxide hosts were evaluated using the same technique and were found to obey the mass-spring relation,

$$E_p = k \times \frac{1}{\sqrt{m_{eff}}} \tag{4.4}$$

where E_p is the energy of the phonon liberated, k is the spring constant and m_{eff} is the effective mass of the spring system.

It is no surprise that this model still largely holds for the varying concentrations of erbium in ceramic yttria subjected to such a study. The notion of 'fractional phonon' mode number is fictitious, in reality it represents the distribution of phonons emitted with differing energies. The phonon mode number is thus a weighted number that is the 'effective' mode. For the low doped samples, both the phonon energy and the phonon modes are close enough to infer

that the phonon energy liberated due to an increase in temperature from the $^4I_{11/2}$ energy-level is absorbed by the lattice is the same for all the low doped concentrations.

The multiphonon experiment and model seems to fail when the concentrations get appreciably large ∼10%. Neither do the phonon energy and mode or the low temperature lifetimes seem to follow any recognizable trends. We believe this is due to increased communication between the active ions.

The Er^{3+} ion is a substituted instead of the Y^{3+} ion in the host matrix. As the concentration of erbium is increased in the solid solution, there is an increase in probability of forming clusters of two or three or more erbium ions. One may calculate the probability thus:

From a pool of 90.00 at. wt. % Y^{3+} and 10.0% at. wt. % Er^{3+} there is a 10% chance of first finding a Er^{3+} ion and a 90% chance of finding a Y^{3+} ion. Referring to Table 4.2, we note that each yttrium holding site has a total coordination number of 12.

Since not all the yttrium sites in the cell are optically active (due to the lack of inversion symmetry for C_{3i}) for dipole-dipole transitions. This reduces the effect of clustering by a factor of a half.

Consecutive probabilities multiply, therefore there is a $(0.1 \times 0.99^{11} \times 0.5)$ chance of having one Er^{3+} ion in an equivalent, optically active site. There are 12 possible positions for the Er^{3+} ion to be in the 12 coordinated sites. We thus get a total probability of,

$$P(1Er^{3+}) = 0.1 \times 0.99^{11} \times 0.5 \times 12 = 0.54 \tag{4.5}$$

Similarly, the probability of finding 2 erbium ions in neighboring optically

Parameter	Property
Crystal Symmetry	body-centered cubic
Space Group	Ia3
Unit cell size	$\sim$10.604 Å
Er^{3+} site symmetry	C_2, C_{3i}
Er^{3+}-Er^{3+} coordination	6@ 3.496 Å, 6@ 3.985 Å

Table 4.2: The following table (4.2) [9] summarizes the crystal structure of $Er^{3+} : Y_2O_3$.

active sites is approximately a third. Thus although there is a greater than half a chance of having isolated Er^{3+} ions in the host matrix, there is a not insignificant possibility of having pairs. The probability of having three active ions within 'talking' distance is $\frac{1}{10}$. Since upconversion and other energy-transfer phenomena occur so frequently in erbium-doped materials, the multiphonon experiments for the 10% at. wt. doped sample are bound to show those effects.

Both these sets of results, when taken together show the limitation of the application of the multiphonon study when it come to highly doped materials.

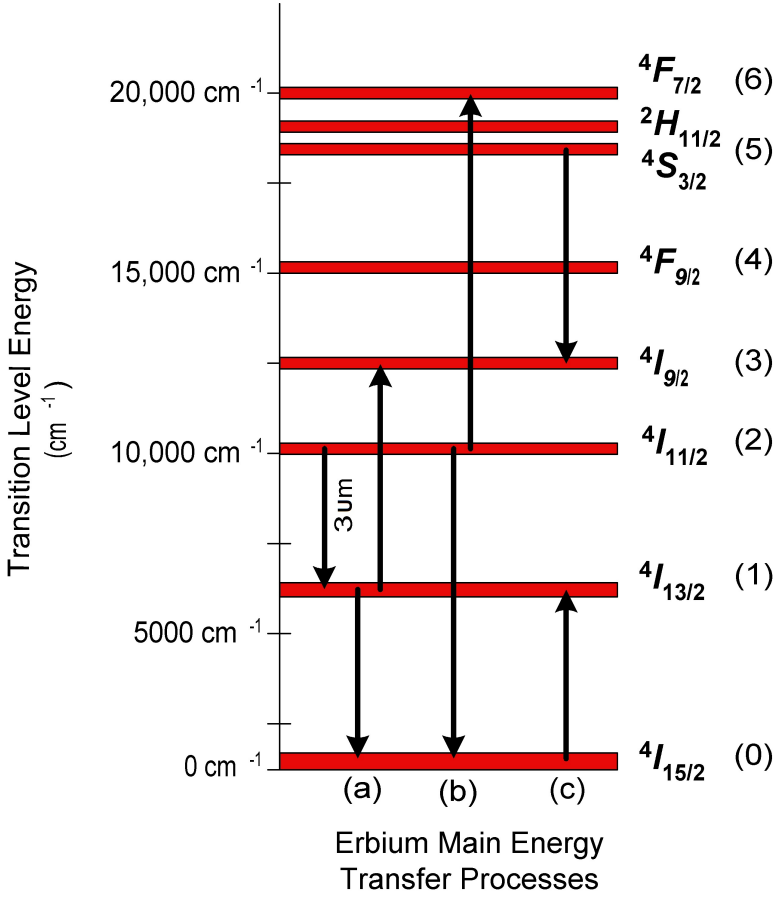

Figure 4.1: Relevant energy levels and energy transfer processes in the standard $Er^{3+}:YAG$

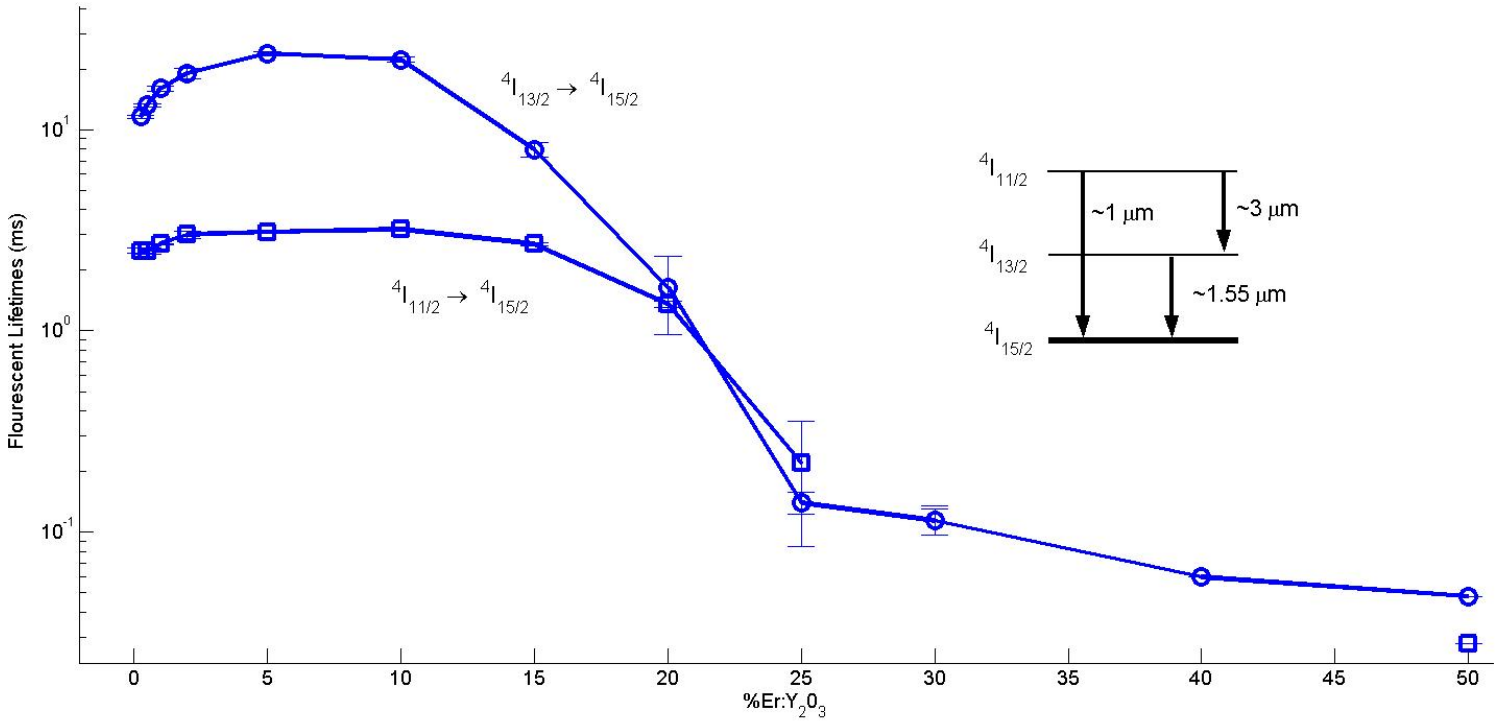

Figure 4.2: Room temperature fluorescence lifetimes for the ${}^4I_{11/2} \rightarrow {}^4 I_{15/2}$ transition.

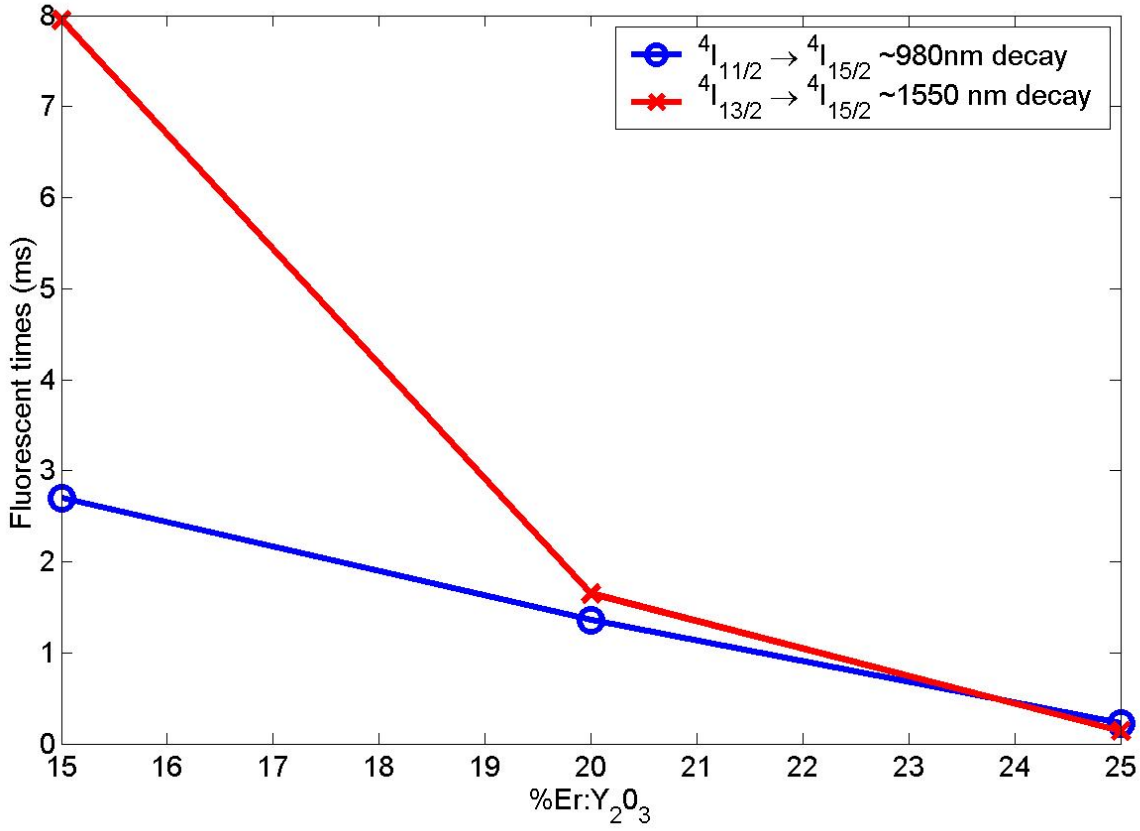

Figure 4.3: The lifetimes for the $^4I_{11/2}$ and $^4I_{13/2}$ energy-levels are similar at relatively high concentrations of erbium.

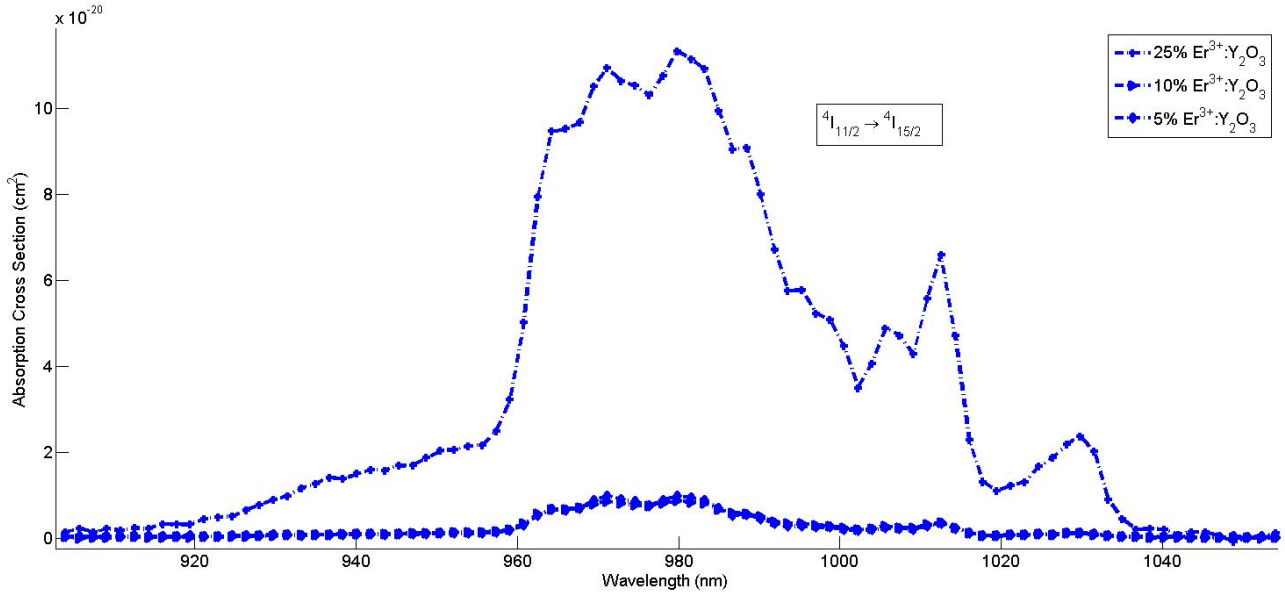

Figure 4.4: Absorption Cross-sections for the $980nm$ band corresponding to $^4\mathrm{I}_{15/2} \rightarrow {}^4\mathrm{I}_{11/2}$ transition

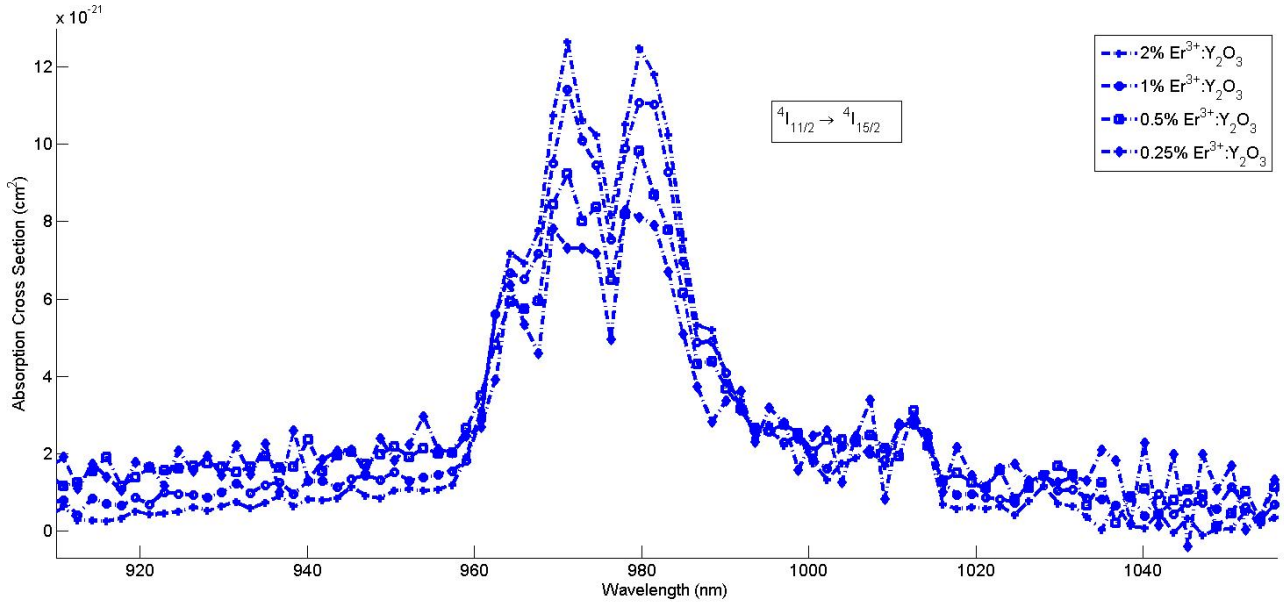

Figure 4.5: Absorption Cross-sections for the $980nm$ band corresponding to $^4I_{15/2} \rightarrow {}^4I_{11/2}$ transition

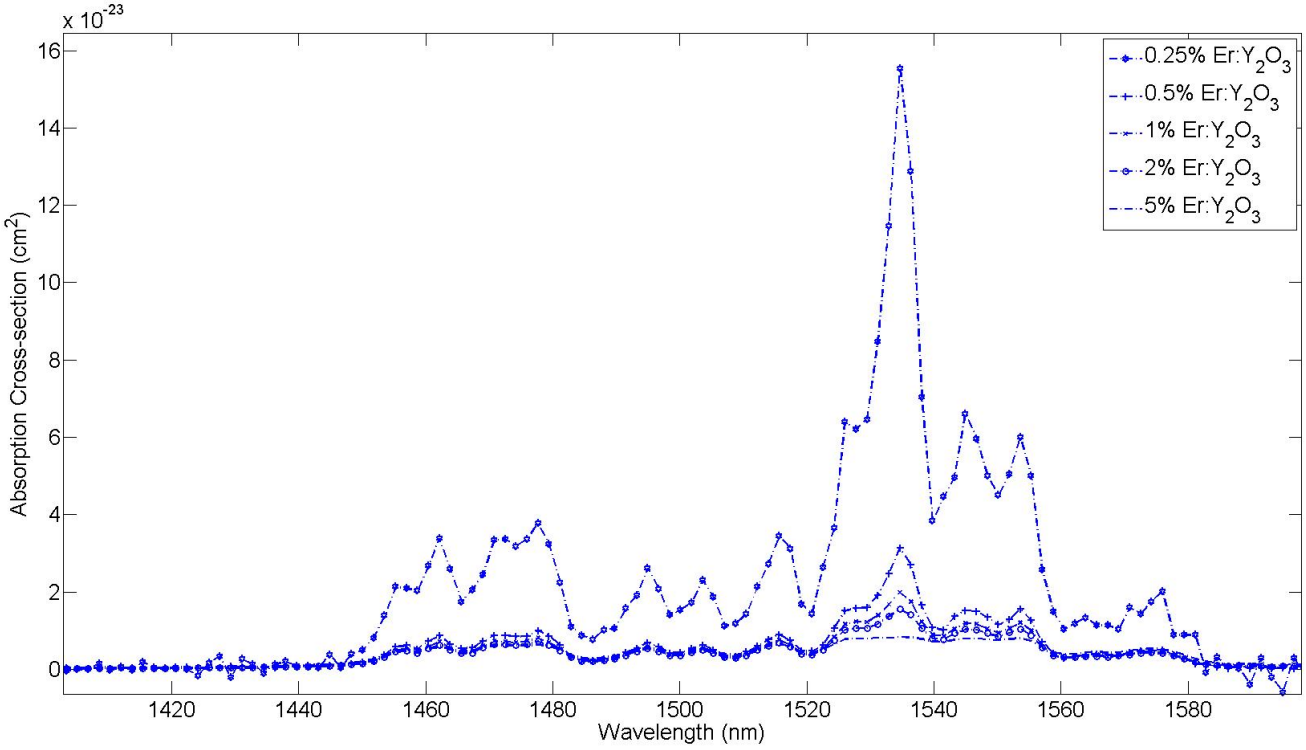

Figure 4.6: Absorption Cross-sections for the $1550nm$ band corresponding to $^4\mathrm{I}_{15/2} \rightarrow {}^4\mathrm{I}_{13/2}$ transition

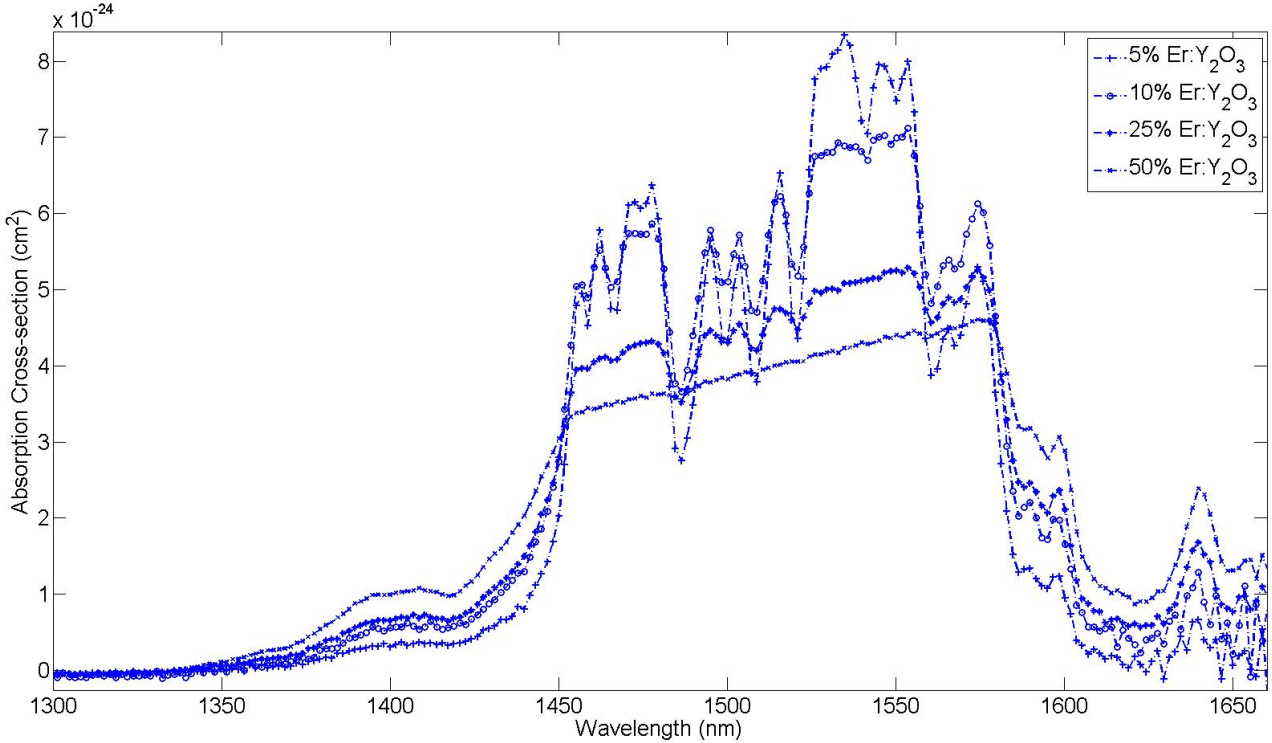

Figure 4.7: Absorption Cross-sections for the $1550nm$ band corresponding to $^4\mathrm{I}_{15/2} \rightarrow {}^4\mathrm{I}_{13/2}$ transition

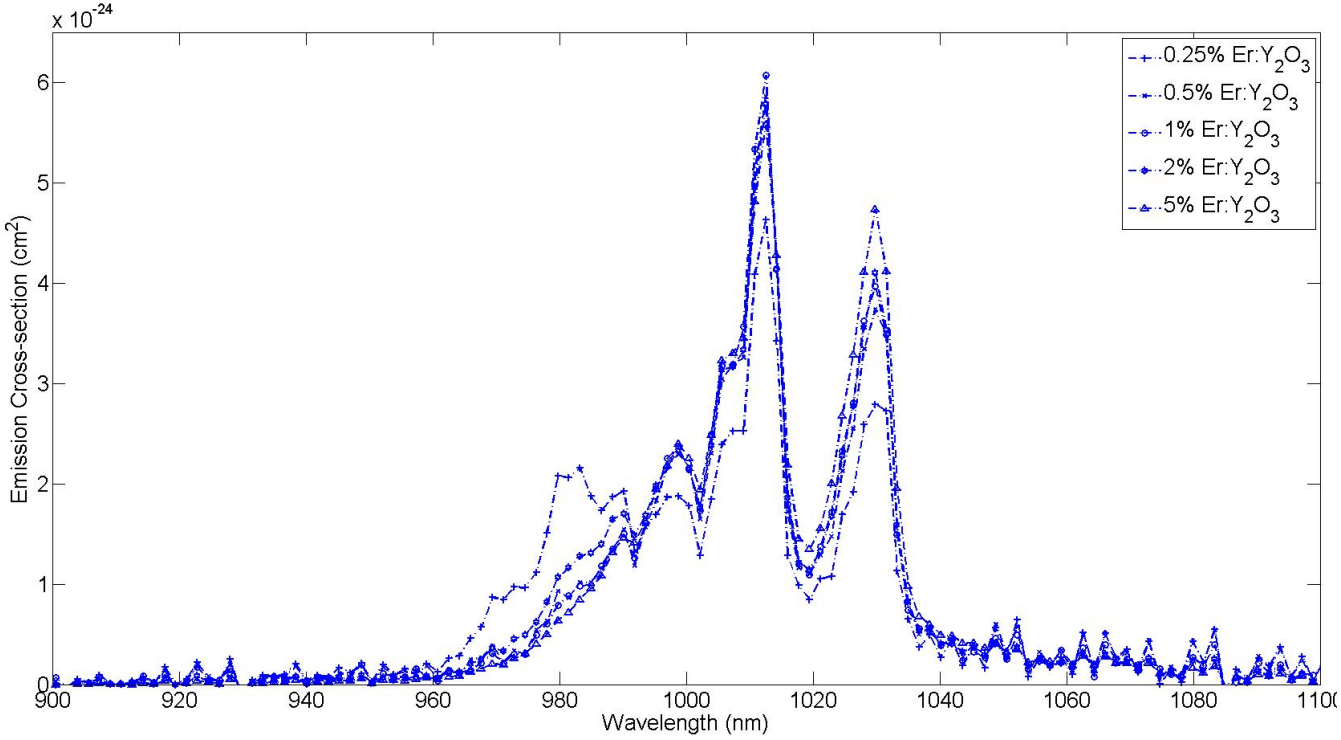

Figure 4.8: Emission Cross-sections for the $980nm$ band corresponding to $^4I_{11/2} \rightarrow {}^4I_{15/2}$ transition

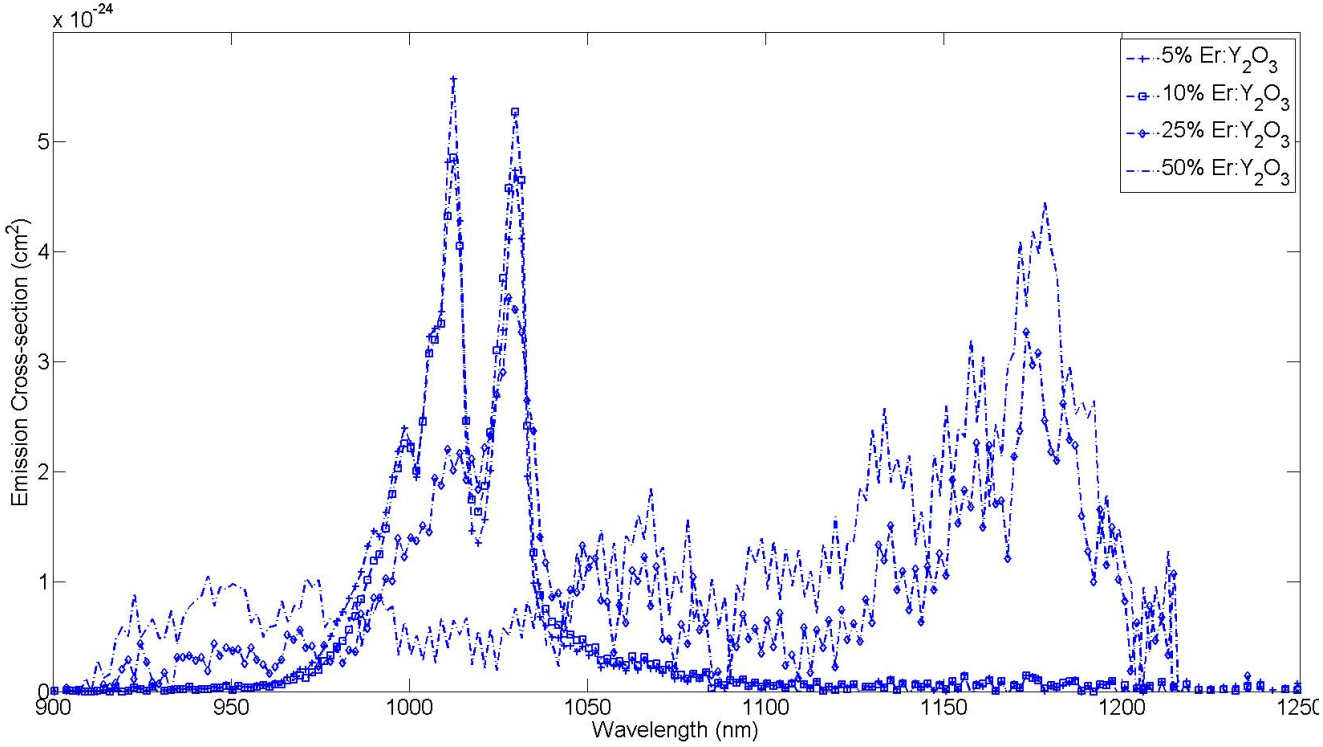

Figure 4.9: Emission Cross-sections for the $980nm$ band corresponding to $^4I_{11/2} \rightarrow {}^4I_{15/2}$ transition

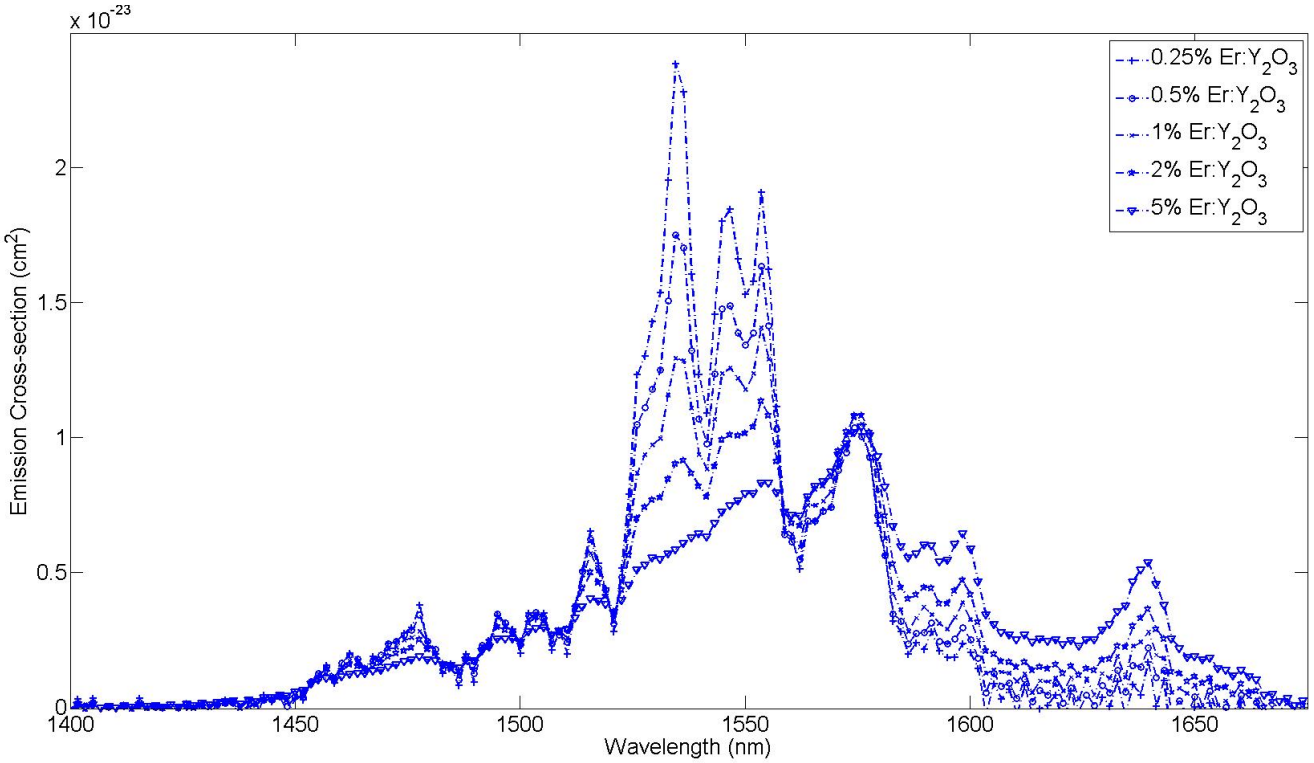

Figure 4.10: Emission Cross-sections for the $1550nm$ band corresponding to $^4\mathrm{I}_{13/2} \rightarrow {}^4\mathrm{I}_{15/2}$ transition

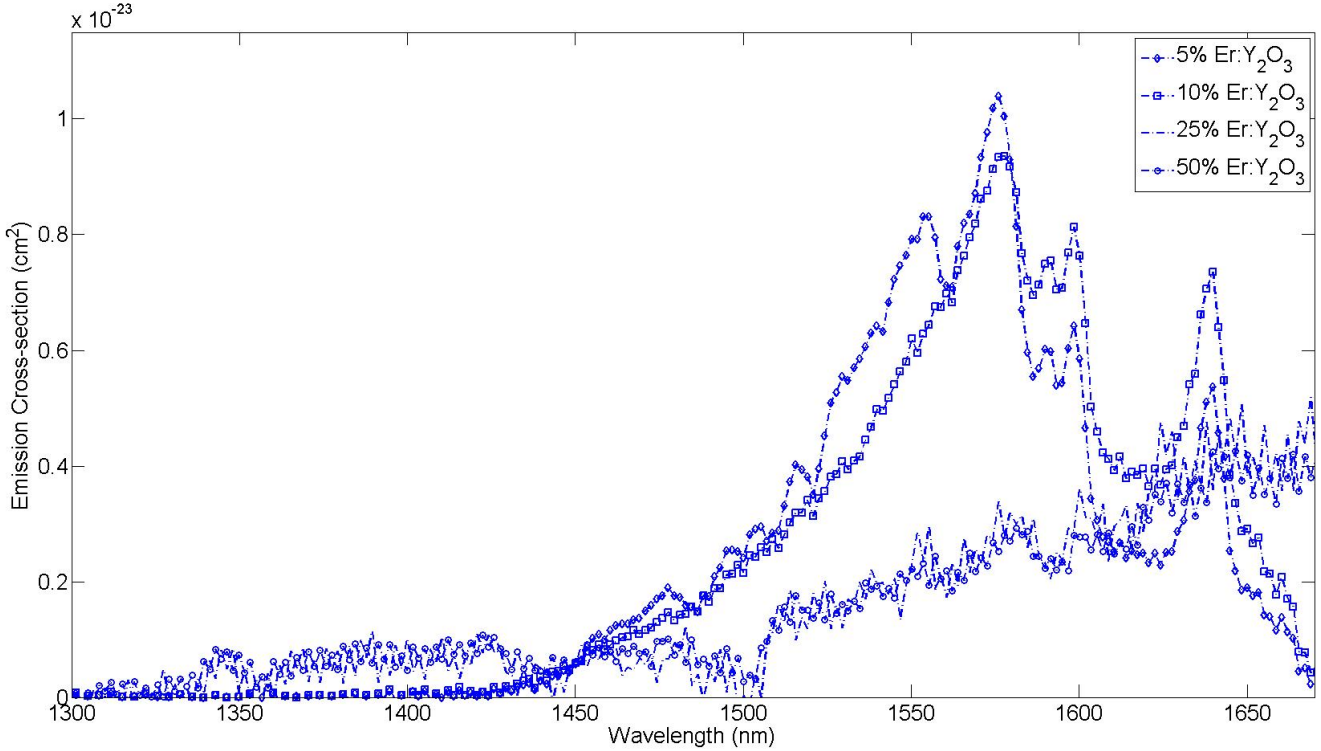

Figure 4.11: Emission Cross-sections for the $1550nm$ band corresponding to $^4\mathrm{I}_{13/2} \rightarrow {}^4\mathrm{I}_{15/2}$ transition

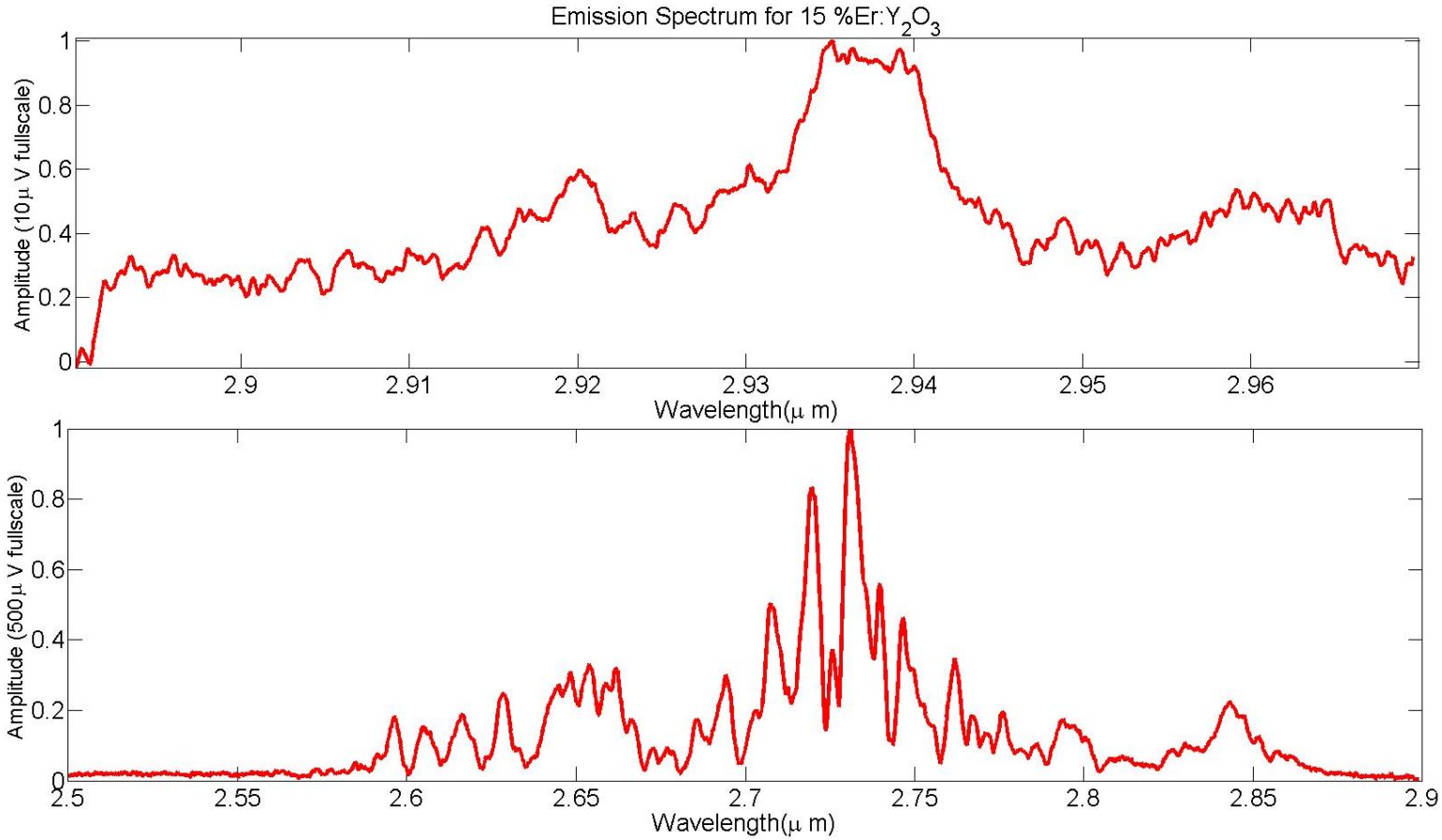

Figure 4.12: Mid IR Emission Spectra for $15\% Er : Y_2O_3$ ceramic. Pump wavelength was $\sim 0.97nm$

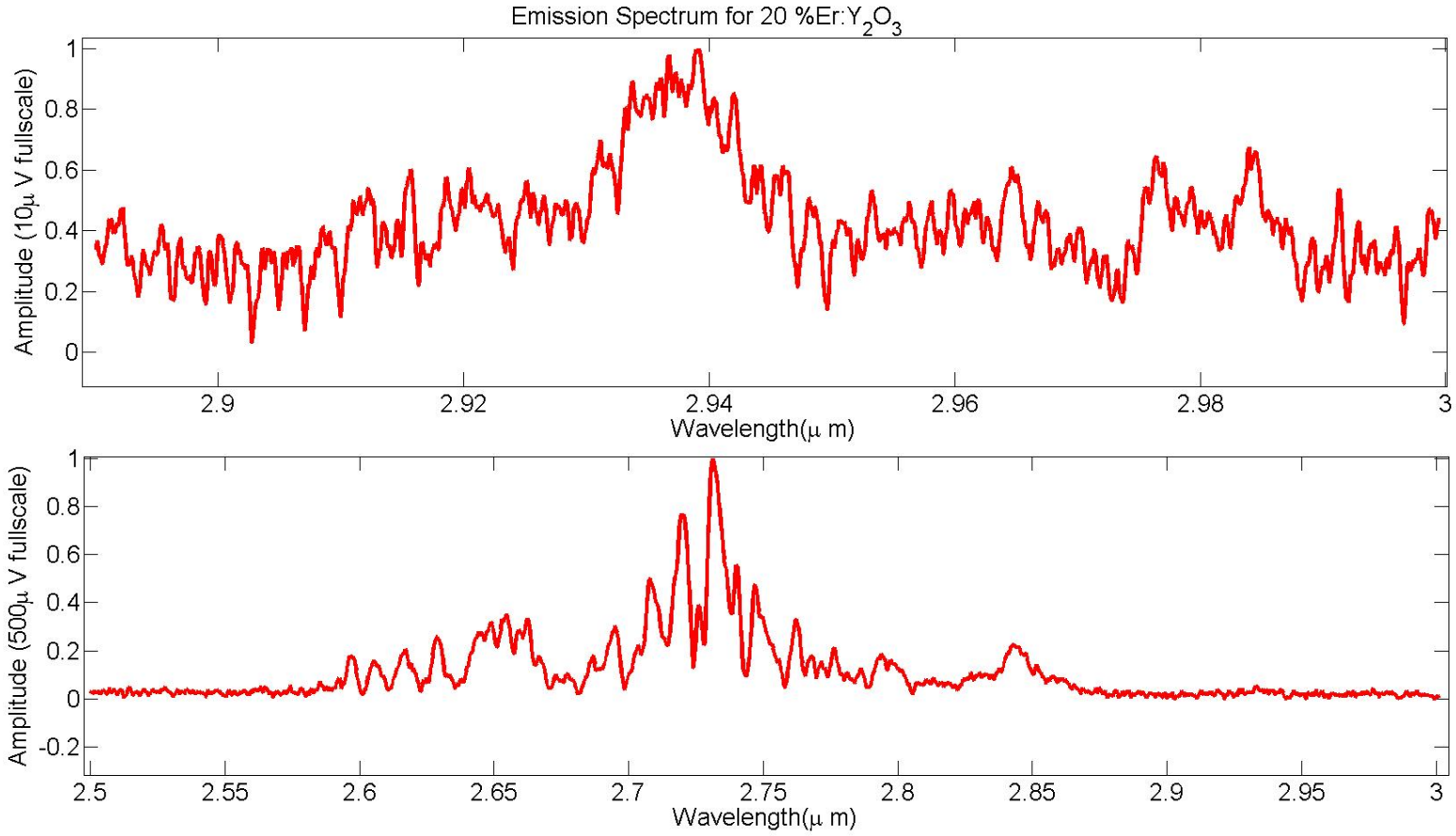

Figure 4.13: Mid IR Emission Spectra for $20\% Er : Y_2O_3$ ceramic. Pump wavelength was $\sim 0.97nm$

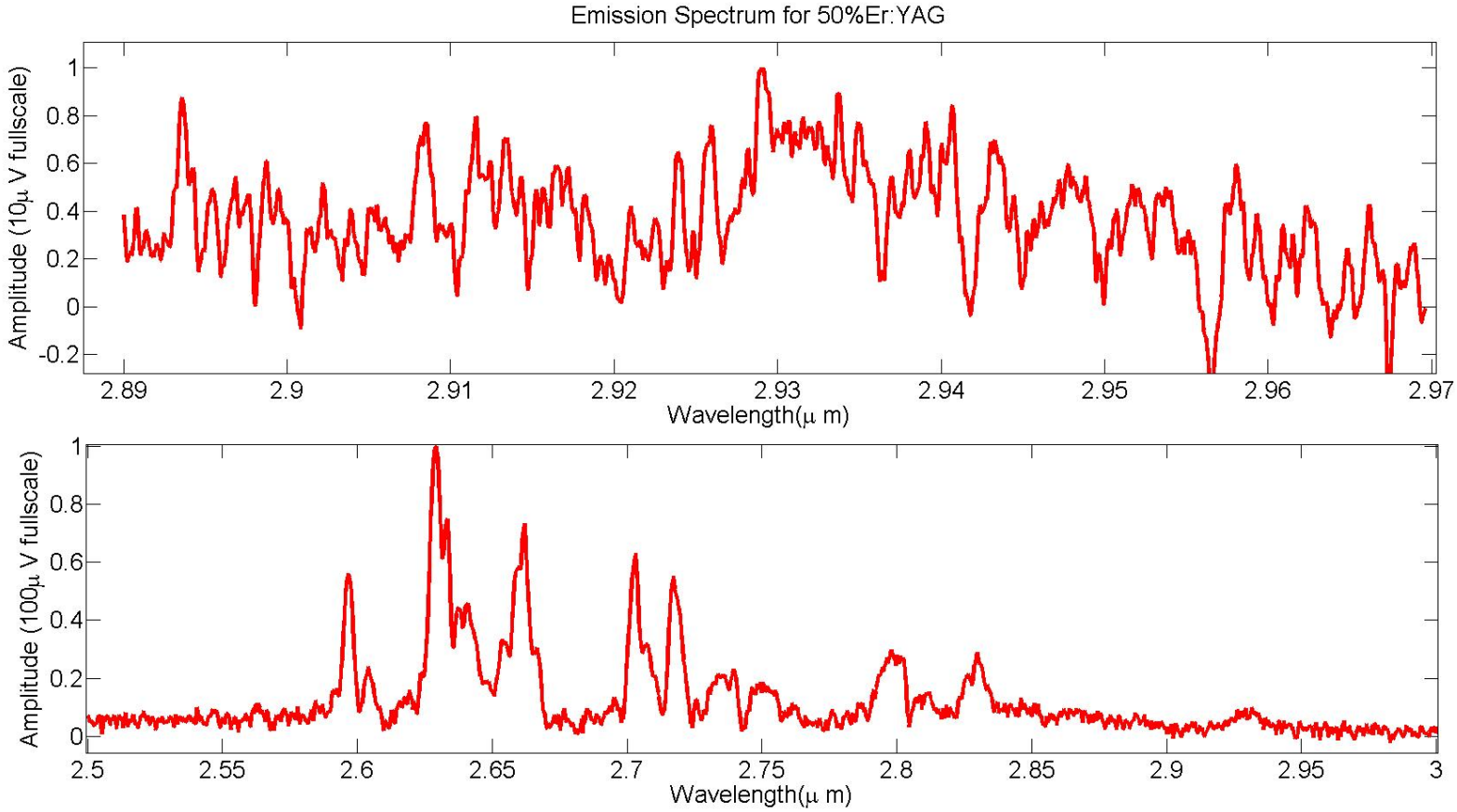

Figure 4.14: Mid IR Emission Spectra for industry standard $50\%Er:YAG$ single crystal system. Pump wavelength was $\sim 0.97nm$

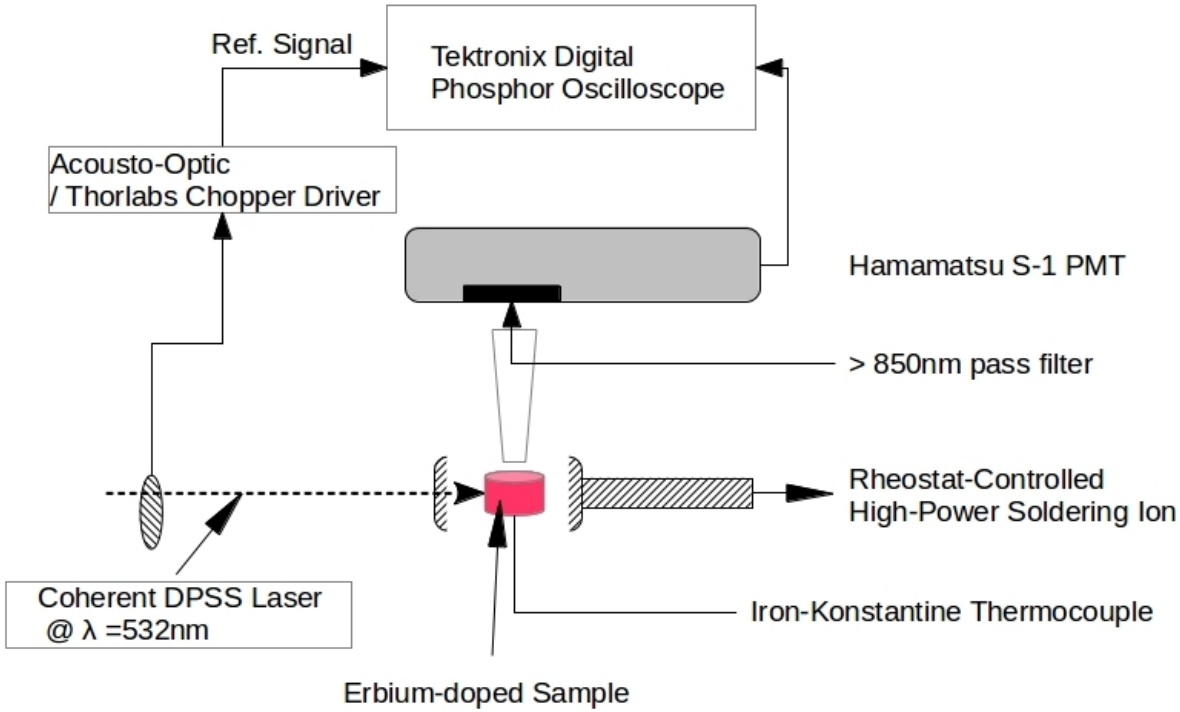

Figure 4.15: Experimental setup to measure the multiphonon rate as a function of temperature for the ${}^4I_{11/2} \rightarrow {}^4 I_{15/2}$ transition.

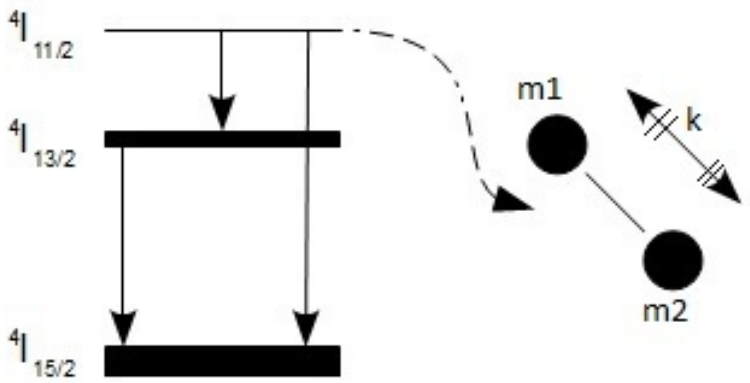

Figure 4.16: Pictorial representation if the active ion coupling to the host lattice

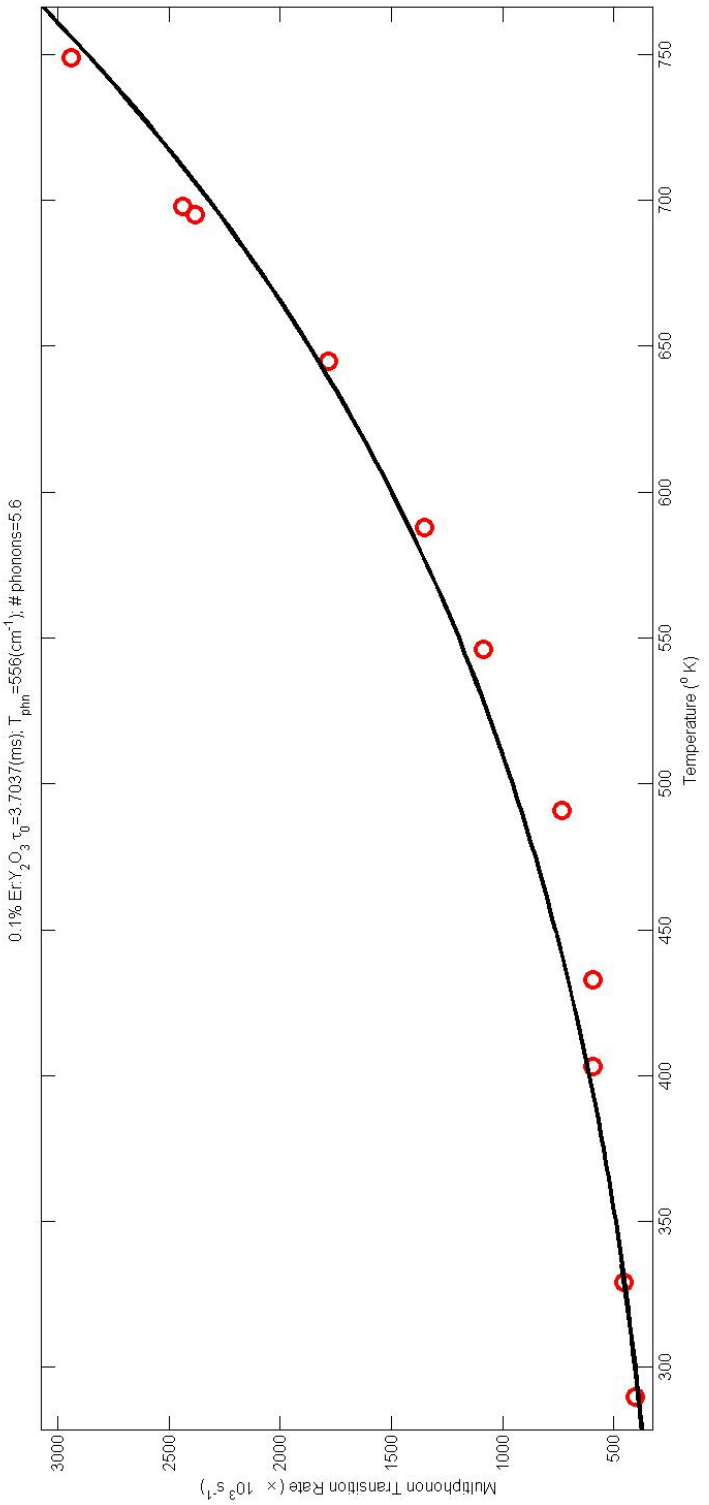

Figure 4.17: 0.1% at. wt. erbium in yttria.

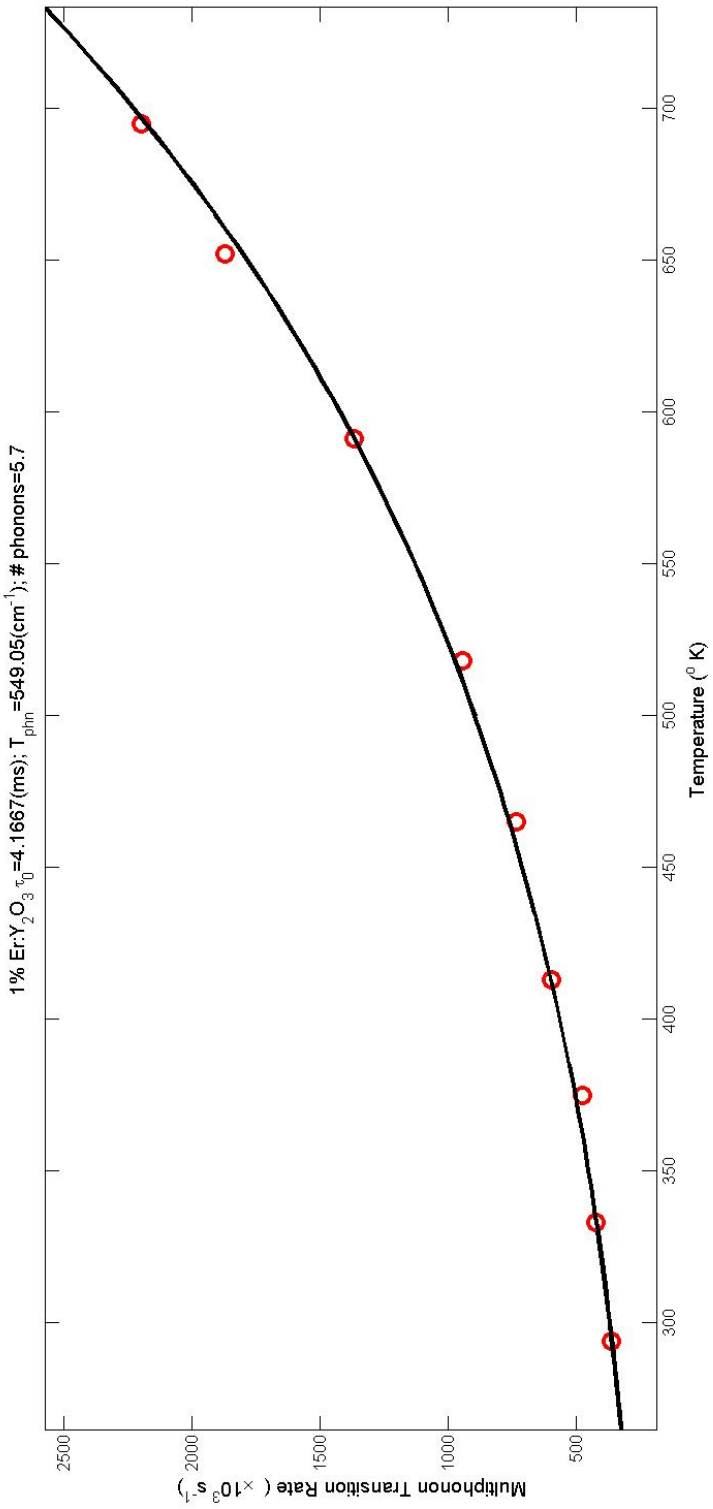

Figure 4.18: 1% at. wt. erbium in yttria.

Acknowledgments

We acknowledge the financial support provided by the Office of Naval Research under grant number N00014-09-0205.

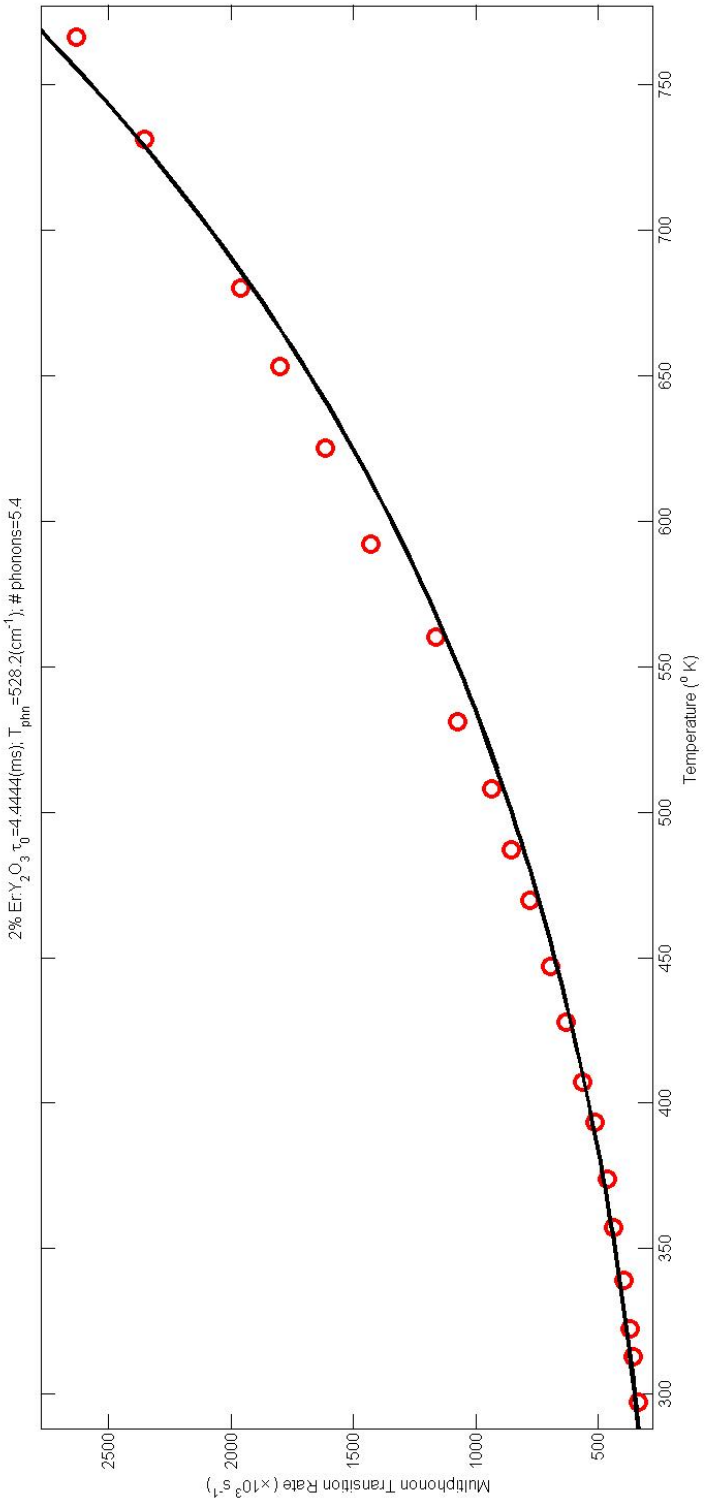

Figure 4.19: 2% at. wt. erbium in yttria.

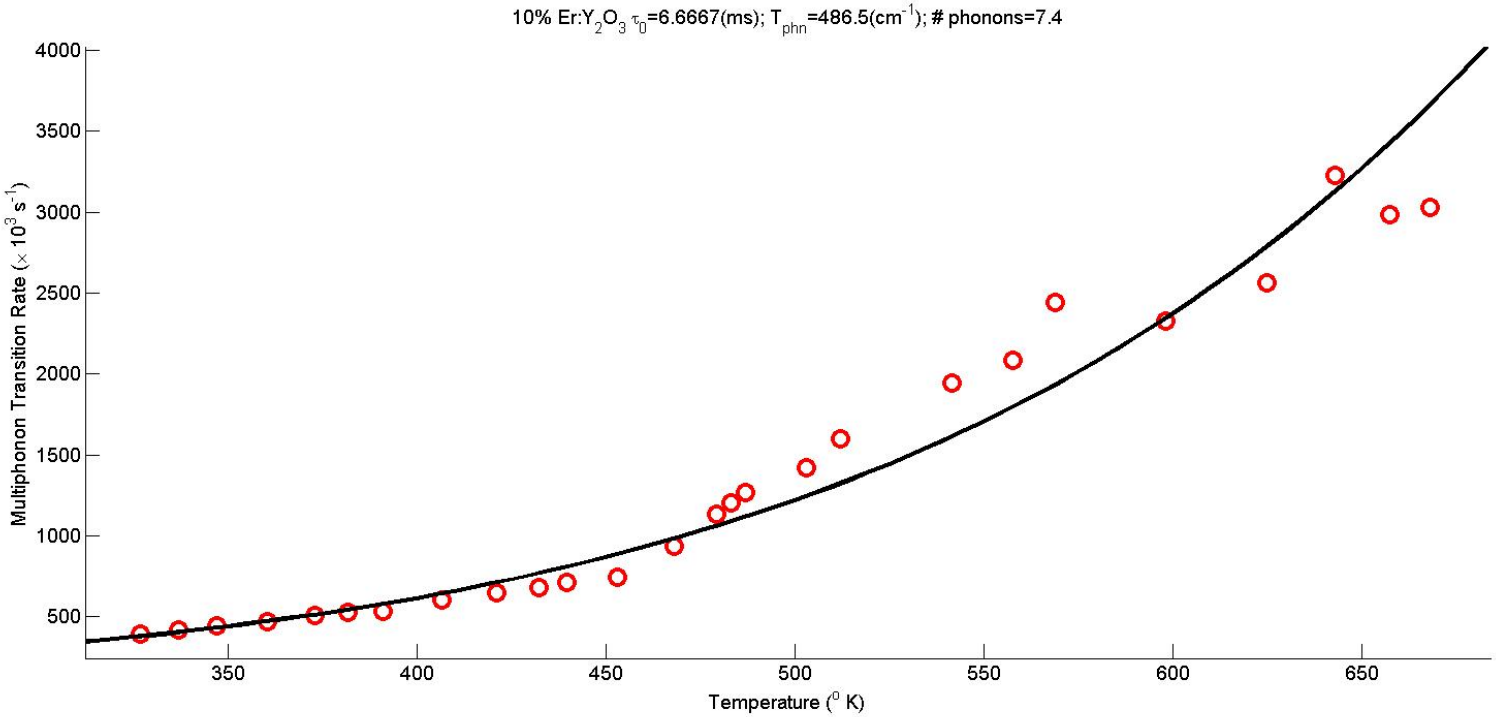

Figure 4.20: 10% at. wt. erbium in yttria.

References

[1] *Quantification and modeling of the dynamic changes in the absorption coefficient of water at λ = 2.94 μm*, R. K. Shori, A. A. Walston, O. M. Stafsudd, D. Fried, J.T. Walsh, Jr., IEEE Journal of Selected Topics in Quantum Electronics, Volume 7, Issue 6, pgs 959-970, Nov/Dec 2001.

[2] *Er:YAG Three-Micron Laser: Performances and Limits*, Serban Georgescu and Octavian Toma, IEEE Journal of Selected Topics in Quantum Electronics, Vol. 11, No. 3, May/June 2005.

[3] *Temperature-Dependent concentration quenching of Fluorescence by cross-relaxation of Nd^{3+}:LaF_3*,C. K. Asawa and C. K. Robinson, Physical Review, Vol. 141, Issue 1, January 1966.

[4] *Codoped Erbium Laser Crystals*, Mario Furtado, PhD Thesis submitted at the University of California, Los Angeles, 2005.

[5] *Stimulated emission from Er^{3+} ions in yttrium aluminum garnet crystals at $\lambda = 2.94\mu m$*, Evgeny V Zharikov, V I Zhekov, L A Kulevskii, T M Murina, Vyacheslav V Osiko, A M Prokhorov, A D Savel'ev, Valery V Smirnov, B P Starikov and M I Timoshechkin. 1975 Sov. J. Quantum Electron. 4 1039-1040.

[6] *Monograph in Paramagnetic Resonance*, A. Kiel, ed. W. Low, Academic Press Inc. New York, pg. 525, 1963.

[7] *Multiphonon Orbit-Lattice Relaxation of Excited States of Rare Earth Ions in Crystals*, L. A. Riseberg, H. W. Moos, Physical Review, vol.174, no.2, 1968.

[8] *Spectroscopic Relaxation Processes of Rare Earth Ions in Crystals*, H. Warren Moos, Journal of Luminescence, 106-121, 1970.

[9] *Correlation between luminescent properties and local coordination environment for erbium dopant in yttrium oxide nanotubes*, Y. Mao, J. Bargar, M. Toney, J. P. Chang, Journal of Applied Physics, vol. 103, 094316, (2008).

[10] *Radiative and Multiphonon Relaxation of Rare-Earth Ions in Y_2O_3*, M. J. Weber, The Physical Review, Second Series, vol. 171, No. 2.

CHAPTER 5

Judd-Ofelt Analysis

The work by Judd [1] and Ofelt [2] introduced a phenomenological approach to treating the *f-f* transition in rare-earth ions is almost 50 years old; it still forms a central piece in the study of any new laser gain medium.

The absorption spectra of concentration dependent of the ceramic material will be analyzed and the *Judd-Ofelt* parameters for the ion:host system will be provided. These intensity parameters may be used to calculate the probability of transitions between any ^4f_n levels of interest for potential laser applications. Important laser parameters may be obtained including absorption and fluorescence intensities, excited-state absorption, radiative lifetimes, quantum efficiency and branching ratios.

* This chapter was greatly benefitted by earlier work on the subject by Dr. W. R. Cochran titled *Erbium in Yttria* [3]. These were internal documents.

5.1 Introduction

J. H. van Vleck first presented the *rare-earth puzzle* in 1937 [4], some two decades before rare-earth ion lasers were made. It was well known that salts of rare-earth showed sharp lines at locations which could only correspond to transitions between the 4f energy-levels. But such transition were *forbidden* by LaPorte's selection rule which states that the algebraic sum of the angular momentum of the

Transition Mechanism	Transition Frequency sec^{-1} (approximate)
Electric-Dipole	1.3×10^8 (for the visible transition in Ce^{3+})
Quadrupole transition	~ 4 (for a $4f \rightarrow 4f$ transition)
Magnetic Dipole	~ 2

Table 5.1: Transition frequencies [4]

electrons in the initial and final state must change by an odd integer for electric dipole transitions (transitions between opposite parity, $\Delta\Sigma_i l_i$ is odd). The transitions are not forbidden for magnetic dipole or electric quadrupole transitions, but then we expect these intensities to be low compared to an electric dipole transition. The magnetic dipole and electric quadrupole transitions exist even in free atoms, *i.e.* in gas phase. For the electric dipole transitions to exist one requires that the ion be subjected to substantial crystal-fields (*i.e.* the effect of the surrounding lattice on the active ion causing an asymmetry). It is also necessary that the field does not have a center of symmetry

The following table 5.1, gives the order of magnitude transition when the differing types of transition mechanisms are considered.

A more extensive list of frequencies is given in [4]; the author evaluates distortion by the crystal field, naturally asymmetric fields and vibrational effects. They are all smaller than the noted transition frequencies.

At the time the experimentally recorded transitions were in the order of a $100 sec^{-1}$ for neodymium and praseodymium.

It took another quarter century before group theoretical foundations were built by Racah(*circa* 1940's) for treating the *rare-earth puzzle*. The advent of computers also contributed to the solution which was put forth simultaneously and independently by B. R. Judd (UC Berkeley) [1] and G. S. Ofelt (John Hopkins University)[2].

5.2 Judd-Ofelt Theory : Principles

The theory provided by Judd and Ofelt is based on the static, free-ion and single configuration approximations. In the static model, the central ion is affected by the surrounding host ions via a static electric field, referred to as the ligand or crystal field. In the free-ion model, the host environment produces the static crystal field, and is treated as a perturbation on the free-ion Hamiltonian. Such that,

$H = H_{free-ion} + V_{crystal-field}$. The $V_{crystal-field}$ introduces the effect of the surrounding host's field.

In the single configuration model, the interaction of electrons between configurations is neglected [10].

$$V_{crystal-field} = \sum_{k,q} \sum_{i} r_i^k Y_{k,q}(\theta_i, \varphi_i) \tag{5.1}$$

Above, the summation over i is above all electrons of the ions of interest. $A_{k,q}$ are structural parameters in the static crystal field expansion, r is the radius and Y are spherical harmonics defined on a sphere. The strength of the formulation is it's direct comparison to experiments via calculation of oscillator strengths f_{ij} (for a transition between the i^{th} state and the j^{the} state).

The Judd-Ofelt formulation provides the following expression for the oscillator strength,

$$f_{ij} = \frac{8\pi m\nu c}{3h(2J+1)} \sum_{\lambda=2,4,6} \Omega_\lambda |\langle f^n[SL]J||U^{(\lambda)}||f^n[S'L']J'\rangle|^2. \tag{5.2}$$

where Ω_λ are the *Judd-Ofelt* parameters, which in practice must be estimated by a best fit of the line strength to the absorption spectra. They contain the radial integrals and crystal field potentials. The *3j* and *6j* symbols enter the calculation via λ (these are co-efficients that arise when considering the coupling of the angular momentum between two and three quantum mechanical systems). Also, m is the mass of the electron, c is the speed of light and ν is the frequency of the emitted photon.

Tabulations by Judd[5] and Kaminskii[6] give the values of the reduced matrix elements $|\langle f^n[SL]J||U^\lambda||f^n[s'L']J'\rangle|^2$. Further details may be found in [10].

The experimental determination of f_{ij} using absorption spectroscopy is based on the following:

$$f_{ij} = \frac{2300mc^2}{\pi e^2 N_A \lambda C L} \int_0^\infty log\left(\frac{I}{I_0}\right) d\lambda \tag{5.3}$$

where, N_A is Avogadro's number, λ is the wavelength, C is the molar concentration, L is the length of the interaction. The $\frac{I}{I_0}$ is the ratio of absorbed to incident intensity.

A comparison between equations (5.2) and (5.3) yields the Judd-Ofelt parameters (Ω_λ).

5.3 The Er^{3+}:Y_2O_3 system

Yttria crystallizes in a cubic bixbyte structure (see Figure 5.1). Y^{3+} lies at the center of the structure surrounded by 6 oxygen ions. The optically active ion Er^{3+} is a substitutional dopant and takes the place of a Y^{3+} ion. Table 9.1 summarizes the crystal structure and provides the coordination number for the erbium sites. As may be noted, there are two equivalent sites available for the erbium ion, the

Parameter	Property
Crystal Symmetry	body-centered cubic
Space Group	Ia3
Unit cell size	∼10.604 Å
Er^{3+} site symmetry	C_2, C_{3i}
Er^{3+}-Er^{3+} coordination	6@ 3.496 Å, 6@ 3.985 Å

Table 5.2: Properties of the Bixbyte Crystal Structure [8]

C_2 and C_{3i} sites (see Figure 5.2). Of which the C_2 site is optically active. Optical activity here is a function of the group symmetry, as stated above, and the C_2 is the only configuration without inversion symmetry (symmetry must be broken to allow electronic dipole transitions).

The following table (9.1) [8] summarizes the crystal structure of the Er^{3+} : Y_2O_3.

We have used new data to update the work provided in [3]. Newer, more accurate refractive indices and absorption data were used to recalculate the absorption oscillation strengths and the radiative transition rates and lifetimes for the ${}^4I_{11/2} \rightarrow^4 I_{15/2}$ ($\lambda \sim 1\mu m$), the ${}^4I_{13/2} \rightarrow^4 I_{15/2}$ ($\lambda \sim 1.55\mu m$), and the ${}^4I_{11/2} \rightarrow^4 I_{13/2}$ ($\lambda \sim 3\mu m$) transitions.

STATES	Transitions from $^4I_{15/2}$ to	$^4I_{13/2}$	$^4I_{11/2}$
2J+1	16	14	12
Energy (cm^{-1})		6520	10250
Wavelength (μm)		1.533742	0.97561
$(U^{(2)})^2$		0.0195	0.0282
$(U^{(4)})^2$		0.1173	0.0003
$(U^{(6)})^2$		1.4316	0.3953
$\Omega_2(\times 10^{-20} cm^2)$		4.59	4.59
$\Omega_4(\times 10^{-20} cm^2)$		1.21	1.21
$\Omega_6(\times 10^{-20} cm^2)$		0.48	0.48
Line Strength($\times 10^{-20} cm^2$)		0.918606	0.319545
n		1.88243	1.892957
Absorption Oscillator Strength ($\times 10^{-6}$)		0.734543	0.405209
Emission Oscillator Strength ($\times 10^{-6}$)		0.839478	0.540279
Radiative Transition Rate (s^{-1})		198.7895	129.3738
Sum of Rates		198.7895	253.1037
Radiative Lifetime (ms)		5.030446	3.95095
Branching Ratio		1	0.511149

Table 5.3: Calculated Er^{3+}:Y_2O_3 characteristics. Updated from [3].

Figure 5.1: The Y_2O_3 bixbyte structure from different perspectives [7]

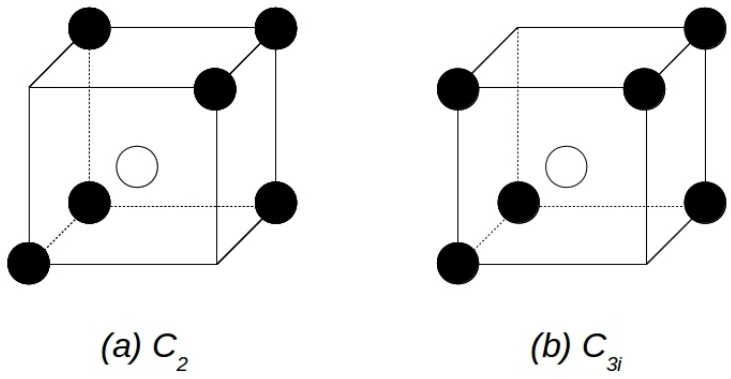

Figure 5.2: Site symmetries for the bixbyte structure. Solid spheres represent the oxygen ions while the hollow sphere are Y^{3+} or Er^{3+}.

References

[1] *Optical Absorption Intensities of Rare-Earth Ions*, B. R. Judd, Phys. Rev. 127, 750761 (1962).

[2] *Intensities of Crystal Spectra of Rare Earth Ions*, G. S. Ofelt, J. Chem. Phys. 37, 511 (1962).

[3] *Erbium in Yttria*, W. R. Cochran, Internal Communications (2010).

[4] *The Puzzle of Rare-earth Spectra in Solids*, J. H. Van Vleck, J. Phys. Chem., 1937, 41 (1), pgs 6780.

[5] *Matrix Elements of Tensor Operators for Configurations of Three Equivalent Electrons*, B. R. Judd, Proceedings Royal Society, A250, 562 (1959).

[6] *Crystalline Lasers*, A. A. Kaminskii, CRC Press (1996).

[7] http://cst-www.nrl.navy.mil/lattice/struk/d5_3.html, Retrieved 2^{nd}August 2012.

[8] *Er coordination in Y_2O_3 thin films studied by extended x-ray absorption fine structure* Trinh Tu Van, John R. Bargar, and Jane P. Chang, Journal of applied physics (2006) Vol. 100 Issue. 2 pg. 023115.

[9] *Correlation between luminescent properties and local coordination environment for erbium dopant in yttrium oxide nanotubes*, Y. Mao, J. Bargar, M. Toney, J. P. Chang, Journal of Applied Physics, vol. 103, 094316, (2008).

[10] *Judd-Ofelt theory: principles and practices*, Brian Walsh, ed. di Bartolo and O. Forte, Advances in Spectroscopy for Lasers and Sensing 2006, Part 1, pgs. 403-433.

CHAPTER 6

Multiphonon-based comparison of erbium-doped yttria in large, fine grain polycrystalline ceramics and precursor forms

We have studied the phonon-induced non-radiative decay in erbium doped yttria (Y_2O_3). The technique employed allows for the evaluation of potential ceramic and crystalline laser materials. The frequency of the dominant phonon that deactivates the fluorescing levels and an approximate prediction of $0K$ lifetime can be determined. Results show no significant quantitative difference between very large grain polycrystalline (with grain size $\sim 200\mu m - 500\mu m$) ceramic, fine grain polycrystalline (with grain size $\sim 0.3\mu m$) ceramic and the precursor powder (with $\sim 30nm$ particle size) of Er^{3+} doped Y_2O_3, when it comes to the dominant phonon frequency and the phonon occupancy number.

The results show that a correct evaluation of the final product can be made in the precursor stage of the process eliminating the need to proceed to crystalline or fully sintered ceramic form to evaluate the spectroscopic properties of the material. It should be noted that the powders must be carefully prepared and handled. Adsorbed species such as water can drastically change the effective lifetimes observed in powders samples.

6.1 Introduction

Crystals large enough to design high powered solid state laser systems are not easily made. Single crystal solid state media also have stringent limitations on their opto-mechanical, thermal properties and general mechanical robustness. This has given impetus to the development of ceramic solid state laser media. Ceramics are expected to have lower processing and fabricating temperatures and the ability to custom design multi-functional laser gain media. This would include spatially non-uniform doping and the mechanical advantages of ceramic media such as a lack of cleavage planes and enhanced toughness due to granular microstructure. Ceramics are also expected to have the simpler stress-optic behavior of amorphous media as compared to single crystal versions of the same compounds.

It is an expensive and time-consuming proposition to create crystalline or fully sintered ceramics in order to evaluate them for use as insulating laser hosts. We provide evidence that there is a clear and simple method to evaluate the properties of such hosts for laser applications while they are in the powder form before further processing.

Quantification of the non-radiative component of the excited state decay is especially of importance. Along with two-ion energy (cross-relaxation, impurity quenching, etc.) transfer processes, phonon de-excitation is the most significant mechanism of loss of energy in excited solid state systems. It is also the limiting quenching process that reduces radiative efficiency. Theories have been proposed to understand two ion interaction (Foerster [1] and Dexter [2]), *i.e.* , quenching, energy transfer and up-conversion. In lightly-doped high purity samples such interactions are not expected because they require the ions to be physically close to each other. However, non-radiative emission can be experimentally studied using

the multiphonon relaxation theory first developed by Kiel [3] and subsequently extended by Riseberg and Moos [4], [5].

We use the general formulation by Riseberg and Moos for calculating the probability of multiphonon non-radiative transitions between the Stark groups (J multiplets) of the ${}^4I_N$ states of trivalent erbium ions in hosts. The fluorescence decay rate of a level is then the sum of the radiative decay and multiphonon relaxation rates. These rates are determined primarily by the order of the process and the strength of the interaction. In the multiphonon decay theory, one assumes the emission of p_i equal energy phonons corresponding to the i^{th} phonon mode. The population of the modes occurs due to thermal excitation. The rate of decay of excited atoms due to both radiative and non-radiative effects (Ω) can be given by,

$$\Omega(T) = \Omega_0(n_i + 1)^{p_i} \tag{6.1}$$

where n_i is the average phonon occupancy number given by the Bose-Einstein formula,

$$n_i = \frac{1}{e^{\frac{E_p}{kT}} - 1} \tag{6.2}$$

Here, E_p is the characteristic phonon energy of the host matrix, k is Boltzmann's constant and T is the temperature in Kelvin. Combining the above formulae one obtains,

$$\Omega(T) = \Omega_0 \left(\frac{e^{\frac{E_p}{kT}}}{e^{\frac{E_p}{kT}} - 1} \right)^{p_i} \tag{6.3}$$

It is evident that as $T \rightarrow 0K$ we should get the radiative transition rate corresponding to the Einstein *"A"* coefficient.

6.2 Sample Preparation

In the present study, 1 at. % erbium-doped yttria powders were prepared by co-precipitation with ammonium hydroxide. A 0.25 mol/L of erbium-doped yttrium nitrate solution was prepared by dissolving yttrium nitrate hexahydrate (99.9%, Arcos Organics) and erbium nitrate pentahydrate (99.9% Arcos Organics) in ultrapure water. A 5 mol% of ammonium sulfate (99.99%, Sigma Aldrich) was added to the nitrate solution and then a 2.0 mol/L of ammonium hydroxide solution (certified ACS plus, Fisher Scientific) was added drop-wise in order to precipitate a yttrium nitrate precursor. The precipitate was aged for 3 hrs at room temperature and washed several times with water to remove the residual reactants. After the final washing, the precipitate was dried at $333K$ overnight under vacuum. The dried precursors were calcined at $1323K$ for 4 hrs under oxygen, flowing at 3 L/min, to yield erbium-doped yttria powders. The polycrystalline erbium-doped yttria transparent ceramics were obtained by sintering compacts of erbium-doped yttria powders using a modified two-step sintering approach as reported elsewhere [6]. The powders were uniaxially pressed into pellets at 15MPa followed by cold isostatical pressing at 200MPa. The pellets were heated to $1773K$, and then cooled down to $1673K$ and held at $1673K$ for 20 hrs to obtain dense opaque ceramics. The opaque ceramics became transparent with average grain size of $0.3\mu m$ after hot isostatic pressing at $1573K$ under an argon pressure of 20MPa for 3 hrs.

Large grain-sized ceramics were prepared using a more conventional sintering process whereby samples were heated to $2273K$ for 6 hrs under a vacuum of less

than 10^{-3}Pa.

The sintered powders were subjected to FTIR characterization, results indicate the vibrational features from molecular water, free hydroxyl groups, NO_3^-, SO_4^- are no longer present on calcination at $1323K$ [6].

6.3 Experimental Results

We present the evaluation and comparison of multiphonon characteristics of three different forms of the same material, erbium (1 $at.\%$) doped yttria, the precursor powder annealed at $\sim 1300K$, fine grain polycrystalline ceramic with grain sizes around $0.3\mu m$ and very large grain polycrystalline ceramic with grain sizes in the $200\mu m - 500\mu m$ range. The lifetimes of various levels are studied as a function of temperature and the data was fit using the multi-phonon decay theory, yielding the characteristic phonon energy and the non-radiative component of the decay of excited states. Y_2O_3 occurs in the bixbyte structure, in which there are two sites that can be occupied by the trivalent ions of C_2 and C_{3i} symmetry. Only the C_2 site is optically active for rare earth dopants.

Weber, in 1968, [7] studied the multiphonon characteristics of the rare-earth ions doped in crystalline Y_2O_3. In the study it was noted that, as a function of temperature, the fluorescence lifetime of the $^4I_{11/2}$ (to $^4I_{15/2}$) state degrades from $3900 \pm 400\mu s$ at $77K$ to $\sim 900\mu s$ at $600K$ for a $0.2\% Er^{3+}$ doped yttria sample.

We have measured the temperature dependence of the same state in the three different forms and found that in the precursor powders the lifetimes drop from $1930 \pm 16\mu s$ at room temperature to $570 \pm 23\mu s$ at 600K. The lifetimes in the fine grain polycrystalline ceramic form drop from $3150 \pm 9\mu s$ at room temperature to $\sim 750 \pm 75\mu s$ at $600K$. The lifetime in the large grain polycrystalline $Er^{3+} : Y_2O_3$

form decreases from $2860 \pm 11\mu s$ to $650 \pm 2\mu s$ in the vicinity of $575K$.

It should be noted that the simple multiphonon model yields a $0K$ lifetime for both the ceramic and crystalline forms within the admittedly large error range from Weber's calculations. Using Judd-Ofelt analysis Weber reported a value of $\sim 6810 \pm 2470\mu s$.

Parameter fitting on the data yields results as shown in Table 7.1. A non-integer phonon occupancy number implies the existence of the combination of the two closest integer occupancy numbers. Strictly, the multiphonon theory applies only to integer phonon occupancies. The plots of fluorescence rates versus temperature is given in figure (6.1). Figure (6.2) shows a representative semi-log plot of fluorescence rate versus temperature. This plot is quasi-linear as expected.

The energy difference between the ${}^4I_{13/2}$ and the ground state ${}^4I_{15/2}$ is approximately $6600cm^{-1}$, and expectedly no phonon-assisted decay was found in the samples up to a temperature of $\sim 900K$.

6.4 Effect of Hydration on Precursor Powders

Great care must be exercised in the handling and measurement of the precursor powder samples. Freshly calcined powders show lifetimes at room temperature of approximately $2ms$, quite similar to bulk ceramic and crystalline samples. Powders that have been exposed lightly to moist atmosphere, a few days at a relative humidity of about 30%, show reduced $\sim 300K$ lifetimes in the range of $\sim 0.7 - 1.2ms$. Powders exposed to small amounts of liquid water have reduced lifetimes as low as $80\mu s$. The exposed powders do continue to predict the phonon energy but not the correct Ω_0. Figure (6.3) shows the measured fluorescence

Table 6.1: Multiphonon Experimental Results

Sample	E_p Phonon energy (cm^{-1})	n_i phonon occupancy	$\tau(0K)$(ms) from eqn. (7.1)	$\tau(\sim 290K)(ms)$
$1\%Er : Y_2O_3$ precursor powder	549 ± 14	5.8 ± 0.2	3.51	$1.93 \pm 16\mu s$
$1\%Er : Y_2O_3$ fine grain polycrystalline	549 ± 3.5	5.4 ± 0.05	4.55	$3.15 \pm 9\mu s$
$1\%Er : Y_2O_3$ large grain polycrystalline	549 ± 3.5	6.0 ± 0.05	4.44	$2.86 \pm 11\mu s$

lifetime of a single powdered sample versus temperature the higher lifetimes correspond to the same sample after calcining at $1300K$ for at least 12 hours. The same sample after a few days of exposure to laboratory air *i.e.* 30% relative humidity and $300K$ degrades to the lower curve. Note repeated heating of the sample to $\sim 600K$ did not restore the original lifetimes. Recalcining for prolonged periods at $1300K$ was necessary to restore the samples to their original lifetimes.

6.5 Conclusion

We have shown that measurements of lifetime versus temperature of powdered precursors predicts the mean phonon frequency and the occupancy to $\pm 5\%$ in the large and fine grain polycrystalline ceramic forms. This implies that at the molecular level the three forms have an equivalent structure and coupling mechanisms. Carefully handled powders also predict the lifetimes at $0K$ within 25%. Despite the large number of defects expected in the powder samples they do predict the polycrystalline ceramic behavior.

The numbers corresponding to theoretically calculated purely radiative lifetimes of the ${}^4I_{11/2}$ state from Weber's Judd-Ofelt formulation, and the estimated radiative lifetimes from Moos and Riseberg's multiphonon formulation are in agreement.

Acknowledgments

This work was made possible by the generous support of the US Air Force Office of Scientific Research under grant number FA 9550-07-1-0566.

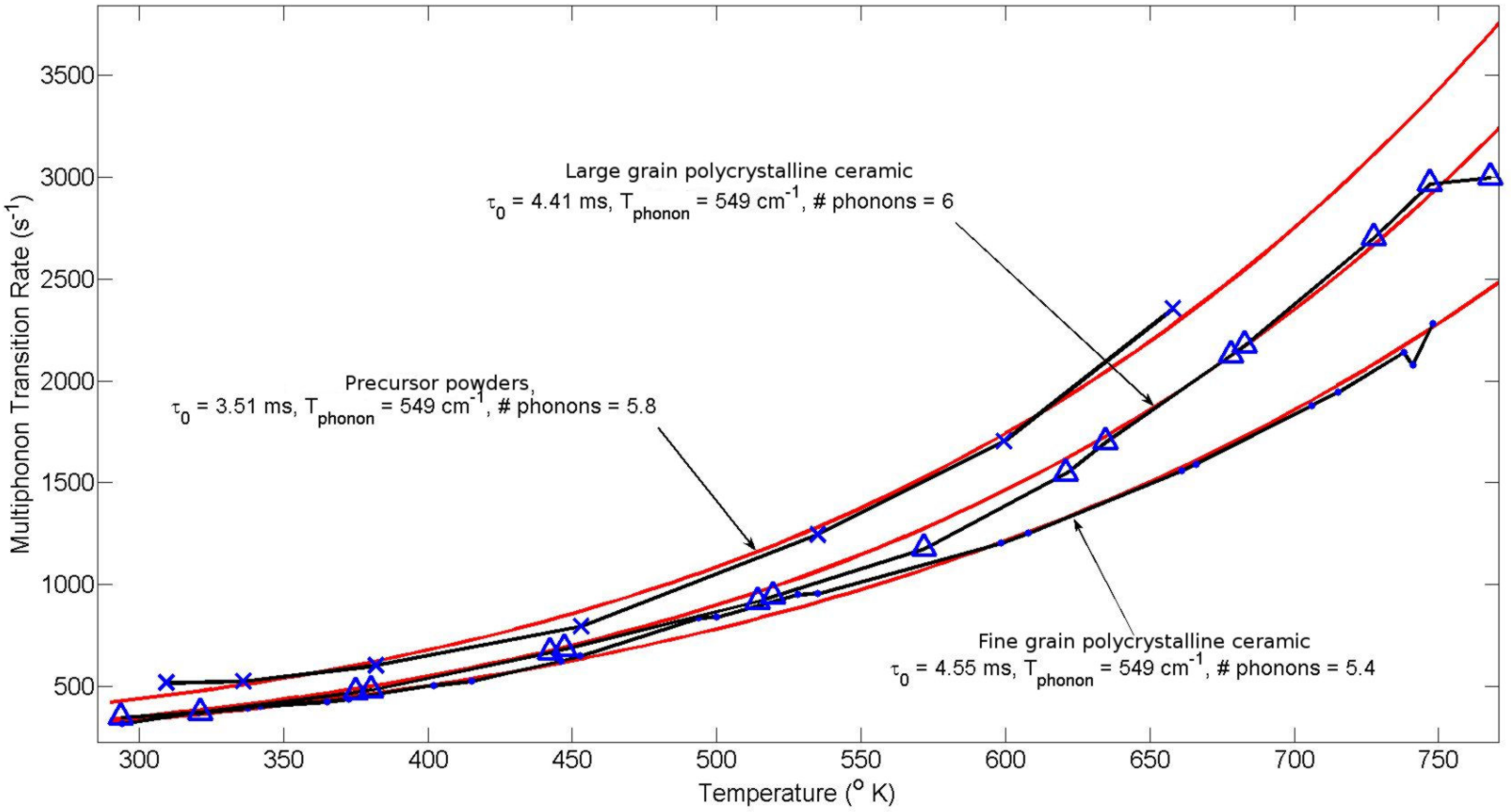

Figure 6.1: Data and multiphonon fit for $1\% Er : Y_2O_3$ in various forms.

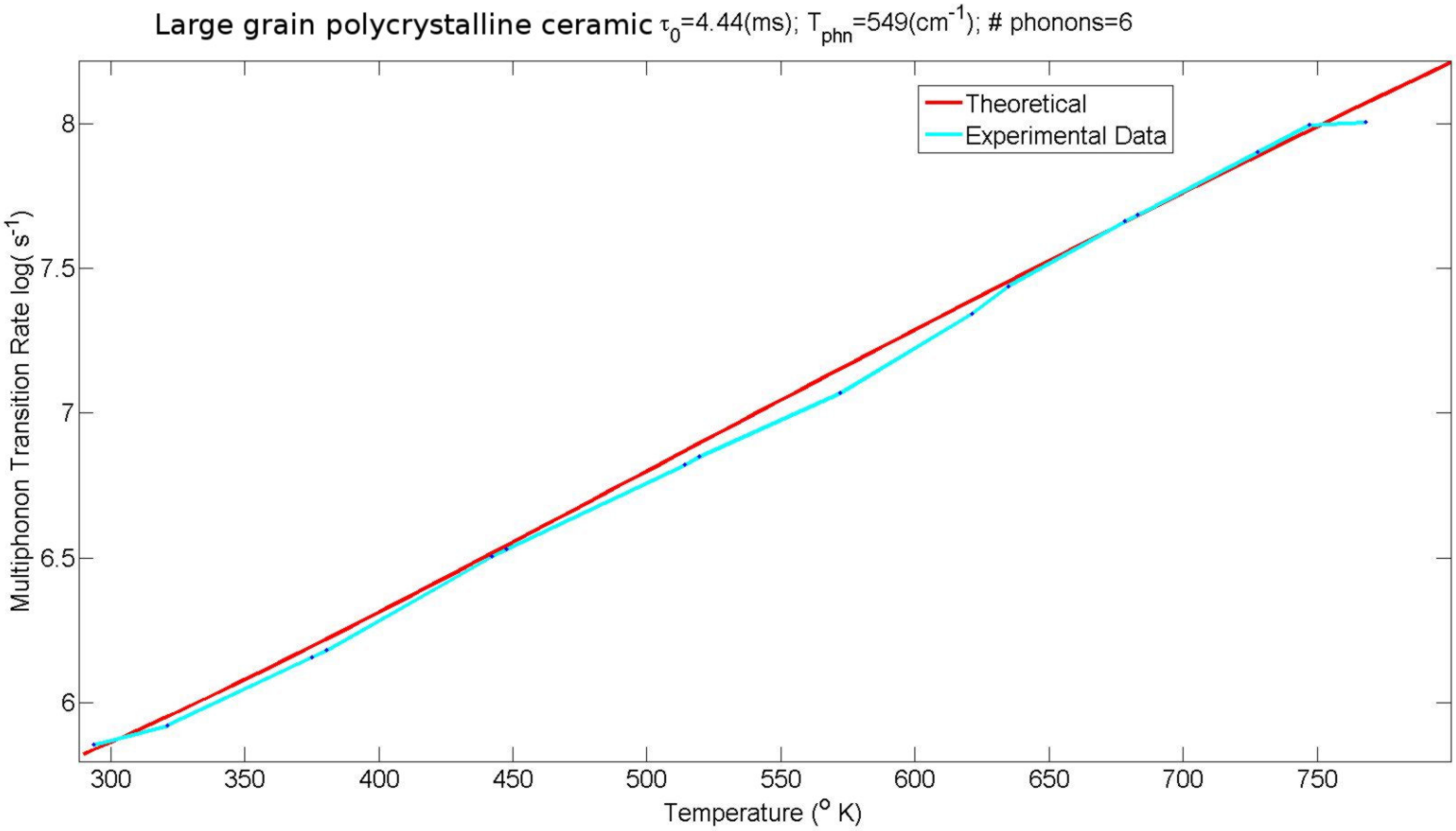

Figure 6.2: Data and multiphonon fit for large grain polycrystalline $1\% Er : Y_2O_3$ in ceramic form. The semi-log fit shows a quasi-linear behavior.

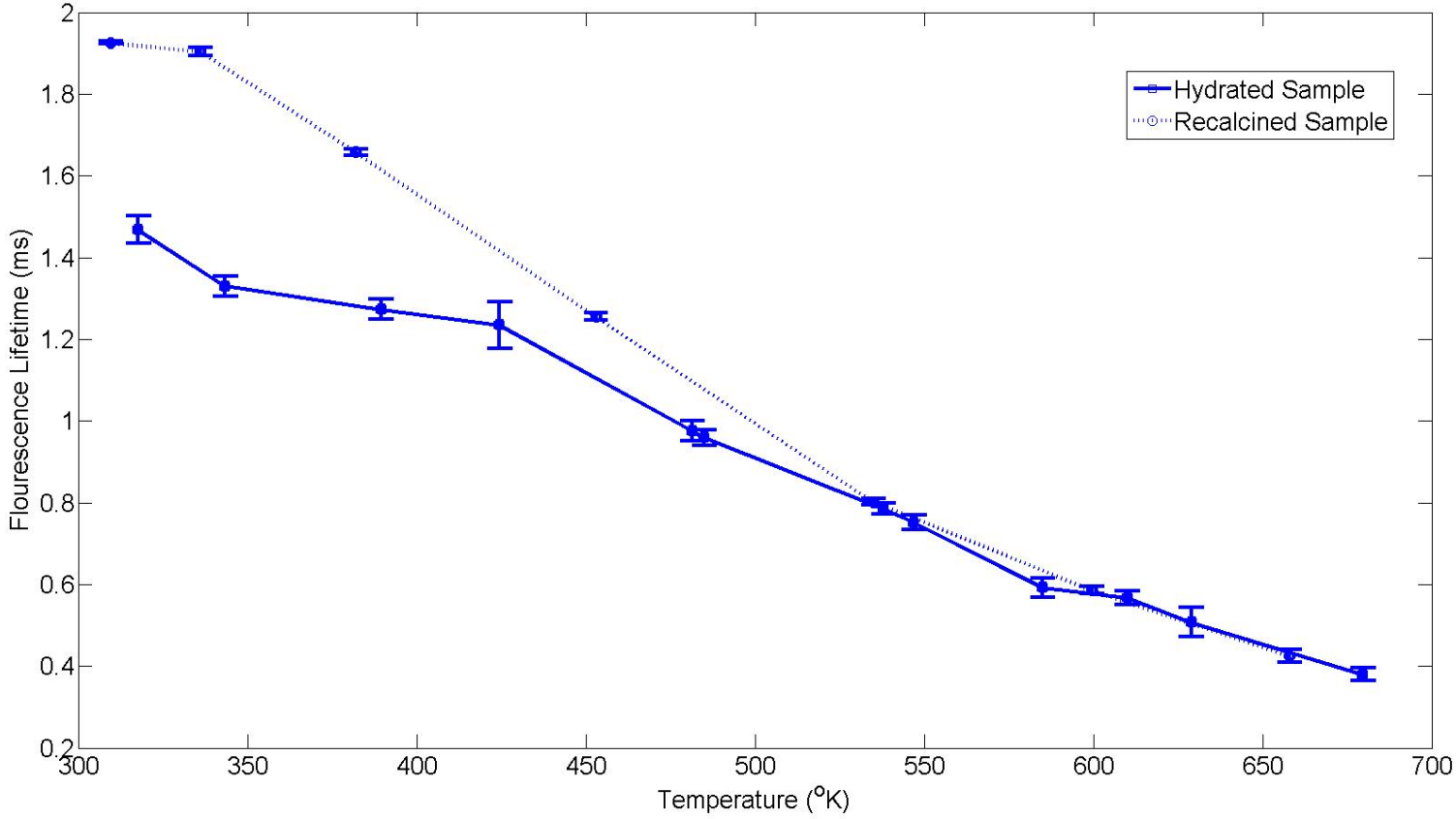

Figure 6.3: Effect of hydration on fluorescence lifetime of $1\% Er : Y_2O_3$ nanocrystalline powders.

References

[1] Th. Foerster, "Zwischenmolekulare Energiewanderung und Fluoreszenz", Annalen der Physik, vol. 437, no. 1-2, pg. 55, 1948.

[2] D. L. Dexter, "A Theory of Sensitized Luminescence in Solids", Journal of Chemical Physics, vol. 21, no. 836 (1953)

[3] A. Kiel,"Monograph in Paramagnetic Resonance", ed. W. Low, Academic Press Inc. New York, pg. 525, 1963.

[4] L. A. Riseberg, H. W. Moos, "Multiphonon Orbit-Lattice Relaxation of Excited States of Rare Earth Ions in Crystals", Physical Review, vol. 174, no.2, 1968.

[5] H. Warren Moos, "Spectroscopic Relaxation Processes of Rare Earth Ions in Crystals", Journal of Luminescence, pg. 106, 1970.

[6] K. Serivalsatit, B. Kokuoz, B. Y. Kokuoz, M. Kennedy and J. Ballato, "Synthesis, Processing, and Properties of Submicrometer-Grained Highly Transparent Yttria Ceramics" ,Journal of the American Ceramic Society, vol. 93, no. 5, pg. 1320, 2010.

[7] M. J. Weber, "Radiative and Multiphonon Relaxation of Rare-Earth Ions in Y_2O_3", The Physical Review, Second Series, vol. 171, no. 2, 1968.

CHAPTER 7

Multiphonon based comparison of the lifetimes of erbium in various oxide hosts

We present a multiphonon study of different insulating solid-state laser hosts doped with erbium in oxide ceramics. Temperature dependence of erbium doped (all 1% at.) yttria (Y_2O_3), lutetia (Lu_2O_3), scandia (Sc_2O_3), lutetium aluminum garnet ($LuAG$), yttrium aluminum garnet (YAG), yttrium gallium garnet ($YGaG$), gadolinium aluminum garnet ($GdGaG$) and, lutetium gallium garnet ($LuGaG$) were measured, and the results were evaluated using the multiphonon theory. The evaluation provides us with the radiative lifetime and characterizes thermal quenching of the excited ion. The transition from ${}^4I_{11/2} \rightarrow {}^4I_{15/2}$ was considered here, it is the upper energy-level for the technologically important $\sim 3\mu$m transition. The technique allows for the evaluation of potential ceramic and crystalline laser materials. The frequency of the dominant phonon that deactivates the fluorescing levels and an approximate prediction of radiative lifetime can be determined.

7.1 Introduction

Solid state lasers based on the Er^{3+} ion fill two important applications: lasers emitting in the $1.5 - 1.6\mu m$ range for eye-safe designators and communications

applications; lasers in the 'water-band' $2.6 - 3\mu m$ region have applications in medical, dental and materials processing fields.

Tuning a laser's emission wavelength can be achieved by changing the host matrix. Although the active ion largely maintains it's energy level structure (see Figure (1)) in various hosts, minor changes in emission wavelength point at slight variations of rare-earth energy levels amongst the hosts. These minor changes in the emission wavelength can, however, significantly affect the technological use of a dopant-host system. For example, the $Er^{3+}:YAG$ system lases at $2.936\mu m$ in the mid-IR region, overlapping with one of the vibrational modes in the water molecule, while the $Er^{3+}:Y_2O_3$ system has been shown to lase around $\sim 2.7\mu m$. The variation is typically small since the *f-orbitals* are well-shielded from the surrounding lattice ions.

There are also other metrics for choosing a suitable laser gain media for applications such as manufacturability, availability of high-powered pumps, efficient cavity design to accommodate the gain media, and other effects of varying pump powers such as thermal lensing in the system and thermal quenching. It is useful to compare various hosts directly to pick a material system targeted toward particular applications.

In this study we've compared a large variety of ceramic oxide hosts to evaluate the effect of normally encountered operating temperatures (300K $\leftrightarrow$ 700K) on lifetimes of the active ion dopant.

Crystals large enough to design high powered solid state laser systems are not easily made. Single crystal solid state media also have stringent limitations on their opto-mechanical, thermal properties and general mechanical robustness. This has given impetus to the development of ceramic solid state laser media. Ceramics are expected to have relatively low processing and fabricating temper-

atures and the added ability to custom design/engineer multi-functional laser gain media. This would include spatially non-uniform doping and the mechanical advantages of ceramic media such as a lack of cleavage planes and enhanced toughness due to granular microstructure. Ceramics are also expected to have the simpler stress-optic behavior of amorphous media as compared to single crystal versions of the same compounds.

We see these materials as an attempt to strike a balance between the current dominant types of insulating hosts - single-crystals and glass. On one hand there is extreme manufacturing complexity - as seen in the manufacture of large-volumes of single-crystal insulating hosts - and on the other there is the relative ease of manufacture, but relative lack of robustness when it comes to glass hosts. Nanocrystallite ceramic hosts hope to provide a golden mean between the two types.

Quantification of the non-radiative component of the excited state decay is especially of importance. Along with two-ion energy (cross-relaxation, impurity quenching, etc.) transfer processes, phonon de-excitation is the most significant mechanism of loss of energy in excited solid state systems. It is also the limiting quenching process that reduces radiative efficiency. Theories have been proposed to understand two-ion interaction notably by Foërster and Dexter, *e*tc that cover quenching, energy transfer and up-conversion [1], [2] and [3].

However, non-radiative emission can be experimentally studied using the multiphonon relaxation theory first developed by Kiel [4] and subsequently extended by Riseberg and Moos [5], [6].

We use the general formulation by Riseberg and Moos for calculating the probability of multiphonon non-radiative transitions between the Stark groups (J multiplets) of the ${}^4I_N$ states of trivalent erbium ions in hosts. The follow-

ing equation fully characterizes the temperature dependence of the multiphonon interaction;

$$\Omega(T) = \Omega_0 \left(\frac{e^{\frac{E_p}{kT}}}{e^{\frac{E_p}{kT}} - 1} \right)^{p_i} \tag{7.1}$$

Here Ω is the rate of decay, E_p is the energy of the non-radiative transition, while p_i is the order of the interaction involved in the interaction corresponding to the ith mode. Ω_0 is the rate of spontaneous emission (Ω_0=$\frac{1}{\tau_{sp}}$). A more complete description of the relation between the size of the multiphonon interaction, the order of the interaction and the effect on the decay rate of a level is provided in [9].

The theory of phonon-assisted non-radiative decay was proposed by Riseberg and Moos [5], [6] and developed by Bendow *et al* [7] assumes that the multiphonon decay is the dominant deactivation mechanism. Quenching of fluorescence via cross-relaxation, impurities or defects are ignored. If those effects are present then the temperature dependence of the fluorescent lifetimes will still yield the dominant phonon frequency (energy) and number, but the rates may not be useful. Non-phonon quenching effects can result in a τ_0 (radiative lifetime) that can be significantly shorter than the true value.

7.2 Sample Preparation

The motivation to consider ceramic oxides for the study was two-fold - the work is in aid of the study of ceramic oxides as potential solid-state laser hosts, and as a pure material-response study. These ceramics samples were manufactured using primarily wet chemistry methods first yielding nanocrystalline powders (similar to [8] or [9]).

The preparation method entails the creation of a small-grained, nanocrystalline powder of the precursor. The precursor is then isostatically pressed and baked/fired under pressure to create nanocrystalline powders that are further processed to create either optical quality or translucent samples.

The method results in a fundamentally different product as compared to single-crystal samples made from a melted precursor where the active ions have greater mobility and can relatively easily agglomerate creating ion clusters. In contrast, the precursor powders pressed as above have a large number of grain boundaries (for instance, *YAG* [8]) that impede the movement of the active ions, in this case erbium. The ion clusters that are commonly seen in single-crystals can have adverse effects like cross-relaxation and quenching of the inverted population causing loss of signal.

Starting off with a relatively low atomic percent of 1% (atomic doping ratio) and the above preparation methods, we may assume that the ions are well separated from each other. This allows us to ignore two and multiple ion effects such as upconversion that would normally affect the energy transfer.

7.3 Experimental

The samples were heated in a brass chamber specially built for the experiment. The temperature of the chamber was carefully monitored using an iron-konstantin thermocouple. We estimate the variance in the temperature readings to be in the range of $\pm 1^o$K. Two holes drilled at 90^o from each other allowed pump light to enter and the fluorescence emission to be observed with minimal direct interference from the pump light. The fluorescence was then further isolated from the pump radiation by appropriate filters and detected via a *S-1* (Hamamatsu Electronics)

surface photomultiplier tube.

The pump light was provided by a Coherent DPSS source ($\lambda_{pump} = 532$nm). The pump was modulated externally by an acousto-optic beam deflector which ensured nanosecond rate square pulse drop-off, which was found to be orders of magnitude faster than the typical lifetimes of any of the erbium doped hosts considered. 50% duty-factor with a chopping frequency of 37Hz was used. This allowed sufficient recovery time for even the longest lieftime material we tested.

Sub-microsecond rise and fall times were available via the acousto-optic device whenever necessary. The ceramic erbium doped yttria samples utilized in this study came from World Labs Co. Ltd, Japan.

7.4 Results

In this study the $^4I_{11/2}$ fluorescent level of erbium was studied in eight different laser material systems. The samples include both single crystals and ceramic samples. The experimentally determined fluorescent lifetimes versus temperature were fit to the multiphonon model (eqn 7.1). When a rare-earth ion decays from an excited state with a lifetime that depends upon temperature, the total decay rate is made up of the sum of the radiative and non-radiative components [9]. Radiative processes include purely electronic and phonon-assisted transitions. Nonradiative transitions are those that reduce the inverted population by phonon-quenching. Ion-to-ion energy transfer exchanges can be eliminated from the picture by using a low dopant ion concentration and postulating the relative isolation from the influence of a similar ion. Phonon-quenching of energy is thus directly coupled to the host lattice. Varying the host lattice then gives rise to a variation in the fitting parameters E_p and p_i. The magnitude and temperature

dependency of the multiphonon emission rate is then dependent on the phonon frequency distribution and the strength of the ion-lattice coupling.

A more complete picture of the phonon characteristics may be obtained by referring to infrared, vibronic and Raman spectra of the host [10].

The temperature dependent lifetimes were analyzed to extract the phonon energy (E_p), the phonon order (p_i) and the spontaneous decay rate at 0^oK (Ω_0). The results are summarized in Table 7.1.

7.5 Discussion

We have collected and analyzed data from 8 different erbium-doped insulating laser material systems that have shown promise as ceramic laser hosts. For comparison, we also provide data from the standard erbium-YAG system.

The phenomenological fit for p_i corresponding to the energy bandgap from $^4I_{11/2}$ to the $^4I_{13/2}$ level can be determined by multiplying the order of phonons by energy of each phonon E_p [11]. We found no change in lifetimes with change in temperature for the $^4I_{13/2} \leftrightarrow {}^4I_{15/2}$ transition, a fit was thus not possible. We believe significantly higher temperatures might be necessary to affect the inverted population. Such temperatures are not only difficult to obtain in a laboratory environment but also of little practical value - those temperatures are not seen in normally operating laser systems.

The notion of a partial order of phonons (where p_i is not an interger number) is fictitious. A non-integer number implies the dominance of multiple closest phonon-modes with significant contributions to the interaction. The closest integer gives the larger contribution to the overall multiphonon relaxation rate due to higher density of effective phonon states - this may however dominate over the

Table 7.1: Multiphonon Experimental Results

Sample	E_p Phonon energy (cm^{-1})	p_i phonon order	$\Omega_0^{-1} = \tau_{sp}(0K)$(ms) from eqn. (7.1)	$\Omega^{-1} = \tau(\sim 290K)(ms)$
$1\%Er : LuAG$	695 ± 5	3.8 ± 0.2	0.098	0.086
$1\%Er : YAG$ (single-crystal) [11]	785 ± 5	4 ± 0.2	0.1	0.1
$1\%Er : Lu_2O_3$	604.65 ± 5	6.8 ± 0.2	2.70	1.8
$1\%Er : Sc_2O_3$	625.5 ± 5	6.5 ± 0.2	4.00	2.44
$1\%Er : Y_2O_3$	549 ± 5	5.4 ± 0.2	4.55	2.86
$1\%Er : YGaG$	556 ± 5	4.7 ± 0.2	1.31	0.96
$1\%Er : GdGaG$	590.1 ± 5	5 ± 0.2	1.53	1.18
$1\%Er : LuGaG$	549 ± 5	4.55 ± 0.2	1.07	0.78

maximum phonon frequency given by the corresponding Raman spectra.

For instance, for 1% Er^{3+}: Y_2O_3 the maximum phonon frequency is around $600cm^{-1}$ [12], while the analysis yields a phonon energy of $\sim 550cm^{-1}$ (Table 7.1).

In the fitting process, the point at which the rates change is typically determined by E_p, and the order (p_i) determines the rate of the change. This makes the fit unique. We found that the fitted model predicts the temperature dependent behavior of the material fairly accurately (a deviation from the experimental of a few percent).

Materials with lower E_p generally have a large number of phonon modes taking part in the process (this compensates to fill the energy-gap to the next lowest energy level); these materials thus show dramatic lifetime changes with changes in temperature.

The increase in the non-radiative rate thus governs the relaxation at sufficiently high temperature [13], [10].

The phonon order (p_i) represents the best fit of a simple analysis model that provides a useful metric on the behavior of these hosts when exposed to high temperatures.

We have also earlier demonstrated that the multiphonon behavior of the precursor forms of the ceramics can be evaluated using the same scheme [9].

The analysis does indicate that lower energy phonons do have an overweighted effect on the effective phonon energy in all the cases considered here. The lower effective mass of the Al-O bond results in a higher-frequency phonon mode (E_p)

that couples into the matrix.

$$E_p = k \times \frac{1}{\sqrt{m_{eff}}} \tag{7.2}$$

where, k is the coupling constant, and m_{eff} is the effective mass of the system (see Figure (2)).

Figure (3) shows that the same 'class' of materials can be generally grouped on a scatter plot. The relative abundance of high-energy optical-phonons generated by the *A*l-O (Al at. wt. 26.9, O at. wt. 15.9) bond in YAG and LuAG seemingly dominates any influence of the yttrium (at. wt. 88.9) or lutetium (at. wt. 174.9).

The optical-phonons coupled out of the active ion's (Er^{3+}) $^4I_{11/2}$ energy level are coupled strongly into the Al-O bond, this gives rise to a high phonon energy (E_p) and a relatively low phonon order fit (p_i).

Replacing the Al-O bond with a *G*a-O (Ga at. wt. 69.7) bond reduces the phonon-energy in the three gallium garnets studied as expected. It should be noted that the bond is weaker corresponding to a small k parameter in equation 7.2.

The sesquioxides don't seem to fit this simple model consistently, the scatter plot shows a range of phonon energies from 604.65 cm^{-1} for Lu_2O_3 (Lu at. wt. 174.9, O at. wt. 15.9), to 549cm^{-1} for Y_2O_3 (Y at. wt 88.9), and 625.5 cm^{-1} for Sc_2O_3. Applying the above model one may arrive at the conclusion that the strength of the *X*-O bond changes. It makes it easier for lower energy phonons to couple into the matrix for the lowest effective mass systems.

It should be noted that the sesquioxides are all reported to be in the bixbyte structure (space group $Ia\bar{3}$), in which there are two sites that can be occupied by the trivalent ions of C_2 and C_{3i} symmetry. Only the C_2 site is optically active

for rare earth dopants.

This approach is limited by the uncertainties associated with the calculated lifetimes at the various temperature, but this can be mitigated by considering the fit for the whole temperature dependent curve.

7.6 Conclusion

From the simple approximation provided by the multiphonon model (equation 7.1), we can extract the effective phonon frequency and the number of phonons involved in the decay interaction. This model was found to be sufficient to predict the temperature-dependencies of multiphonon relaxation from the $^4I_{11/2}$ level in erbium across a wide variety of hosts. The set of hosts included garnets and oxides that have been pipped as suitable ceramic laser hosts. We also augment the data with others from literature (see plot (3)). The scatter plot also shows that host matrices that are similar in structure largely behave similarly. The different constituents give us the variation in accordance with known laws (equation 7.2).

The ease of the experimental method and fit makes this a quick method of evaluating the suitability of potential laser hosts for high-powered operation.

Larger values for both E_p and p_i indicate a high characteristic temperature and strong dependence on temperature, implying unfavourable performance for the laser gain media when pumped at high-flux densities or when operated at high temperatures.

7.7 Acknowledgement

This work was made possible by the generous support of the US Navy/Office of Naval Research under grant number N00014-09-1-0205.

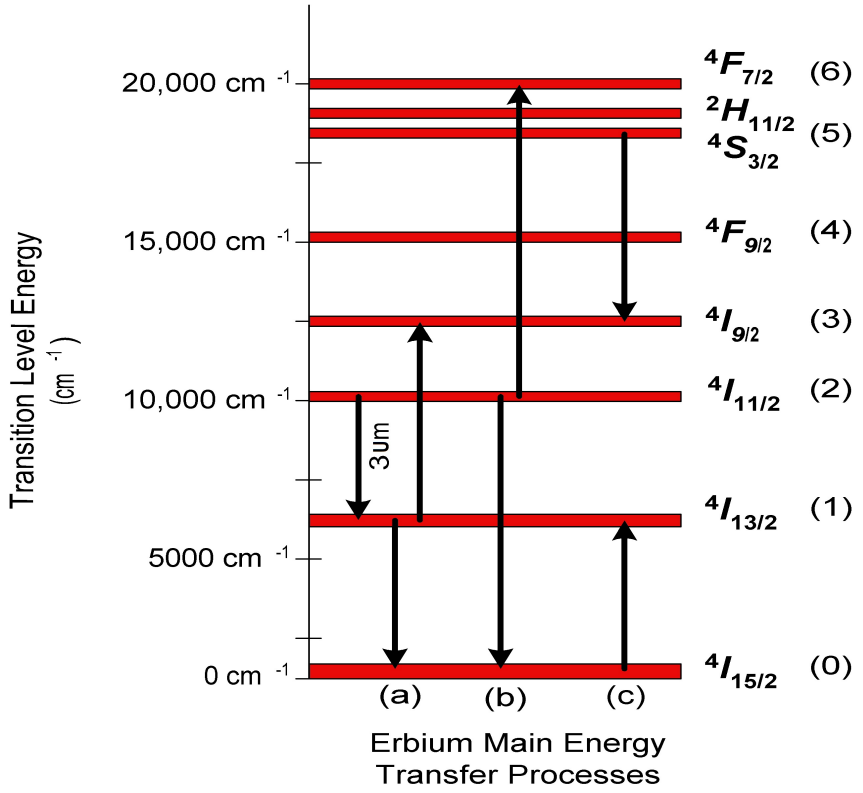

Figure 7.1: Two ion processes in erbium doped in isulating hosts.

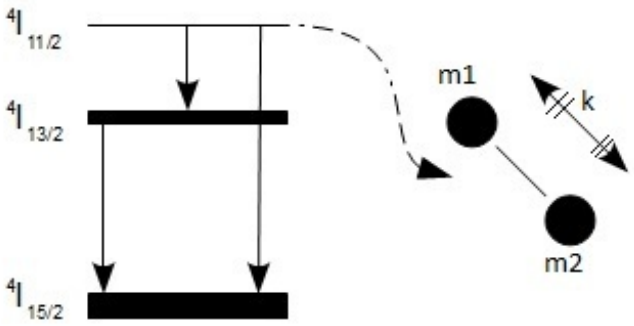

Figure 7.2: The above schematic shows the optical phonon coupling into the matrix. Relevant optical transitions are also shown, we studied the effect of multiphonon generation on the $^4I_{11/2}$ energy level.

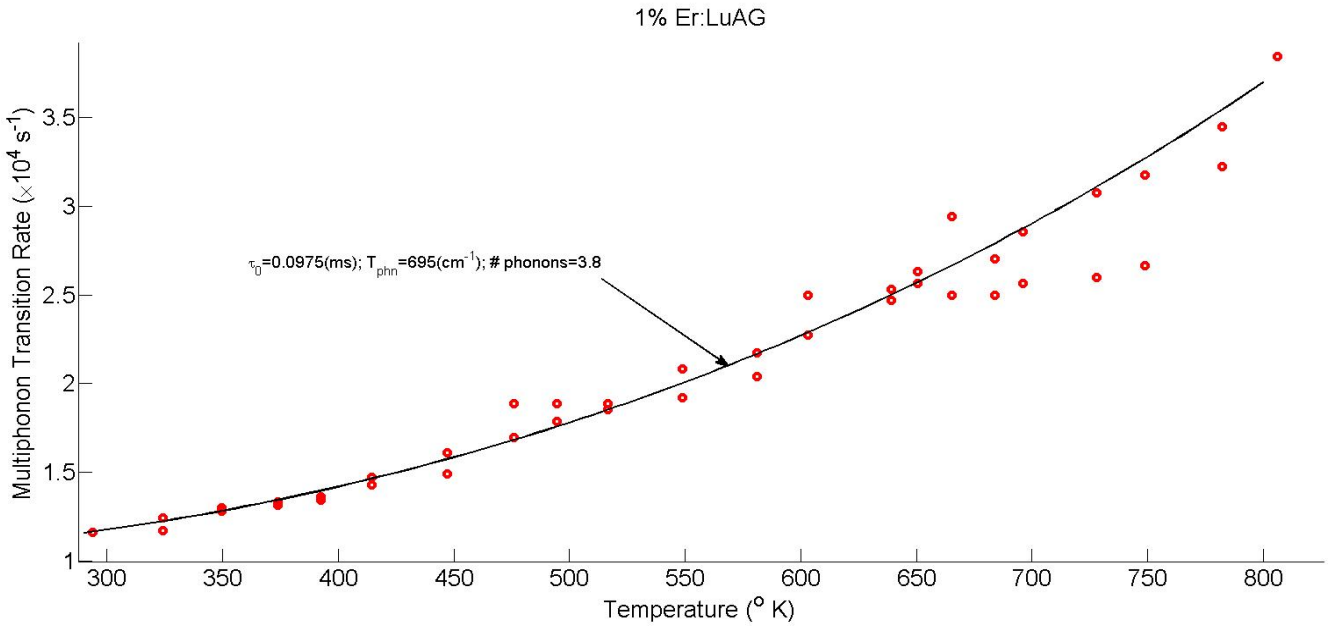

Figure 7.3: Multiphonon fit (following equation 7.1) for 1% doped Er^{3+}:$LuAG$.

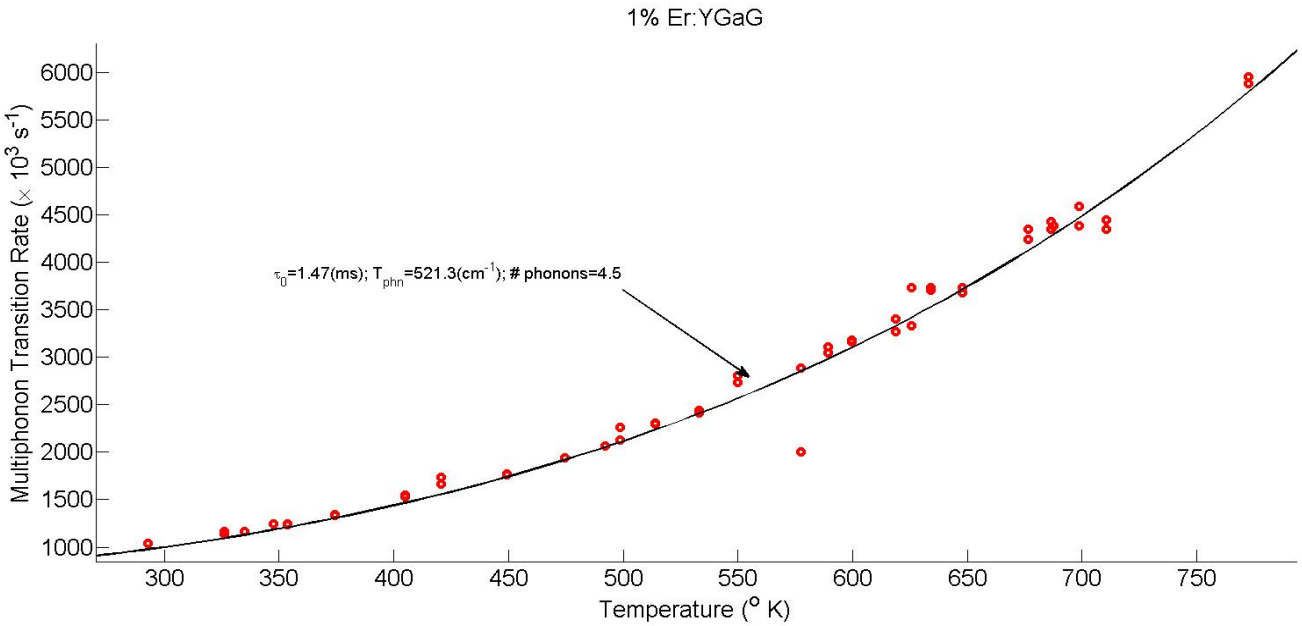

Figure 7.4: Multiphonon fit (following equation 7.1) for 1% doped Er^{3+}:$YGaG$.

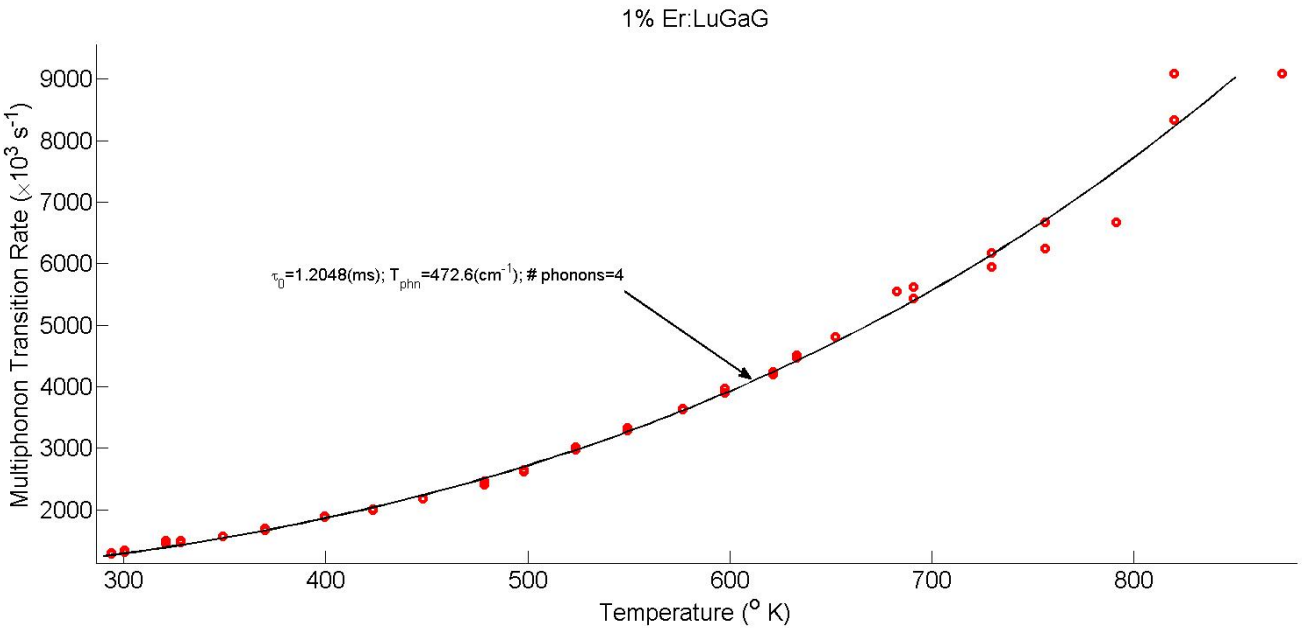

Figure 7.5: Multiphonon fit (following equation 7.1) for 1% doped Er^{3+}:$LuGaG$.

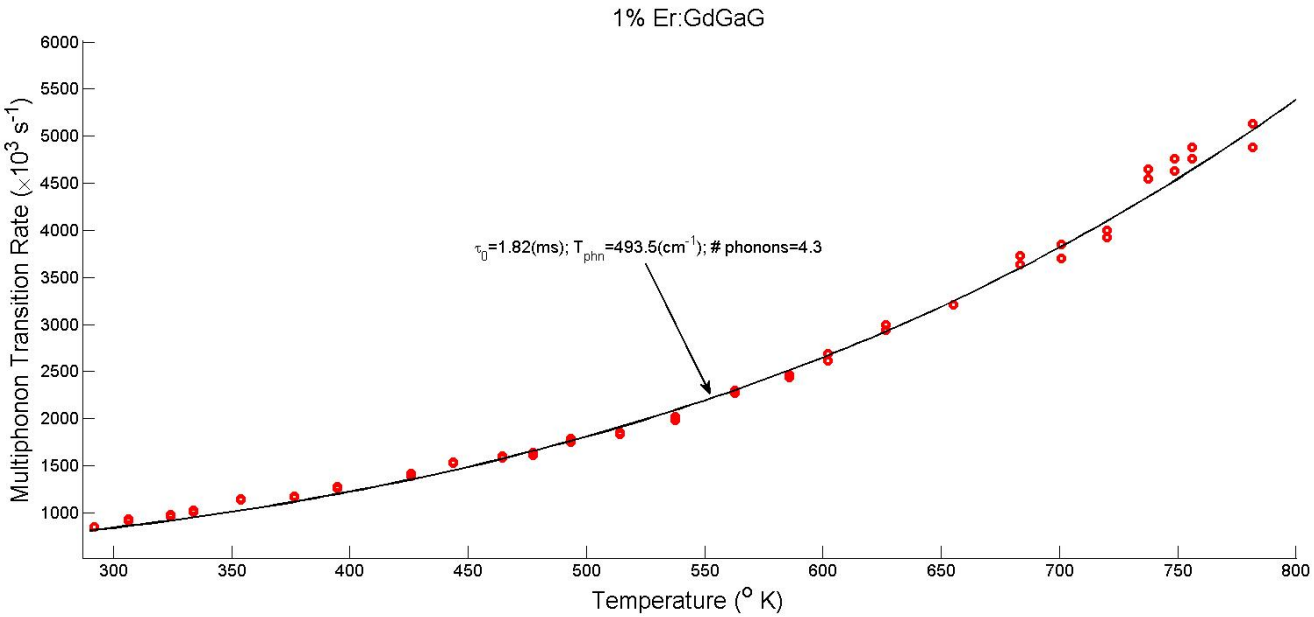

Figure 7.6: Multiphonon fit (following equation 7.1) for 1% doped Er^{3+}:$GdGaG$.

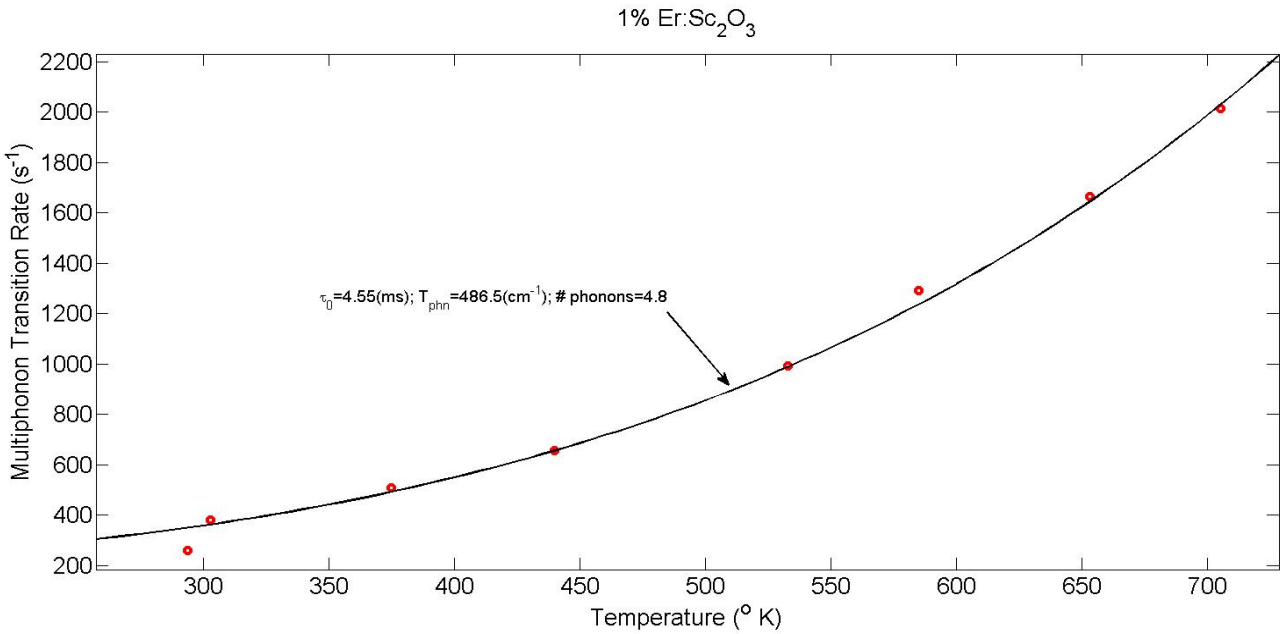

Figure 7.7: Multiphonon fit (following equation 7.1) for 1% doped Er^{3+}:Sc_2O_3.

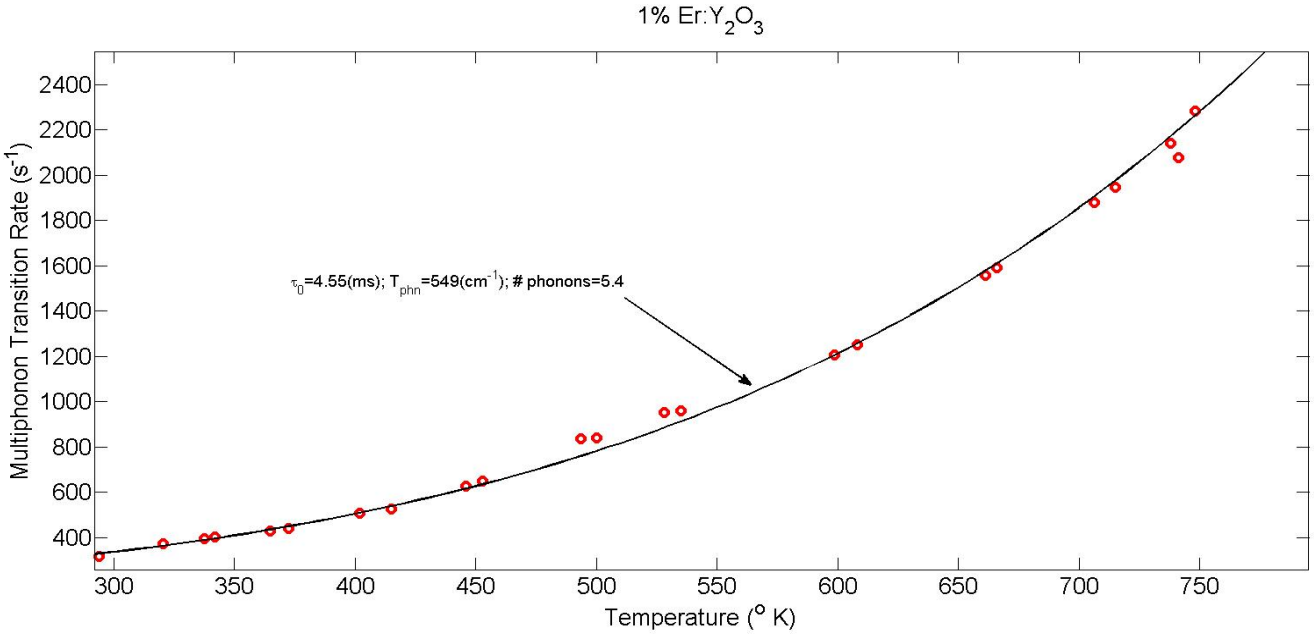

Figure 7.8: Multiphonon fit (following equation 7.1) for 1% doped Er^{3+}:Y_2O_3.

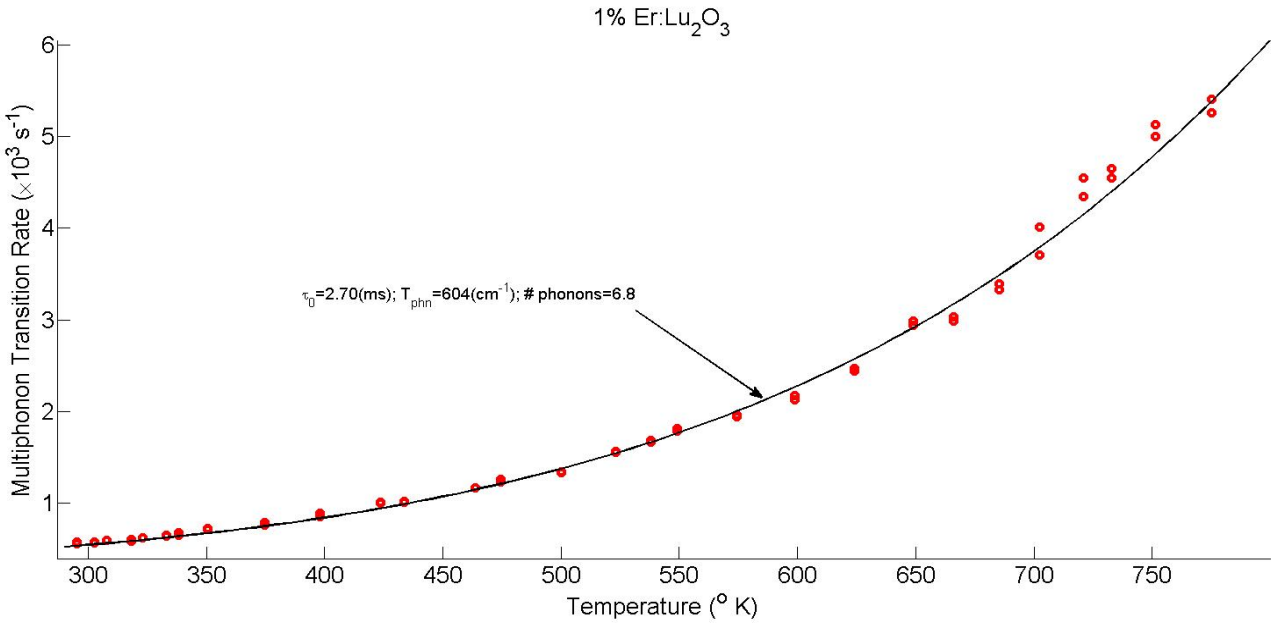

Figure 7.9: Multiphonon fit (following equation 7.1) for 1% doped Er^{3+}:Sc_2O_3.

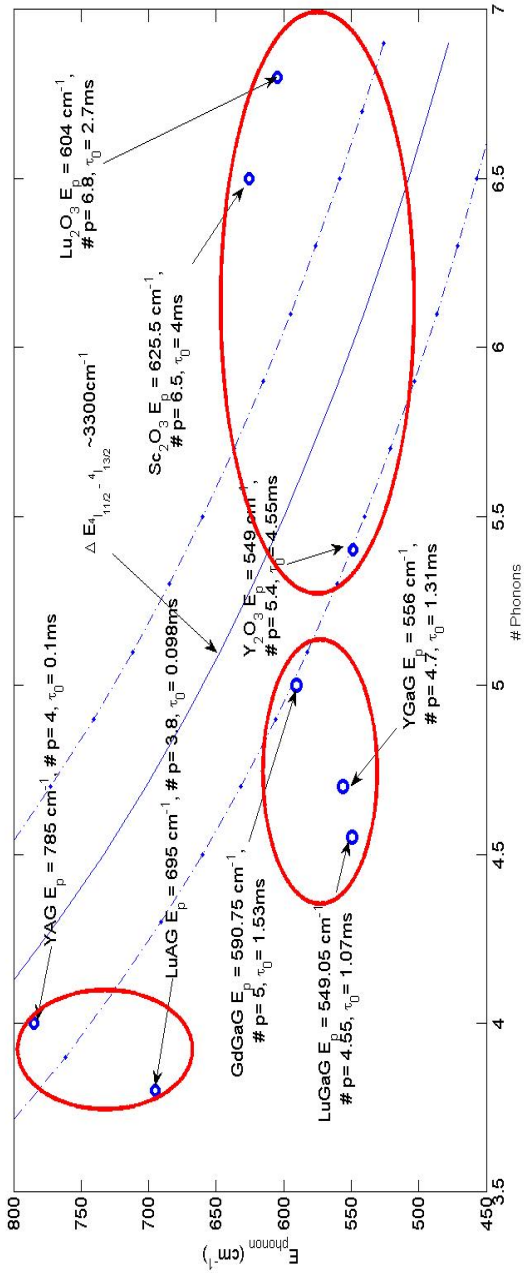

Figure 7.10: Scatter plot showing groupings based on the fitting parameters from equation 7.1.

References

[1] *Intermolecular energy transference and fluorescence*, Th. Förster, Ann Physik, vol. 2, issue. 1-2, pgs. 55-75, 1948.

[2] *A Theory of Sensitized Luminescence in Solids*, D. L. Dexter, The Journal of Chemical Physics, vol. 21, no. 5, pg 836, May, 1953.

[3] *Cooperative Optical Absorption in Solids*, D. L. Dexter, Physical Review, vol. 126, no. 6, June 15, 1962.

[4] *PhD dissertation, The John Hopkins University*, A. Kiel, 1962.

[5] *Multiphonon Orbit-Lattice Relaxation of Excited States of Rare Earth Ions in Crystals*, L. A. Riseberg, H. W. Moos, Physical Review, vol.174, no.2, pg 429, 1968.

[6] *Spectroscopic Relaxation Processes of Rare Earth Ions in Crystals*, H. Warren Moos, Journal of Luminescence, pgs 106-121, 1970.

[7] *Temperature dependence of intrinsic multi phonon absorption in crystals*, B. Bendow, Applied Physics Letters, vol. 23, no.3, pg 133,1 August 1973.

[8] *Fabrication of Polycrystalline, Transparent YAG ceramics by a solid state reaction method*, A. Ikesue, I. Furusato and K. Kamata, Journal of the American Ceramic Society, vol 78, Issue. 1, pgs: 225-228, 1995.

[9] *Multiphonon-based comparison of erbium-doped yttria in large, fine grain polycrystalline ceramics and precursor forms*, A. Joshi, O. M. Stafsudd, K. Serivalsatit and J. Ballato, Optical Materials, Volume 34, Issue 1, November 2011, pgs 9598.

[10] *Radiative and Multiphonon Relaxation of Rare-Earth Ions in Yttrium Orthoaluminate*, M. J. Weber, Physical Review B, vol. 8, No. 1, pg 54,July 1973.

[11] *Multiphonon Relaxation Studies of* $^4I_{11/2}$ *and* $^4I_{13/2}$ *Energy Levels in Er:YAG and Er,Pr:YAG Laser Crystals*, M. K. Furtado, R. K. Shori, O. M. Stafsudd, J. Stone-Sundberg and M. Kutka. Advanced Solid-State Photonics, Technical Digest (Optical Society of America, 2005), paper MB10.

[12] *Vibrational Spectroscopy of the C-form of Yttrium Sesquioxide*, Y. Repelin, C. Proust, E. Husson and J. M. Beny,Journal of Solid State Chemistry, 118, pg. 163, 1995.

[13] *Radiation from the* $^4T_2$ *State of* Cr^{3+} *in Ruby and Emerald*, P. Kisluk and C. A. Moore, Physical Rev. vol. 160, no. 307, 1967.

CHAPTER 8

Concentration dependent upconversion luminescence from the $^4I_{11/2}$ and the $^4I_{13/2}$ energy levels in the bulk Er^{3+}:Y_2O_3 ceramic system

A concentration-dependent study of upconversion in bulk erbium doped yttria ceramics at multiple upconverted emission wavelengths is reported. Erbium is an interesting ion providing multiple paths to emit multiple wavelengths. Upconversion properties of erbium doped yttria were studied on pumping with two pumps, $\lambda = 1545$nm (populating the $^4I_{13/2}$ energy level) and $\lambda = 977$nm populating the $^4I_{11/2}$ energy level. Varying concentrations of erbium in yttria show remarkable upconversion properties to the $^4S_{3/2}$, $^4F_{9/2}$ and $^4I_{9/2}$ energy levels. Power dependence of upconversion luminescence is also presented. We also show that the upconversion mechanisms in the bulk form are certainly different than the often studied nanocrystalliine form.

The upconversion properties of erbium doped in various hosts is very well-known. Erbium was the first ion to show upconversion [1], with the availability of high-powered near-IR pumps at $\sim 810nm$ and $\sim 980nm$ and the invention of the tunable Ti:Sapphire laser in 1980s, the study of upconversion in erbium has been carried out in multiple hosts.

8.1 Introduction

Upconversion refers to the generation of higher energy photons from multiple lower energy ones. It relies on serendipitous spacing between energy-levels, such as ones seen in certain rare-earth ions, and appropriate pump wavelengths. Using active-ions such as erbium, upconversion has been leveraged to produce visible emitting phosphors in the visible. Laser action has also been reported in Upconversion is also responsible in enabling technologically important transitions - *e*.g. emission from the erbium ion (in *Er:YAG*) near the water absorption peak around $\sim 3\mu m$. There upconversion serves as an 'in-built' pump to overcome unfavorable population profiles due to inverted lifetimes (the lifetime of the lower level is longer than that of the upper level). This is also heavily dependent on the concentration of the active ion. All these reasons have necessitated an in-depth study of upconversion yield as the erbium concentration changes.

The upconversion properties of erbium doped in various hosts has been studied extensively. Erbium was the one of the first ions to show significant upconversion [1], with the availability of high-powered near-IR pumps at $\sim 810nm$ and $\sim 980nm$ and the invention of the tunable Ti:Sapphire laser in 1980s, the study of upconversion in erbium has been carried out in multiple hosts.

We here provide power dependent studies, spectra and discussion to help elucidate the mechanisms in bulk yttria as a function of concentration.

8.1.1 Importance of Upconversion in Erbium

With its rich variety of transitions and conveniently placed absorption bands, erbium has become an important ion to generate telecommunication wavelengths ($\sim 1.3\mu m$ and $\sim 1.5\mu m$). Erbium doped in insulating hosts has well-known emis-

sions at other wavelengths around $\sim 3\mu m$ (the ${}^4I_{11/2} \rightarrow {}^4 I_{13/2}$ transition). This emission line is important because the vibrational modes of the water molecule have energies very close to the energy of the $2.94\mu m$ photon (from the $Er : YAG$ system). This allows for high absorption of the radiation into the water molecule ($\alpha \sim 10^4 cm^{-1}$). This method for injecting energy into dental tissue has been leveraged for use in dental surgery to great advantage [2].

The $\sim 3\mu m$ transition (${}^4I_{11/2} \rightarrow {}^4 I_{13/2}$) is academically interesting since in most hosts (*e*.g. YAG, Y_2O_3, etc.) the lifetimes are inverted from what they should ideally be; in the $Er : YAG$ system the upper-level lifetime is around $\sim 100\mu s$, while the lower-level (${}^4I_{13/2}$) has a lifetime of $\sim 5 - 6ms$. This makes continuous-wave laser action practically impossible. Continuous-wave laser action has been obtained in these crystals; and the only way to explain such a laser is depopulation of the terminal level due to upconversion.

The situation in the system under consideration here ($Er : Y_2O_3$) is qualitatively similar, though significantly more unfavorable. The upper level lifetime for the ${}^4I_{11/2}$ state in yttria is in the $3 - 5ms$ range and the lower level lifetime (${}^4I_{13/2}$) is in the $10 - 12ms$ range for a wide concentration range. With the admission of this vital 'in-built' pump for the $\sim 3\mu m$ transition, the study of upconversion becomes even more important. The self-termination of the upper level in the $\sim 3\mu m$ transition is now thought to be overcome by up-conversion processes ${}^4I_{13/2} \rightarrow {}^4 I_{15/2} + {}^4 I_{13/2} \rightarrow {}^4 I_{9/2}$; these deplete the terminal level and feeds the upper one via multi-phonon transitions (dotted arrows in figure(9.1)) [3].

Erbium doped yttria nanocrystalline powders have been also been pipped as potential phosphors for their ability to generate red, green and, blue emission from near-IR radiation efficiently [4], [5].

8.1.2 Study of Upconversion in Erbium doped yttria

Yttria crystallizes in the bixbyte structure and has two sites for rare-earth ion substitution - one has the point group symmetry C_2 and the other C_{3i}. Of the two the documented emissions are from the C_2 site - that is the only site without inversion symmetry - allowing pure electronic dipole transitions in the 4f shell. C_{3i} dipole-dipole transitions are forbidden [6].

The main topics of discussion in the field include pathways to upconverting to different wavelengths and effect of pump power on intensity of upconversion luminescence.

Auzel [7] in 2004 summarized the state of erbium upconversion to green after pumping either at $\sim$ 980nm or $\sim$ 1550nm in various hosts. These hosts have included a wide variety of oxides, fluorides or chalcogenides where universally upconversion was thought to operate via either ETU or ESA.

While pathways are easily conjectured, they are not generally confirmed. Emission spectra and pump-power dependency often helps to complete the picture.

Largely, the evidence for these mechanisms rests on the number of electron excitation 'jumps' (n) needed to produce the emitted photon of the correct frequency. This is usually put forth as,

$$I_{upconverted} \propto I_{pump}^{n} \tag{8.1}$$

where, $I_{upconverted}$ and I_{pump} are the intensities of the upconverted signal and the pump signal respectively. Pump-intensity (or more conveniently power) dependence of upconversion luminescence intensity is generally addressed by a log-log

plot, with the slope giving us the number of steps taken to reach the higher energy levels. Pollnau, *et al* [9] addressed the issue with a simple model which has been used often in literature to explain upconversion in rare-earth ions. It relates the emitted population N to the number of steps needed for the emission. The model however only considers energy-transfer upconversion (ETU) and excited-state absorption (ESA).

In 2002, the enhancement of red emission from the ${}^4F_{9/2}$ energy level was studied in bulk and nanocrystalline erbium doped yttria [8]. Excitation at 815nm was used for the experiment. It was shown that the relative amounts of enhancement for the green and the red emission differed for the two forms of the cubic material system.

In 2003, it was conjectured that the enhancement of the red emission as concentration of the active ion was increased was due to an ion-pair cross-relaxation process (${}^4I_{7/2}$,${}^4I_{11/2} \rightarrow {}^4F_{9/2}$,${}^4F_{9/2}$), that directly populates the ${}^4F_{9/2}$ state [4], [5]. Ytterbium co-doped nanocrystalline powders were analyzed there; not surprisingly we observe a similar increase in red emission as the concentration increases; but it is not just the red-emission that increases with concentration. We also note an increase in emission from the ${}^4I_{9/2} \rightarrow {}^4I_{15/2}$ transition corresponding to the $\sim 840nm$ band (see figure (8.4).

It has since been conjectured that cross-relaxation mechanisms play a large part in producing red emission from erbium under near-IR pump ($\sim 980nm$) [4] at high concentrations. These results are however for the nanocrystalline form of the system.

Here we have shown that the emission of certain wavelengths seem to move in concert as concentration changes. We believe this shows that some of the paths to upconverting low energy photons to higher energy ones in erbium are linked.

These results may be further used to explain upconversion dynamics in erbium doped materials.

The results of our experiments also show that, the efficiency of upconversion changes for different emission wavelengths as the concentration changes.

8.2 Upconversion Experiments with $\lambda_{pump} = 977nm$

8.2.1 Experimental

Nanocrystalline hot-isostatic pressed ceramic samples of varying concentration were subjected to $977nm$ radiation. The upconverted spectra were measured through a 1/2m Jarrell-Ash spectrometer equipped with a suitable broad-band photo-multiplier tube (Hamamatsu R636). The pump beam was chopped and a lock-in (EG&G) was used to collect the data. The nominal resolution of the setup was $\sim$ 1nm.

The power-dependent measurements were done by using suitably picked band-pass filter combinations. The same detector was used for both experiments.

We had at our disposal 0.25%, 1%, 2%, 15% and 25% (at.wt.) doped Er^{3+} : Y_2O_3. These samples were procured from World Lab Co. Ltd., Japan.

8.2.2 Results

The plots 8.5, 8.6 and 8.7 show the power dependence of upconversion as concentration of the dopant is increased. The table 9.3 provides a summary of the obtained n values.

The upconversion spectra provided (figures (8.3 and (8.4)) were obtained after excitation from the 977nm pump. The plots show phenomena correlating the

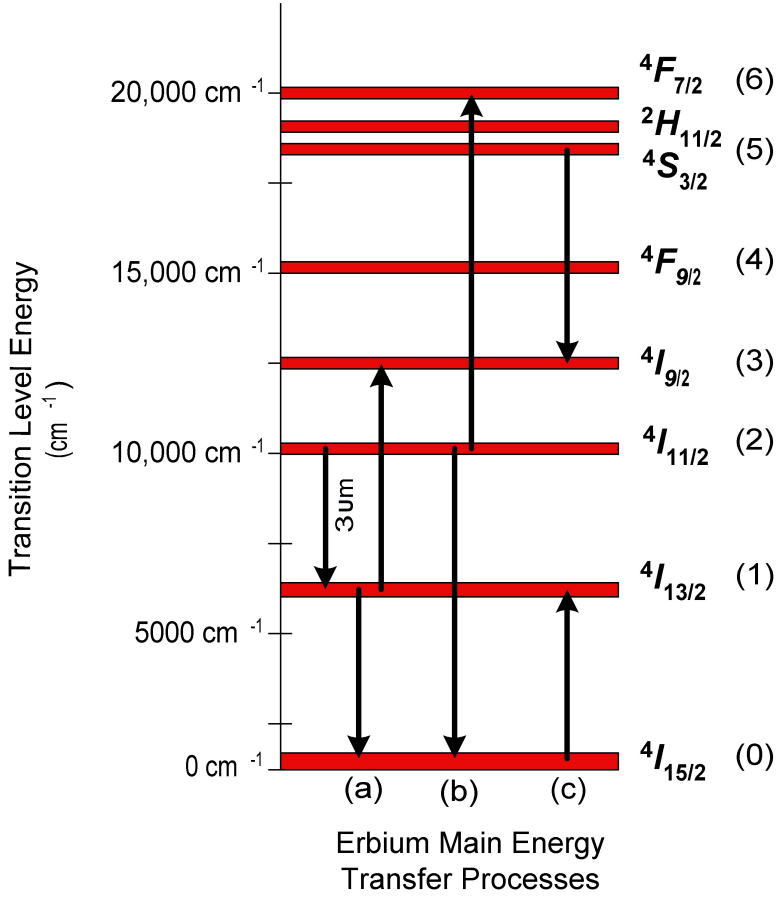

Figure 8.1: The main inter-ion energy transfer processes in Er^{3+}.

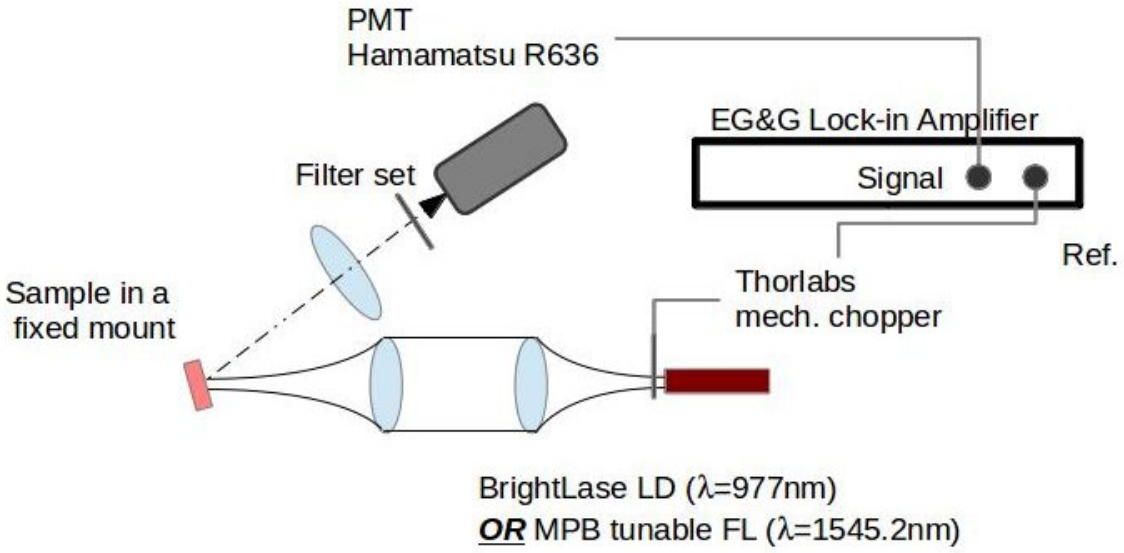

Figure 8.2: Sketch of the experimental setup.

increase in concentration with the increase in emission from the $^4F_{9/2}$ energy level that has been reported elsewhere. They also show a similar concerted increase in emission from the $^4I_{9/2}$ energy level. The emission is comparatively small, but the trend is unmistakable.

With the excitation around $\sim 1\mu$m, we expect excited electrons to require approximately 2 'jumps' to produce emission around 0.5μm. This can be verified from the data in table 9.3 for green emission. The red emission also yields an n value of around 2.

The intensity of near-IR emission from the $^4I_{9/2}$ level yields n values around 0.3 for the relatively low-doped material. This however climbs to numbers slightly ≤ 1 for the highly doped samples where connectivity between the active ions is assumed to be high.

8.3 Upconversion Experiments with $\lambda_{pump} = 1545nm$

8.3.1 Experimental

Nanocrystalline hot-isostatic pressed ceramic samples of varying concentration were subjected to $\sim 1545nm$ radiation from a tunable fiber-laser(MPB Single Mode Er^{3+} Fibre Laser).

The power-dependent measurements were done by using suitably picked band-pass filter combinations. The same detector was used for both experiments.

The same set of samples were used as before.

8.3.2 Results

The results of using the $\sim$ 1550nm pump on the bulk material are summarized in the following table 8.2. The plots 8.8, 8.9 and 8.10 contain the raw data.

The analysis of this data followed the precedent set by the experiments with the 977nm pump. It is expected that the $^4S_{3/2}$ state should require approximately 3 'jumps' when the concentration rises to a point where the active ions are close enough for direct or co-operative energy transfer. This is borne out by the data in the $\geq 0.5\% \leftrightarrow 2\%$ range, where the n value is close to 3. It however seems that at higher concentrations, the value drops to the $1.5 \leftrightarrow 2$ range.

The concentration dependence of emission from $^4F_{9/2}$ energy level follows a similar trend. At very low concentrations the n value is ≤ 0.8.

The near-IR emission upconversion 'jumps' required is generally in the $\geq 1 \leftrightarrow \leq 1.5$ range.

Table 8.1: Trend of upconversion per concentration when the active ion is pumped at 977nm.

	$^4S_{3/2}$	$^4F_{9/2}$	$^4I_{9/2}$
$0.25\%Er:Y_2O_3$	1.8	1.7	0.25
$0.5\%Er:Y_2O_3$	2.1	1.8	0.24
$1\%Er:Y_2O_3$	2.1	2.1	0.3
$2\%Er:Y_2O_3$	2.1	1.9	0.23
$15\%Er:Y_2O_3$	1.7	1.7	0.9
$25\%Er:Y_2O_3$	1.4	1.8	0.75

8.4 Discussion

Note the co-doping of ytterbium in erbium yttria, as studied in the above papers [4] and [5], is primarily responsible for the efficient transfer of photons into the ${}^4I_{11/2}$ level (from the $Yb^{3+}\ {}^2F_{5/2}$ energy-level). We do not consider that co-doping with ytterbium causes a major change in the upconversion mechanism to higher energy-levels from the ${}^4I_{11/2}$ level.

The intensity of upconverted luminescence that is achieved by adding n pump photons is dependent on the pump intensity I^n_{pump}. The value of n may range from n for very little upconversion, to 1 for the upper state decay and ≤ 1 for very large upconversion rates for intermediate states providing the ground state population [9]. The latter measure of upconversion implies a highly efficient transfer of electrons to the upper level that could be achieved by excited state absorption or some other energy-transfer mechanism.

The general scenarios given in [9] cover perhaps the simplest and the most likely means to upconversion, energy-transfer upconversion (ETU) and excited-state absorption (ESA). The other processes perhaps causing the significant deviation seen in this system transferring energy between levels include cross-relaxation and three-ion energy transfer processes. These processes rely on the presence of neighbors within 'talking' distance and are bound to be enabled as the concentration increases.

From the upconversion spectra with the 977nm pump (figure (8.3)), we note the increase in red and $\sim 850nm$ emission (figure (8.4)) as concentration increases.

At very-low concentrations, where the active ions may be assumed to be fairly isolated and homogeneously distributed in the ceramic, we see practically no red and $\sim 850nm$ emission. As the concentration increases and energy can be

Table 8.2: Trend of upconversion per concentration when the active ion is pumped at 1545nm.

	$^4S_{3/2}$	$^4F_{9/2}$	$^4I_{9/2}$
$0.25\%Er:Y_2O_3$	0.72	0.78	-0.007
$0.5\%Er:Y_2O_3$	2.3	1.02	1.4
$1\%Er:Y_2O_3$	3.5	2.1	0.89
$2\%Er:Y_2O_3$	3.1	2.2	1.2
$15\%Er:Y_2O_3$	1.7	1.5	1.5
$25\%Er:Y_2O_3$	1.8	1.7	1.4

transferred from one active-ion to another (ETU), we note an increase in emission for the above wavelengths implying multiple ion processes being dominant. With the lack of evidence for a threshold indicating photon-avalanche effects, ETU and/or cross-relaxation are perhaps the most viable processes to populate the above energy levels in erbium. This maybe further explored by considering the data in Table 1.

The model generally applied to evaluate the number of steps required for upconverted emission relies primarily on the ESA and ETU mechanisms, cross-relaxation mechanisms of populating levels are not included. As a result, the model is largely unsuitable to study upconversion in erbium where cross-relaxation mechanisms seem to be important. But deviations from the model are perhaps useful to gauge the influence of cross-relaxation in the system. The power dependent measurements yield the upconversion step value ('n').

For the 977 nm pump, surprisingly, the analysis results in similar 'n' values for emission from both the $^4S_{3/2}$ and the $^4F_{9/2}$ energy-level for a large range of concentrations. Except for highly doped samples the upconversion step value is close to 2, which implies a two-step upconversion pathway made possible largely via ETU or ESA. The 'n' number of steps taken cannot, as understood in the conventional sense, be the same for both emissions in the red and green regions.

The argument for the $^4I_{9/2}$ level's lower than 1 'n'-value is however less clear. The 'n'-value for the $^4I_{9/2}$ energy-level seems to approach 1 around the $15\%Er : Y_2O_3$ mark. We conclude that the processes populating the $^4I_{9/2}$ energy-level rely on a high number of erbium neighbors for efficient upconversion, this hints at cross-relaxation and multiple ion processes being operative.

Given that the pump is $977nm$, it is easy to explain the upconversion of the near-infrared radiation to $\sim 450 - 550nm$ via excited-state absorption from the

resonant $^4I_{11/2}$ energy level. This ion is initially pumped into the $^2H_{11/2}$, the population then decays into the $^4S_{3/2}$ level non-radiatively [4], [5].

The upconversion into the $^4F_{9/2}$ level is conjectured to be the cross-relaxation of ions from the $^4F_{7/2}$ and $^4I_{11/2}$ energy-levels [4] ($^4F_{7/2}$,$^4I_{11/2} \rightarrow^4 F_{9/2}$,$^4F_{9/2}$). Although, the $^4F_{9/2}$ level can also be filled by the direct emission from the higher energy-levels, emitting photon energies with equal to the difference between the energy levels.

The concerted increase in emission from both the $^4F_{9/2}$ and $^4I_{9/2}$ energy-levels, as concentration increases however, has gone unnoticed (figures (8.3)).

We believe this also could be an instance of cross-relaxation populating the $^4I_{9/2}$ energy level ($^4S_{3/2}$,$^4I_{13/2} \rightarrow^4 I_{9/2}$,$^4I_{9/2}$).

Considering the 1545nm pump, beginning with $0.25\%Er:Y_2O_3$ and moving towards $2\%Er:Y_2O_3$, we note that the upconversion step value initially increase for the visible wavelengths, as concentration increases the 'n' value for both wavelengths decreases. For the very lightly doped sample, 0.25%, we expect that the active ions are separated by a large average distance between the neighbors makes the upconversion process very inefficient. For the $^4I_{9/2}$ energy level, the upconverted intensity is independent of the pump intensity. ESA within one ion thus may be ruled out as the dominant upconversion process.

As the active ion concentration is increased the 'n' value generally increases for the three energy-levels, generally peaking at the 1 to 2 % range for the visible emission. ETU, which relies on energy-transfer between neighbors might be the operative process here. The 'n' value decreases slightly for all the three levels as the concentration increases to 25%, indicating that the upconversion process becomes inefficient due to some form of concentration quenching or is perhaps driven more by cross-relaxation.

8.5 Conclusion

A concentration dependent study of upconverted luminescence from erbium's $^4S_{3/2}$, $^4F_{9/2}$ and $^4I_{9/2}$ energy levels in yttria has provided enough reason to pursue a further investigations to explain intra-ion energy transfer paths. We note a common trend in increase in upconversion luminescence with an increase in erbium concentration from the $^4F_{9/2}$ and $^4I_{9/2}$ levels hitherto overlooked by the community. Also, the unsuitability of the current model to explain the luminescence from the above levels is discussed. Cross-relaxation is also conjectured to play a major role in transferring energy to both the levels.

Erbium-doped ceramic lasers show great potential to replace current single-crystal lasers in telecommunication and medical fields. Erbium yttria also has been widely studied over the last few years as a upconverting phosphor. Given the above results regarding effect of concentration on emission from erbium-doped yttria, further work needs be done in order to conclusively prove the upconversion pathways in the ceramic material.

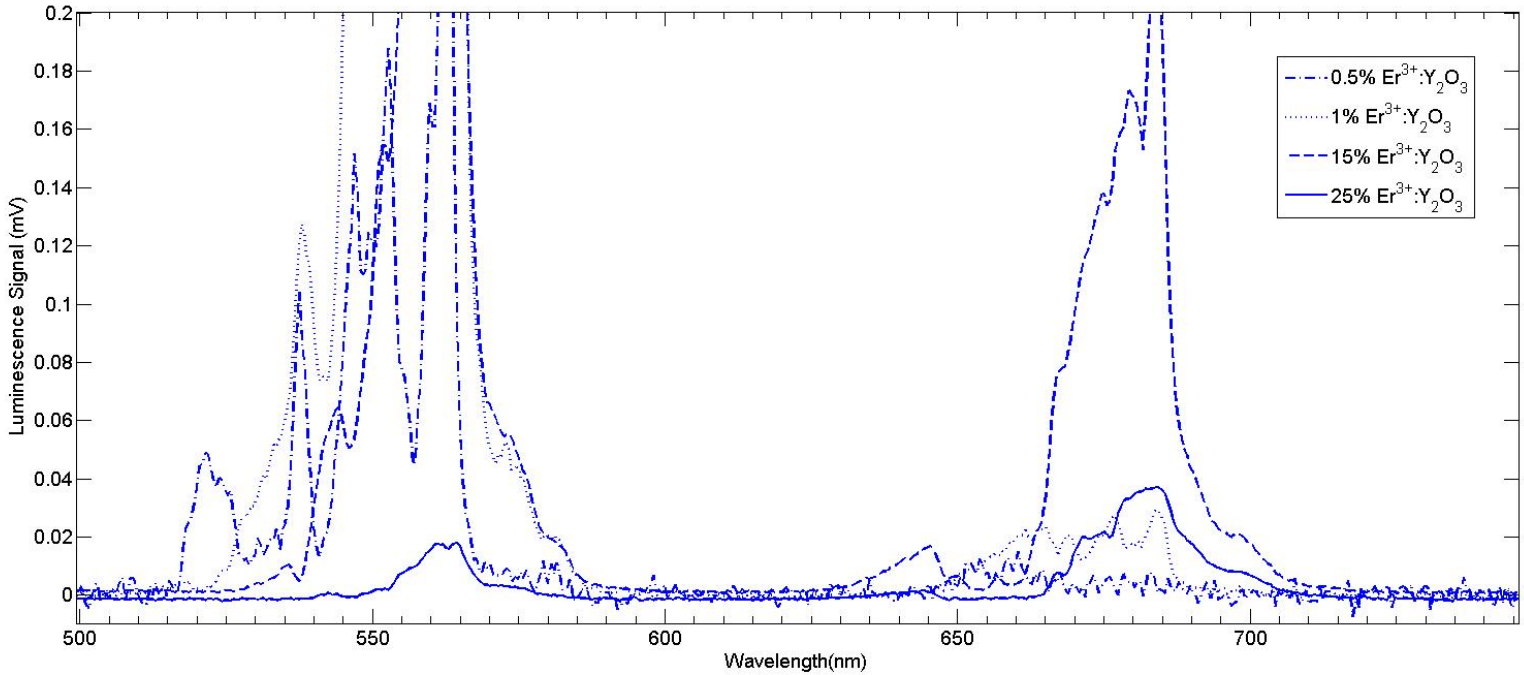

Figure 8.3: Upconversion emission spectra for varying doped $Er^{3+} : Y_2O_3$. As the concentration increases we see two emerging phenomena - fewer photons are emitted from the ${}^2H_{11/2} + {}^4S_{3/2}$ manifolds, there is increased emission from the ${}^4F_{9/2}$ manifold.

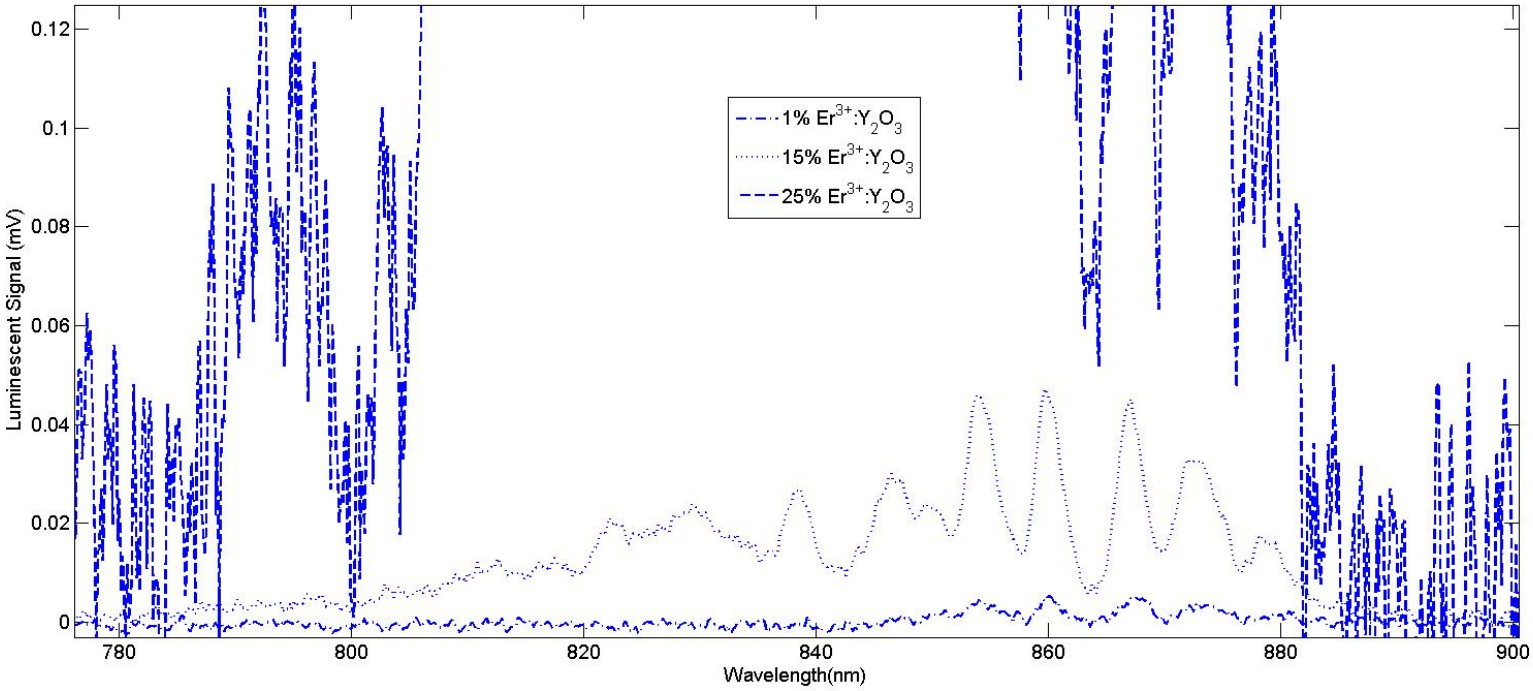

Figure 8.4: Upconversion emission spectra for varying doped $Er^{3+} : Y_2O_3$. Emission from the near-IR energy level ($^4I_{9/2}$) changes in two ways as the concentration of erbium increases: the number and energy of the photons increases.

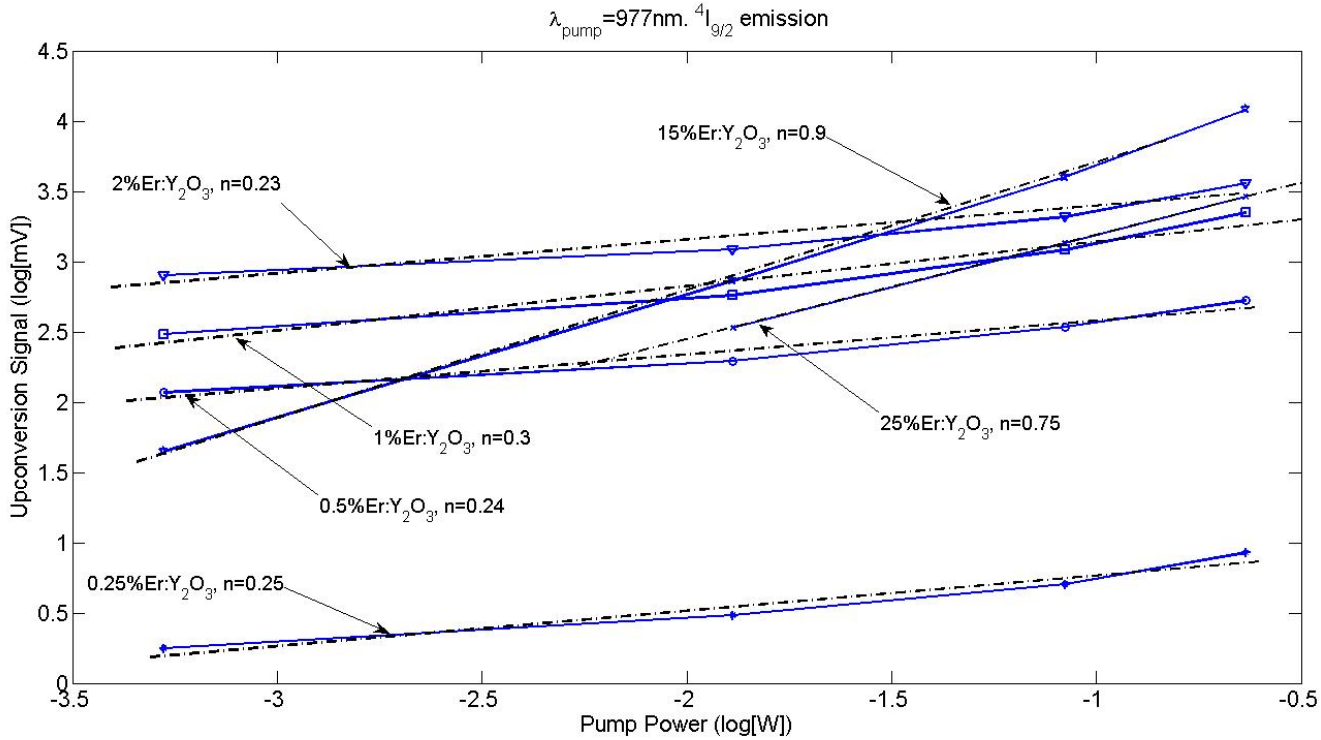

Figure 8.5: Power dependence of upconverted luminescence for the ${}^4I_{9/2} \rightarrow {}^4I_{15/2}$ under the influence of pumping at 977nm ${}^4I_{15/2} \rightarrow {}^4I_{11/2}$.

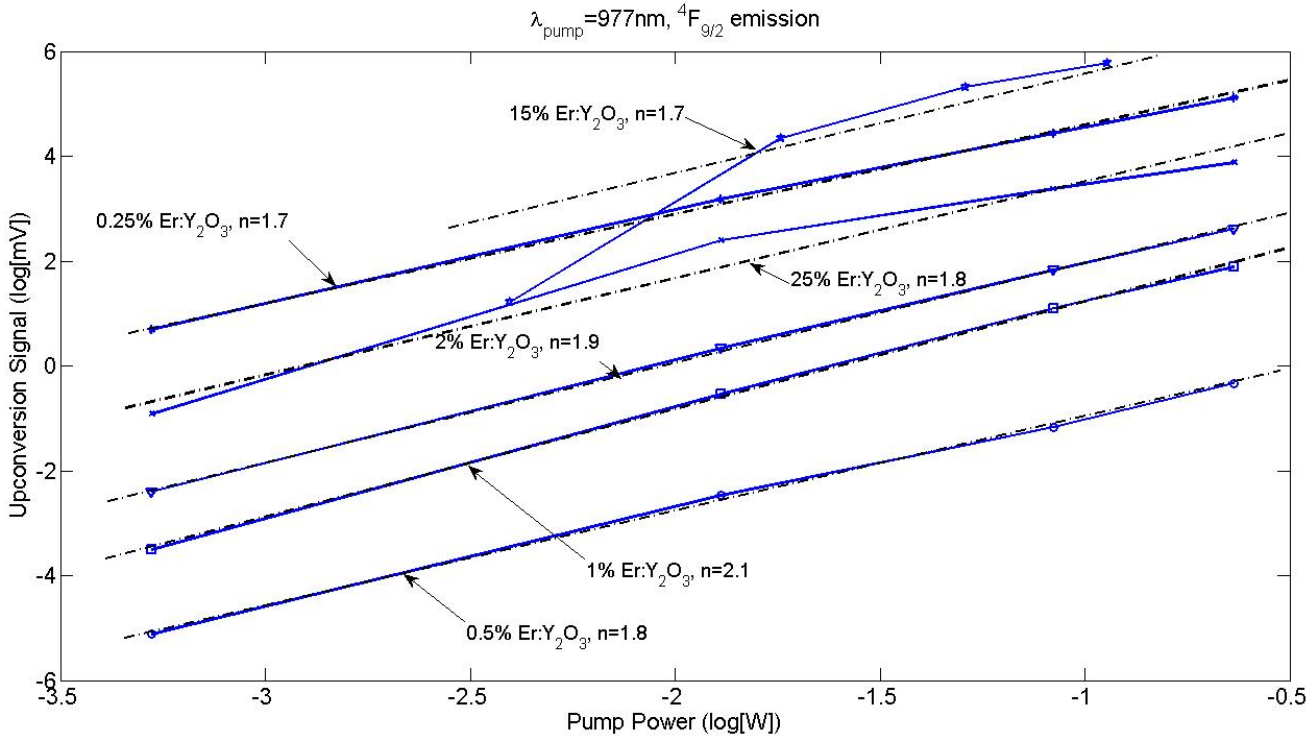

Figure 8.6: Power dependence of upconverted luminescence for the ${}^4F_{9/2} \rightarrow {}^4 I_{15/2}$ under the influence of pumping at 977nm ${}^4I_{15/2} \rightarrow {}^4 I_{11/2}$.

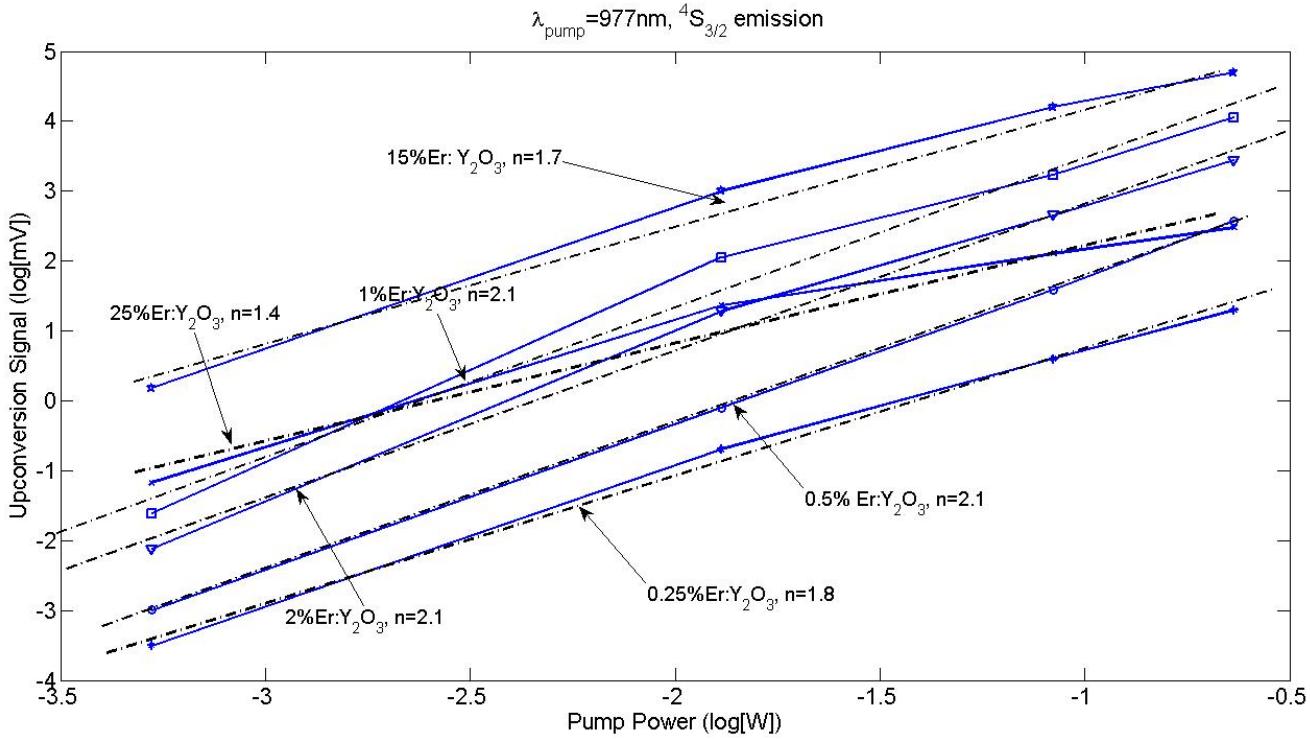

Figure 8.7: Power dependence of upconverted luminescence for the ${}^4S_{3/2} \rightarrow {}^4 I_{15/2}$ under the influence of pumping at 977nm ${}^4I_{15/2} \rightarrow {}^4 I_{11/2}$.

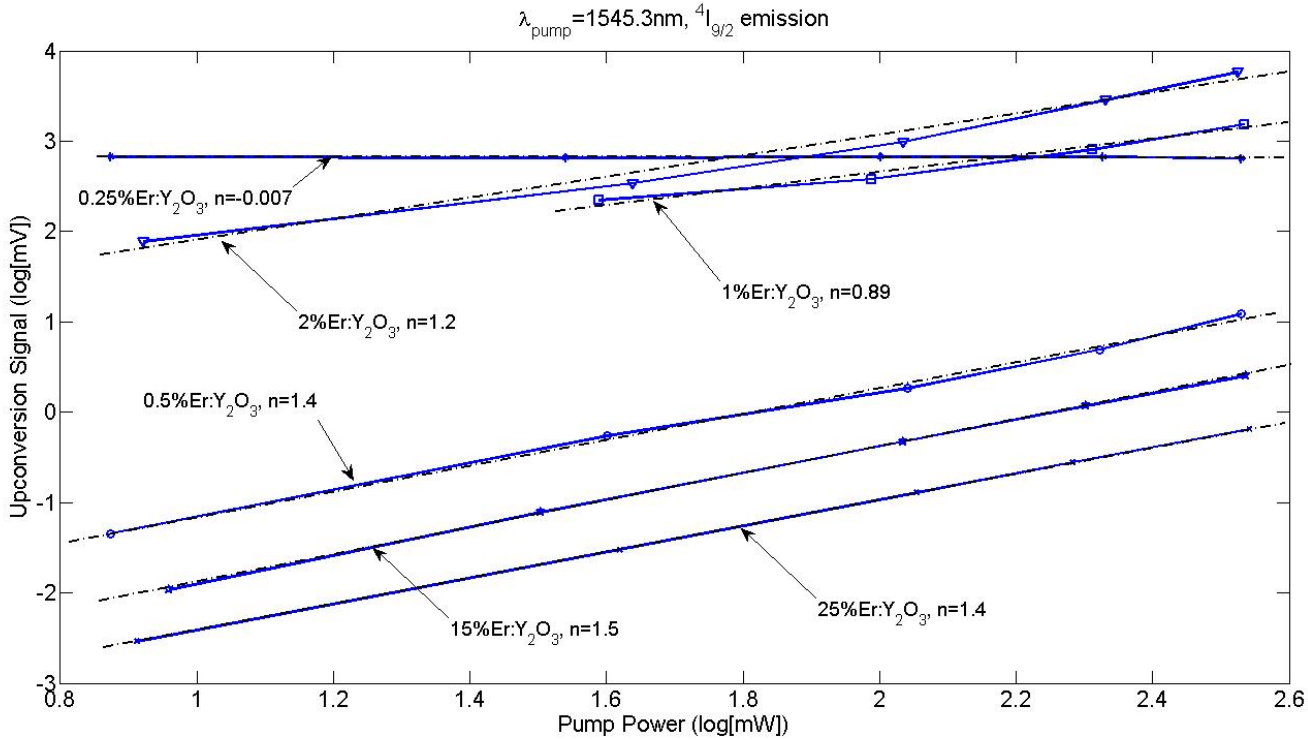

Figure 8.8: Power dependence of upconverted luminescence for the ${}^4I_{9/2} \rightarrow {}^4 I_{15/2}$ under the influence of pumping at 1545nm ${}^4I_{15/2} \rightarrow {}^4 I_{13/2}$.

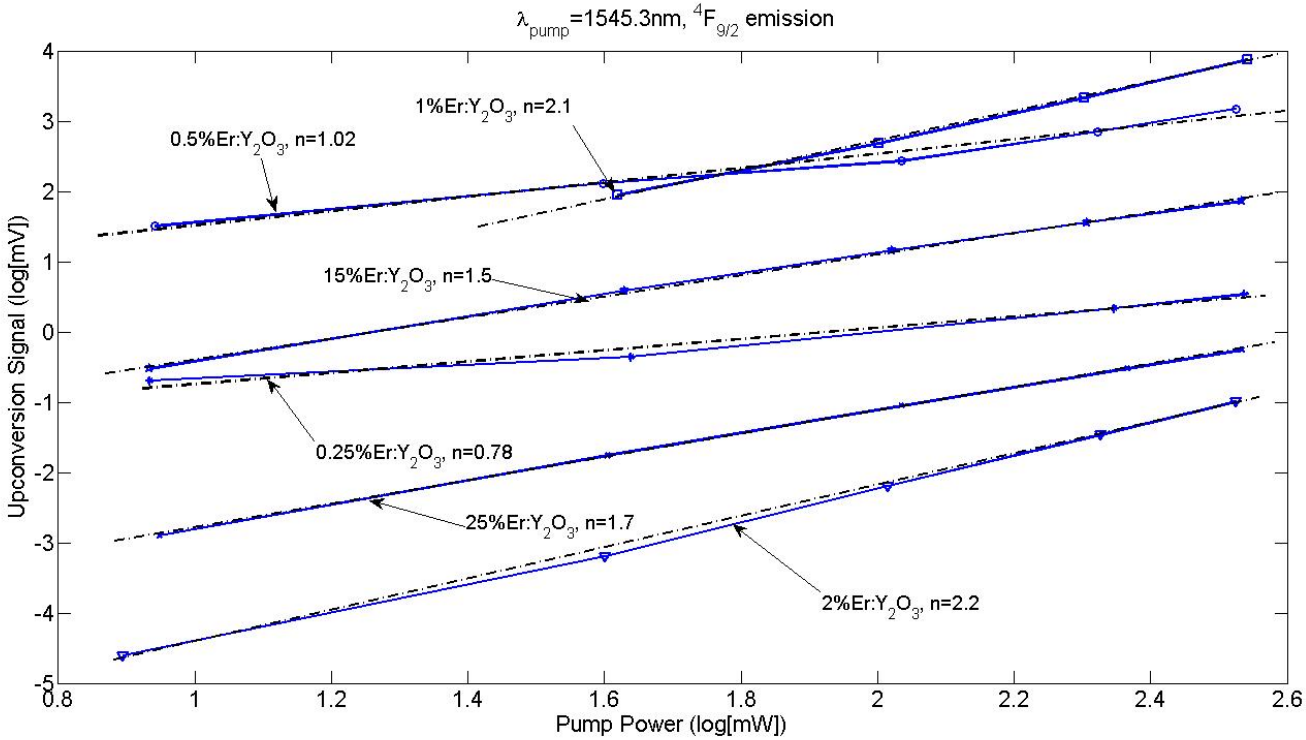

Figure 8.9: Power dependence of upconverted luminescence for the ${}^4F_{9/2} \rightarrow {}^4 I_{15/2}$ under the influence of pumping at 1545nm ${}^4I_{15/2} \rightarrow {}^4 I_{13/2}$.

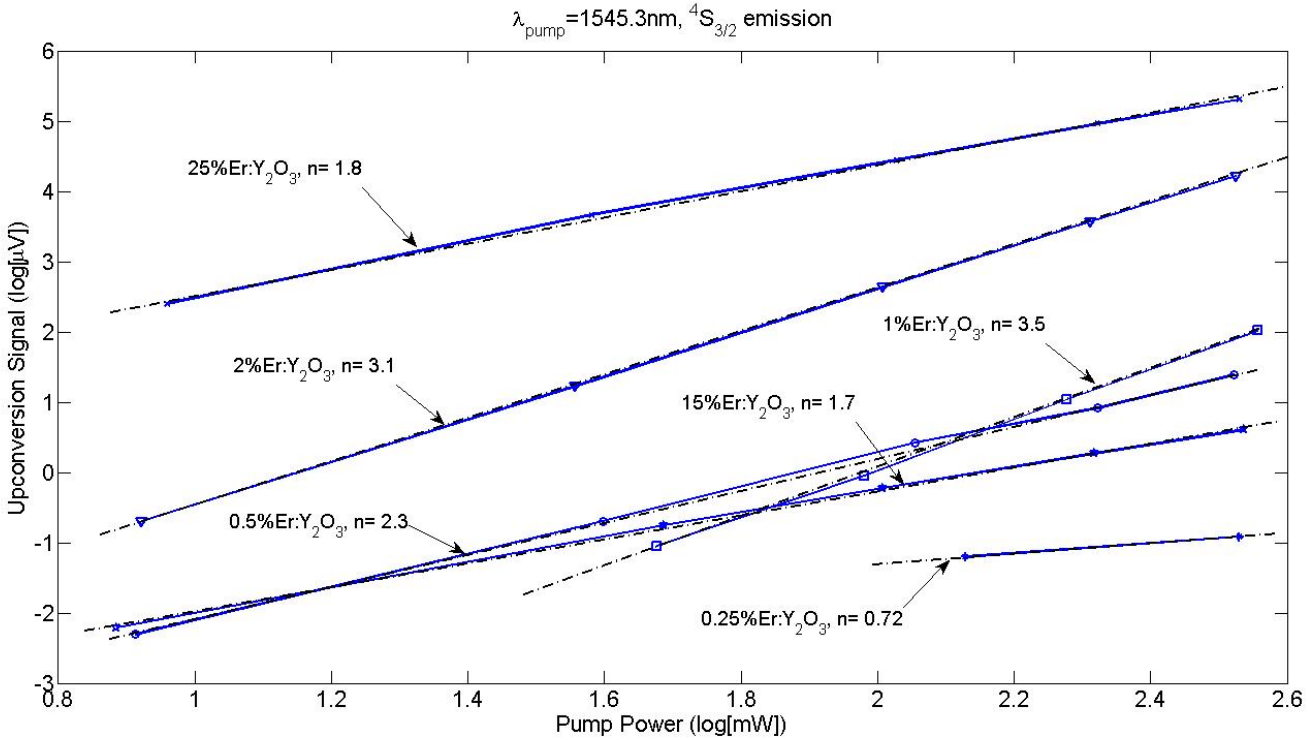

Figure 8.10: Power dependence of upconverted luminescence for the $^4S_{3/2} \rightarrow^4 I_{15/2}$ under the influence of pumping at 1545nm $^4I_{15/2} \rightarrow^4 I_{13/2}$.

References

[1] *Materials and devices using double-pumped-phosphors with energy transfer.*, F. E. Auzel, Proc. IEEE, vol. 61, pg 758, 1973.

[2] *Quantification and modeling of the dynamic changes in the absorption coefficient of water at λ =2.94 μm*, R. K. Shori, A. A. Walston, O. M. Stafsudd, D. Fried, J.T. Walsh, Jr., IEEE Journal of Selected Topics in Quantum Electronics, Volume 7, Issue 6, pgs 959-970, Nov/Dec 2001.

[3] *Er:YAG Three-Micron Laser: Performances and Limits*, Serban Georgescu and Octavian Toma, IEEE Journal of Selected Topics in Quantum Electronics, Vol. 11, No. 3, May/June 2005.

[4] *Effect of Yb^{3+} Codoping on the Upconversion Emission in Nanocrystalline $Y_2O_3 : Er^{3+}$*, F. Vetrone, J-C Boyer, J. A. Capobianco, A. Speghini and M. Bettinelli, The Journal of Physical Chemistry B, vol. 107, No. 5, Feb 2003.

[5] *Concentration-dependent near-infrared to visible upconversion in nanocrystalline and bulk $Y_2O_3 : Er^{3+}$* F. Vetrone, J-C Boyer, J. A. Capobianco, A. Speghini and M. Bettinelli, Chemical Materials, Vol. 15, pgs 2737-2743, April 2003.

[6] *Multiphonon-based comparison of erbium-doped yttria in large, fine grain polycrystalline ceramics and precursor forms*, A. Joshi, O. M. Stafsudd, K. Serivalsatit and J. Ballato, Optical Materials, Vol. 34, Issue 1, Nov. 2011, pgs. 9598.

[7] *Upconversion and Anti-Stokes Processes with f and d Ions in Solids*, F. Auzel, Chemical Reviews, Vol. 104, No.1, 2004.

[8] *Enhancement of Red Emission ($^4F_{9/2} \rightarrow^4 I_{15/2}$) via Upconversion in Bulk and Nanocrystalline Cubic Y_2O_3:Er^{3+}*,J. A. Capobianco, F. Vetrone, and J. Christopher Boyer,J. Phys. Chem. B, 2002, 106 (6), pp 11811187

[9] *Power Dependence of upconversion luminescence in lanthanide and transition-metal-ion systems*, M. Pollnau, D. R. Gamelin, S. R. Lüthi, H. U. Güdel and M. P. Hehlen, Physical Review B, Vol. 61, no. 5, Feb 2000.

CHAPTER 9

Explaining energy-transfer in Er^{3+}:Y_2O_3 using two pump wavelengths

Erbium ions in inorganic, insulating gain media show a wide variety emission wavelengths - including ultra-violet, visible (red, green and blue), near-IR (∼800nm, ∼980nm, ∼1550nm) and mid-IR (∼3000 nm). Erbium is an interesting ion providing multiple paths to emit multiple wavelengths. The energy levels corresponding to these wavelengths can be populated by converting lower-energy photons into higher energy photons by various energy-tranfer mechanisms. Different energy-transfer mechanisms may be present at different concentrations of erbium in the insulating host matrix. Some of these mechanisms are difficult to prove experimentally.

We present a study utilizing a dual-pump scheme to elucidate some of the energy-transfer mechanisms in erbium-doped ceramic yttria. The parameters controlled in this study were the concentration of the active ion, the pump wavelengths and pump power.

Apart from upconverting lasers, erbium doped hosts can be used to make phosphors for multiple uses. The results of the experiment show that, the efficiency of upconversion changes for different emission wavelengths as the concentration changes. This by itself in not however a novel deduction, Pollnau, Huber, Hehlen, etc. have shown such dependence before. We have shown that the emission of

certain wavelengths seem to move in concert as concentration changes. We believe this shows that some of the paths to upconverting low energy photons to higher energy ones in erbium are linked. These results may be further used to explain upconversion dynamics in erbium doped materials. The results help shed light on some of the more curious behavior of the erbium ion, such as why certain wavelengths should have a higher intensities of emission than other, perhaps preferred, ones.

9.1 Introduction

9.1.1 Pathways to upconvert low-energy photons to higher energy ones

Upconversion in activated rare-earth ions is a form of electronic energy transfer. Energy transfer was initially put forth in it's bare-bones form in relation to biological energy-transfers from a 'sensitized' molecule to an 'acceptor' molecule [1]. Förster expanded the above report when he proposed the theory of 'resonant transfer' between one sensitized molecule and an acceptor molecule. Energy is absorbed in one localized part while being liberated in a different part well separated from the other. The effect could be fluorescense or oxidative metabolism [2].

Förster cited the example of the fluorescing aromatic acids of proteins, tryptophane, tyrosine, and phenylanine where non-radiative energy transfer was recognized to be only reason fluorescence was seen in different parts of the molecule. Considering dipole-dipole interactions one arrives at following form of the energy-

transfer rate equation,

$$\Omega_{s\to a} \propto \frac{1}{r^6} \tag{9.1}$$

where, $\Omega_{s\to a}$ is the rate of energy-transfer and r is the distance between the molecules.

Dexter extended Förster's 1948 work, by formulating models that allowed the transfer of energy by forbidden transistions [3]. Forbidden resonant energy tranfer mechanisms are the primary models that are responsible for energy transfer in rare-earth ions doped in inorganic matrices. An ion with the allowed transition absorbs the incoming energy and causes an excitation (is 'sensitized'). The energy is then transferred, possibly, through multiple 'steps' eventually exciting the 'acceptor' ion, which may emit the higher energy photon. The transition, it should be noted, is forbidden due to the incongruency between the energies of the incoming radiation and the higher emitting energy-level (by direct absorption). For this process to occur there must be co-operative energy transfer between two ions or excited state absorption in a single ion, this is also known as upconversion.

Ion-pair resonance was then experimentally observed in the $PrCl_3$ system [4]. Here the $^3P_0$ energy level was directly excited and emission was seen from the $^3P_2$ energy level.

Margolis, *et al* [5] confirmed and revealed more anamalous emission out of $Ce^{3+} : PrCl_3$.

Resonance fluorescence was detected from the $^3P_0$ state when irradiated at a wavelengths where it well-known that a single Pr^{3+} does not absorb - wavelengths higher than the $^3P_2$ state [4]. This corresponded to the sum of the excitation energy of the emitting state and that of discrete lower excited states - a cooperative

mechanism. The results were subsequently confirmed by Margolis, *et al* [5]. This experiment also reported a 'simultaneous transition' or as we now recognize it 'co-operative' energy-transfer between two praseodymium ions - one ion was noted to been excited to the $^1G_4$ and the other to $^3P_0$. These are not normally observed in fluorescence measurements but can be seen with a large enough pump intensity.

Specific mechanisms were proposed to explain the observation by Dexter in 1962[6], including 'double' and 'triple' excitation. This included energy-transfer from an initial state to the final state, via an intermediate state. This presents the starting point for all subsequent energy-transfer mechanism studies.

Auzel's review papers, the first one in 1973 [7] and another one in 2004[8], effectively summarize our current understanding of energy transfer mechamisms. Excited State Absorption (ESA), Energy Transfer Upconversion (ETU), cross-relaxation into a level and complex multi-ion processes seem to be various ways of generating higher energy photons (see Figure (9.2)). ESA and ETU have been well addressed [9], [8]. There are many similarities between the two mechanisms, such as dependence on excitation density and n-photon order of upconversion. Moreover, nothing forbids both these models to be simultaneously operative [8]. This causes confusion in experimental circles. Experimental methods to distinguish between the two processes have not been sufficiently addressed. We here propose perhaps the beginning of such an experimental study.

While pathways are easily conjectured, they are not generally confirmed. Emission spectra and pump-power dependency often helps to complete the picture.

Largely, the evidence for these mechanisms rests on the number of electron excitation 'jumps' (n) needed to produce the emitted photon of the correct fre-

quency. This is usually put forth as,

$$I_{upconverted} \propto I_{pump}^{n} \tag{9.2}$$

where, $I_{upconverted}$ and I_{pump} are the intensities of the upconverted signal and the pump signal respectively. Pump-intensity (or more conveniently power) dependence of upconversion luminescence intensity is generally addressed by a log-log plot, with the slope giving us the number of steps taken to reach the higher energy levels. Pollnau, *et al* [9] addressed the issue with a simple model which has been used often in literature to explain upconversion in rare-earth ions. It relates the emitted population N to the number of steps needed for the emission. The model however only considers energy-transfer upconversion (ETU) and excited-state absorption (ESA).

One of the paths explored extensively has been the co-doping of specific 'sensitizer' atoms such as ytterbium in erbium-doped materials. This allows the experimentalist to target specific energy-levels with optical excitation and observe emission from energy-levels in the 'acceptor' ion.

The field continues to be guided by practical considerations even now such as the development of upconverting lasers and phosphors.

We present the use of two excitation sources that allow the population of specific energy-levels in the erbium-doped yttria matrix. Populations in certain energy-levels when modulated show changes in upconverted emission - this verifies the dependence of the intermediate states population on the upconversion mechanism.

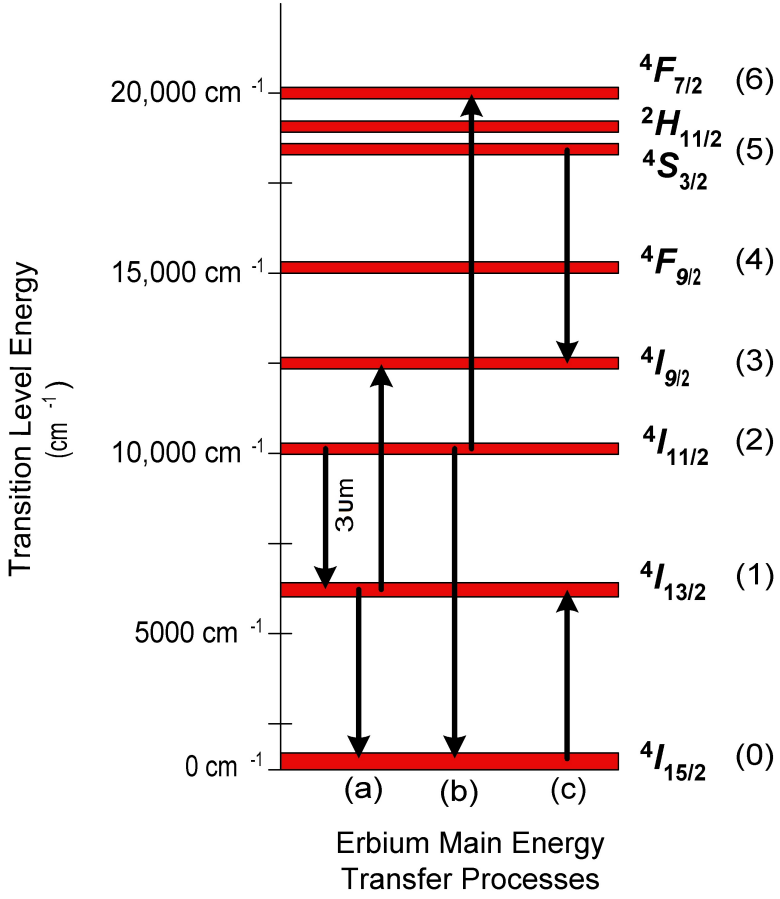

Figure 9.1: The main inter-ion energy tranfer processes in Er^{3+}.

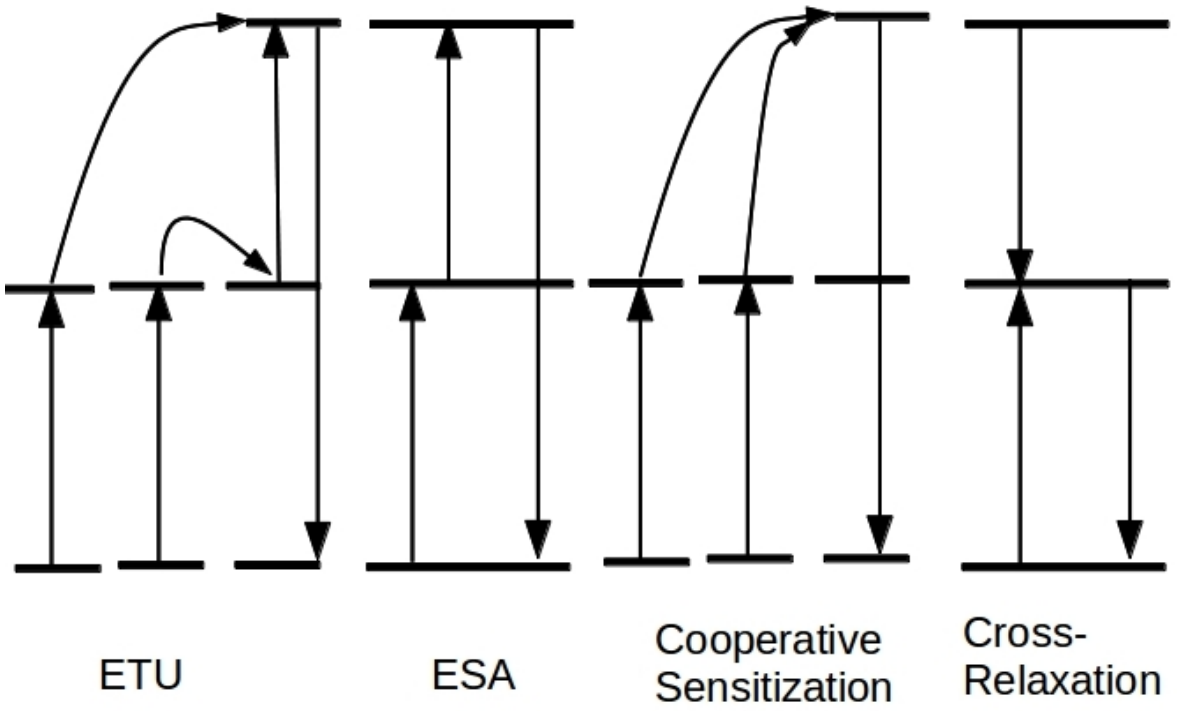

Figure 9.2: A summary of the known energy-upconversion mechanisms.

9.1.2 Feedback loops in RE energy-transfer

Until recently the experimental study of rare-earth energy-transfer systems has viewed the problem as a simplistic linear, time-invariant problem. As with all real-world systems these models provide a very weak commentary on the facts. It has been only recently that *feedback* has been suggested to be a component of such systems. Evidence stating the *abnormality* of 'n' values (especially 'n' values larger than expected or reasonably possible - [10]) was cited as giving credence to the new hetero-LEET *feedback* mechanism (Apart from that the experimental evidence is weak - until this study).

For instance, a larger than 'reasonable'n values - or couched in different terms evidence for emission of higher intensity light than expected seems to adequately evidence by n values of 5 or 8 (for instance) from the $^4I_{9/2}$ level under 980nm pump light ([10]). We should note that energy storage times drop dramatically at energy-levels higher than $^4F_{9/2}$ in this system due to increasing probability of thermal quenching at room temperatures and even heating due to pump.

It should be noted that this process is rooted in the photo-avalanche (PA) 'idea' of energy being stored in an intermediate level that spontaneously plays an important role in the upconversion mechanism. The implications of the new process being set in motion by a PA process are:

- There is a time-delay τ_δ for the onset of the energy-transfer effect that is typical of feedback systems
- There is an intermediate energy-level involved where energy is temporarily stored
- And that the energy may be transferred to a 'different' energy-level where it may manifest itself

These are all properties of feedback mechanisms - taken together it means that the *dynamics* of the normal and expected energy-downconversion is irreversibly changed - which is amply demonstrated by the larger or smaller than expected 'n' values. It also indicates, as is generally recognized in the class of feedback systems - the mechnisms are largely true for *all* rare-earth doped material systems regardless of the individual differences in energy-level parameters such as lifetimes, and oscillator strengths. Provided the active-ion is the same, we expect the system *dynamic* is the same. This allows us to study particular systems and apply the mechnisms to other material systems.

There are also positive and negative feedback mechnisms that enhance or dampen the system response. Anamalous behaviour of the 'n'-value for downconversion from certain energy-levels is again a indication of there being both positive and negative feedback mechnisms at play.

With an independent light source, as is used in this study, one may independently modulate the 'storage' energy-level allowing one to see negative and positive feedback machenisms separately. This is dicussed in detail further in this manuscript.

Following a similar track of reasoning, one would expect an increase in 'damping' mechanisms to dominate when the 'n' values are far below 1 and still produce upconverted radiation. Here 'damping' mechanisms would include resonant energy transfer to other energy-levels, or quenching mechanisms including cross-relaxation, etc.

The common ground in the argument is that either 'positive' or 'negative' energy feedback loops require an intermediate level, or perhaps more broadly set of levels that exchange energy, to play a significant role.

9.1.3 Quantitative Analysis

We expect the active ions to be homogeneously distributed in the ceramic material as compared to single-crystal hosts, where bunching is a known problem. The Er^{3+} and Y^{3+} occupy the same sites in the host yttria matrix.

Yttria occupies two sites in the yttria matrix : the non-centrosymmetric C_{2v} and the centrosymmetric C_{3i} site . Erbium substitutes into the yttrium site and of the two sites the C_{2v} site is optically active.

The relative populations of the substitutional active rare-earth ions in the Y^{3+} site have been studied in the electron paramagnetic resonance (EPR) community [11], [12]. The literature alludes to a random distribution in the two yttrium sites (1:1).

However other literature seems to provide divergent views on the population difference in the two sites it has also been reported that the proportions favor the optically active C_{2v} site ($C_{2v} : C_{3i}$=1:3) [13].

It is assumed for the following discussion that the distribution of active ions in the C_{2v} and C_{3i} is equal in proportion. The following table (9.1) [14] summarizes the crystal structure of the $Er^{3+} : Y_2O_3$.

From a pool of 99.75 at. wt. % Y^{3+} and 0.25 at. wt. % Er^{3+} there is a 0.25% chance of first finding a Er^{3+} ion and a 99.75% chance of finding a Y^{3+} ion. Of the erbium ions, we may assume half are in the optically active C_2 site. Consecutive probabilities multiply, therefore there is a $(0.0025 \times 0.9975^{11} \times 0.5)$ chance of having one Er^{3+} ion in an equivalent, optically active site. There are 12 possible positions for the Er^{3+} ion to be in the 12 coordinated sites. We thus get a total probability of,

Parameter	Property
Crystal Symmetry	body-centered cubic
Space Group	Ia3
Unit cell size	∼10.604 Å
Er^{3+} site symmetry	C_2, C_{3i}
Er^{3+}-Er^{3+} coordination	6@ 3.496 Å, 6@ 3.985 Å

Table 9.1: Properties of the $Er^{3+}Y_2O_3$ crystal structure.

$$P(1Er^{3+}) = 0.0025 \times 0.9975^{11} \times 0.5 \times 12 = 0.01459 \tag{9.3}$$

We expect the rate of energy transfer to drop off dramatically with distance (Eqn.9.1), this implies that the energy transferred from a cell not immediately next to the site being considered will have a muted effect on the energy-transfer mechanism.

Similarly there is a $((0.0025)^2 \times (0.9975)^{10} \times 0.5)$ chance of having two Er^{3+} in the coordinated, optically active equivalent sites. There are 66 possible poitions for the Er^{3+} ion in the 12 coordinated sites. Thus we get a total probabilty of,

$$P(2Er^{3+}) = (0.0025)^2 \times 0.9975^{10} \times 0.5 \times 66 = 0.0002 \tag{9.4}$$

The table (Tab. 9.2) gives the probabilities for finding single, pairs and triplets of erbium ions in 0.25%, 2% and 25% at. wt. erbium-doped yttria.

9.2 Dependence of upconversion radiation with varying concentrations of the active ion under pump wavelength $\lambda = 980nm$

Pump power-dependence of emission from the $^4S_{3/2}$, $^4F_{9/2}$ and $^4I_{9/2}$ energy-levels was measured while pumping the $^4I_{11/2}$ energy-level with the $\lambda = 977$nm. This experiment provides an important baseline for the dual-pump experiment that follows.

Erbium Concentration	Pr($1Er^{3+}$)	Pr($2Er^{3+}$)	Pr($3Er^{3+}$)
0.25%	1.459×10^{-2}	2.011×10^{-4}	1.6804×10^{-6}
2%	9.608×10^{-2}	1.079×10^{-2}	7.337×10^{-4}
25%	6.335×10^{-2}	1.116×10^{-1}	1.291×10^{-1}

Table 9.2: List of probabilities of finding 1, 2 or 3 active ions in a cluster. The cluster radius is limited to distances noted in 9.1 corresponding to direct erbium-to-erbium co-ordination.

9.2.1 Experimental

Nanocrystalline hot-isostatic pressed ceramic samples of varying concentration were subjected to 977nm radiation. The pump beam was chopped and a lock-in (EG&G) was used to collect the data.

The power-dependent measurements were done by using suitably picked band-pass filter combinations. The same detector was used for both experiments.

We had at our disposal 0.25%, 1%, 2%, 15% and 25% (at.wt.) doped Er^{3+} : Y_2O_3. These samples were procured from World Lab Co. Ltd., Japan.

9.2.2 Results

With the excitation around $\sim 1\mu$m, we expect excited electrons to require approximately 2 'jumps' to produce emission around 0.5μm. This can be verified from the data in Table (9.3) for green emission. The red emission also yields an n value of around 2.

The intensity of near-IR emission from the $^4I_{9/2}$ level yields n values around 0.3 for the relatively low-doped material. This however climbs to numbers slightly ≤ 1 for the highly doped samples where connectivity between the active ions is assumed to be high. This phenomena is the target of the second dual-pump experiment.

9.2.3 Discussion

The intensity of upconverted luminescence that is achieved by adding n pump photons is dependent on the pump intensity I^n_{pump}. The value of n may range from n for very little upconversion, to 1 for the upper state decay and ≤ 1 for very large upconversion rates for intermediate states providing the ground state

Table 9.3: Trend of upconversion per concentration when the active ion is pumped at 977nm.

	$^4S_{3/2}$	$^4F_{9/2}$	$^4I_{9/2}$
$0.25\%Er:Y_2O_3$	n=1.8	n=1.7	n=0.25
$0.5\%Er:Y_2O_3$	n=2.1	n=1.8	n=0.24
$1\%Er:Y_2O_3$	n=2.1	n=2.1	n=0.3
$2\%Er:Y_2O_3$	n=2.1	n=1.9	n=0.23
$15\%Er:Y_2O_3$	n=1.7	n=1.7	n=0.9
$25\%Er:Y_2O_3$	n=1.4	n=1.8	n=0.75

population [9]. The latter measure of upconversion implies a highly efficient transfer of electrons to the upper level that could be achieved by excited state absorption or some other energy-transfer mechanism.

The general scenarios given in [9] cover perhaps the simplest and the most likely means to upconversion, energy-transfer upconversion (ETU) and excited-state absorption (ESA). The other processes perhaps causing the significant deviation seen in this system transferring energy between levels include cross-relaxation and three-ion energy transfer processes. These processes rely on the presence of neighbors within 'talking' distance and are bound to be enabled as the concentration increases.

The model generally applied to evaluate the number of steps required for upconverted emission relies primarily on the ESA and ETU mechanisms, cross-relaxation mechanisms of populating levels are not included. As a result, the model is largely unsuitable to study upconversion in erbium where cross-relaxation mechanisms seem to be important. But deviations from the model are perhaps useful to gauge the influence of cross-relaxation in the system. The power dependent measurements yield the upconversion step value ('n').

For the 977 nm pump, surprisingly, the analysis results in similar 'n' values for emission from both the $^4S_{3/2}$ and the $^4F_{9/2}$ energy-level for a large range of concentrations. Except for highly doped samples the upconversion step value is close to 2, which implies a two-step upconversion pathway made possible largely via ETU or ESA. The 'n' number of steps taken cannot, as understood in the conventional sense, be the same for both emissions in the red and green regions.

The argument for the $^4I_{9/2}$ level's lower than 1 'n'-value is however less clear. The 'n'-value for the $^4I_{9/2}$ energy-level seems to approach 1 around the $15\%Er : Y_2O_3$ mark. We conclude that the processes populating the $^4I_{9/2}$ energy-level rely

on a high number of erbium neighbors for efficient upconversion, this hints at cross-relaxation and multiple ion processes being operative. We shall see further on that the $^4I_{9/2}$ energy-level plays an important role in upconversion to the higher energy manifolds.

9.3 Dual-pump experiments. Continuous pump at λ =980nm, modulated pump at λ =1550nm

9.3.1 Experimental

The dual-pumping experiments were devised to discover pathways to upconversion. The experiment involved monitoring the emission fluorescence magnitudes from the $^4S_{3/2}$ ($\lambda =\sim$ 540nm) , $^4F_{9/2}$ ($\lambda =\sim$ 680nm) and $^4I_{9/2}$ ($\lambda =\sim$860nm) under the influence of lower energy pumps near-IR pumps.

The modulated pump experiment is based on the following: we can change the relative population difference in either the $^4I_{11/2}$ state or the $^4I_{13/2}$ state directly by cw pumping with the $\sim$ 980 nm pump and the $\sim$ 1550nm pump respectively. We may modulate either one of these pumps. With the modulated beam at fixed power, we can then upconvert and cause inversion in the higher energy levels. By using a lock-in amplifier in the setup, we collect the upconverted emission that is a direct effect of the modulated beam. But since the population in a level affected by the cw pump may have changed, we could see a corresponding change in the upconversion emission due to the modulated beam. This would prove the involvement of the energy level affected by the cw pump.

For instance, population was pumped into the $^4I_{11/2}$ energy-level directly with the 977nm pump (λ_{cw}) running continously reasonably ensuring available ions for upconversion $from$ $^4I_{11/2}$; the 1545nm pump ($\lambda_{modulated}$) was thereafter intro-

duced enabling upconversion from ${}^4I_{13/2}$ to the higher energy levels. $\lambda_{modulated}$ was mechanically chopped, while λ_{cw} was not, and the signal was collected by a broad-band photomultiplier tube (Hamamatsu R636) after conditioning through a lock-in amplifier (EG&G).

Since $\lambda_{modulated}$ was chopped and the reference supplied to the lock-in amplifier, the effect of $\lambda_{modulated}$ was monitored against a background of the sample being continously pumped by the cw pump.

The roles of λ_{cw} and $\lambda_{modulated}$ were thereafter switched, and the effect of first wavelength against a constant availability of inverted electrons in energy level ${}^4I_{11/2}$ was measured. This was repeated for the varying concentrations of erbium in the ceramic. No noticable trends were seen with this arrangement.

The powers available for the two pumps were very different (1545nm has a maximum output of $\sim$ 25mW, and the 977nm laser was used with a maximum power around 1W), the results therefore provide a qualitative description of the upconversion pathways. This information is nonetheless useful as the first step in discovering and confirming the upconversion pathways in the erbium ion. See figure (9.3) for the experimental setup. Further studies along the same lines with comparable pump powers might provide quantitative data regarding the amount of upconversion through various paths.

9.4 Results and Discussion

To simplify the following summary and discussion, we assume that upconversion has no or a negligibly small time delay associated with it compared to mudulation frequency. Also, we note that compared to the lifetimes of the pumping levels the energy levels populated by upconverted electrons have lifetimes that are small.

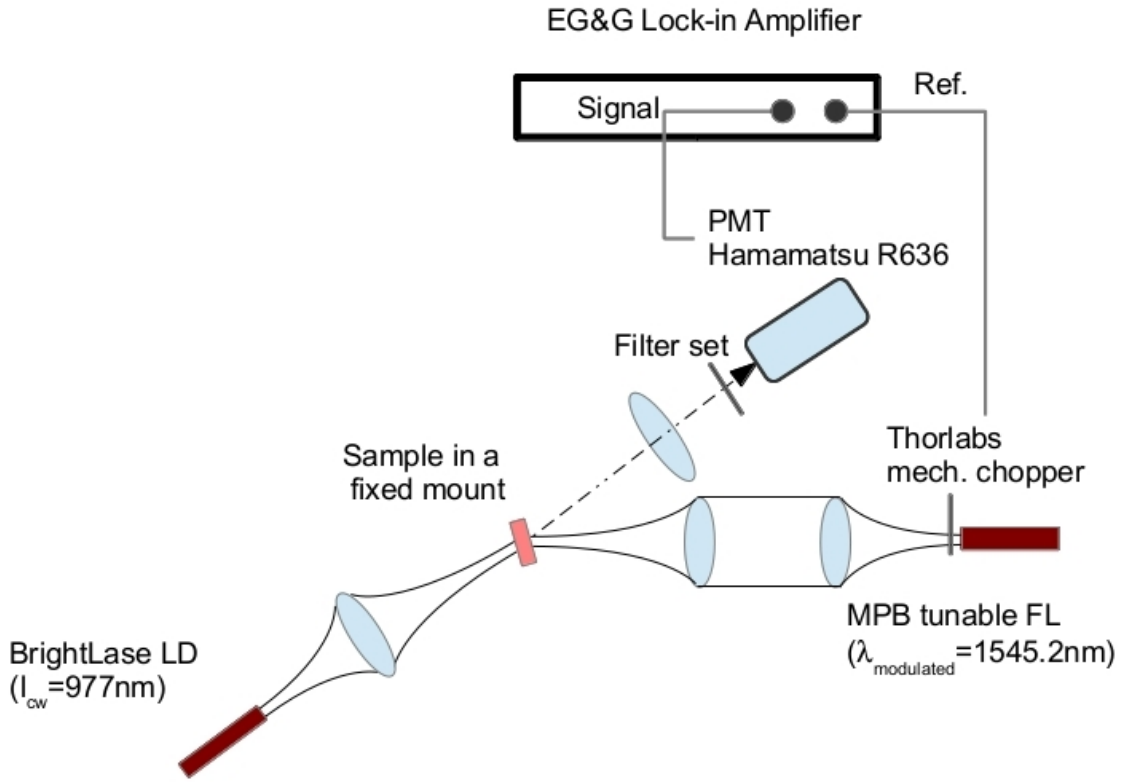

Figure 9.3: Sketch of the experimental setup.

The lifetimes of ${}^4S_{3/2}$ and ${}^4F_{9/2}$ state have been measured in nanocrystalline erbium-doped yttria [15] (around 11μs for ${}^4S_{3/2} \rightarrow {}^4 I_{15/2}$ and $\leq 7\mu$s for ${}^4F_{9/2} \rightarrow {}^4 I_{15/2}$, for $\leq 1\%$ active ion) at various concentrations of the active ion, these lifetimes are orders of magnitude faster than the decays for the ${}^4I_{11/2}$ and ${}^4I_{13/2}$ states.

We've measured the lifetimes for the ${}^4I_{11/2} \rightarrow {}^4 I_{15/2}$ and ${}^4I_{13/2} \rightarrow {}^4 I_{15/2}$ transitions for varying concentrations in the bulk form and have found them to be in the millisecond scale. The lifetimes for the ${}^4I_{11/2} \rightarrow {}^4 I_{15/2}$ range from $\geq$10ms for low doping to $\sim$0.03ms for highly doped and, the lifetimes for the ${}^4I_{13/2} \rightarrow {}^4 I_{15/2}$ range from $\sim$2ms to $\sim$0.01ms [16].

As might be readily seen, the longer the lifetime of a particular energy-level the higher the chance an excited atom has to get doubly or even triply excited. The lifetimes of these states is critical to the upconversion process.

We see no evidence of thresholding effects under normal (single-pump) upconversion experiments. Thresholding is understood to be a sign of photon-avalanche effects. We base the following discussion on ESA, ETU, cross-relaxation and other multiple-ion processes such as cooperative sensitization and concentration quenching [8].

At a low doping percentage, we expect the erbium ion to be fairly well segregated from the neighbouring active ions. All upconversion processes are within the isolated erbium ions. We see that at a doping level of 0.25% there is no noticable effect from having a population available in the ${}^4I_{11/2}$ energy level. See figure (9.4). Upconversion here is a simple process where inverted electrons from the ${}^4I_{13/2}$ energy level are simply further inverted to either the ${}^4I_{9/2}$ energy level producing the near-IR emission or the ${}^4S_{3/2}+{}^4H_{11/2}$ energy levels producing green emission. Once the latter energy level is 'activated', it enables the production of

red emission from the ${}^4F_{9/2}$ energy level after the emission of a suitable photon.

At concentrations where there is appreciable communication between the active ions (2% and 25% $Er^{3+} : Y_2O_3$) we see that the background interferes with the pump revealing some of the pathways directly.

Consider the $2\%Er^{3+} : Y_2O_3$ sample: emission from the ${}^4S_{3/2}$ level shows an increase in upconverted photons once the continous-wave 'background' pump is at some appreciable power level. Emission from the ${}^4F_{9/2}$ level also shows an increase with an increase in the 'background' pump. On the other hand, there is no change in the emission from ${}^4I_{9/2}$ level. See figure (9.5). Together these results shows the involvement of the ${}^4I_{9/2}$ level in generating visible photons. A mechanism such as : ${}^4I_{9/2} \rightarrow {}^4 I_{13/2} + {}^4 I_{9/2} \rightarrow {}^2 H_{11/2} + {}^4 S_{3/2}$ suggests itself. This would be consistent with a two-ion process which is more likely in a sample doped at 2%.

At a concentration of 25%, we note a sharp drop in the ${}^4I_{9/2}$ (near-IR emission) and ${}^4S_{3/2}$ (green emission), with a corresponding increase in emission from ${}^4F_{9/2}$, see figure (9.6). We expect at this concentration substantial 'communication' between the active ions. The cw pump-aided processes such as: ${}^4I_{15/2} \rightarrow {}^4 I_{11/2} + {}^2 H_{11/2}, {}^4 S_{3/2} \rightarrow {}^4 I_{11/2}$ would reduce the green emission. Emission from the ${}^4F_{9/2}$ level might also decrease due to ${}^4F_{9/2} \rightarrow {}^4 I_{13/2} + {}^4 I_{15/2} \rightarrow {}^4 I_{11/2}$ filling up both the upper and lower level of the mid-IR $\sim 2.7\mu m$ laser; but this is a minor effect.

When the concentration is as high as 25% we expect that every active ion is amply surrounded by other active ion facilitating cross-relaxation and co-operative mechanisms. We cannot ascertain a trend that relates to the 977nm pump in anyway in presence of the 1545nm background.

It follows that for the lowest doping concentration, 0.25%, there is a high probability of the activated ion being isolated. This supports our assumption that

the upconversion processes are largely within the single ion. Similarly, the energy-transfer processes in the 2% doped sample also largely occur within the single-ion, although the effect of two erbium ions exchanging energy due to proximity is possibly comparable (due to comparable probabilities) to the low doped, single-ion processes. The deviations seen are then perhaps due to an over-weighted effect of two-ion processes. The 25% Er^{3+}:Y_2O_3 shows comparable probabilities for two and three ion coordinated erbium ions. The energy transfer effects are an indicaton that these may be ≥ 2 ion processes.

9.5 Conclusion

A concentration dependent study of upconverted luminescence from erbium's $^4S_{3/2}$, $^4F_{9/2}$ and $^4I_{9/2}$ energy levels in yttria has provided enough reason to pursue a further investigations to explain intra/inter-ion (depending on the co-ordination number) energy transfer paths. The pathways maybe deduced by taking the dual-pump experiment together with the qunatitative model developed earlier (see figure (9.7)). Using a two pump scheme we may change the populations of intermediate energy-levels (in this case the $^4I_{13/2}$ energy-level using the 1545nm pump) and monitor the dependence of upconversion due to the 977nm pump. We may pick up the effect of the intermediate level ($^4I_{13/2}$), and thus pick out the exact upconversion pathways at varying concentrations.

As expected upconversion mechanisms change with an increasing concentration of the active ion. At low enough doping concentrations (such as 0.25%) the system is a single-ion system. At higher concentrations (2% and 25%) we see increasing effects of two-ion and multiple ion effects (see Section on Quantitative Analysis).

We note a common trend in increase in upconversion luminescence with an increase in erbium concentration from the $^4F_{9/2}$ and $^4I_{9/2}$ levels hitherto overlooked by the community.

With the 980nm pump modulated, we note a concerted decrease in signal from the $^4I_{9/2}$ and $^4F_{9/2}$ energy-levels at a concentration of 25%. At the intermediate 2% concentration, we note little change in the near-IR upconverted emission, and a corresponding increase in the visible emission. A simple mechanism however is elusive. At the lowest concentration level, the only trend is a near-linear increase in the red emission from the $^4F_{9/2}$ energy-level. The following pathway seems evident: $^4I_{15/2} \rightarrow^4 I_{13/2}$ followed by $^4I_{13/2} \rightarrow^4 F_{9/2}$. Also, the unsuitability of the current model to explain the luminescence from the above levels is discussed. Cross-relaxation is also conjectured to play a major role in transferring energy to both the levels.

Erbium-doped ceramic lasers show great potential to replace current single-crystal lasers in technologically significant telecommunication and medical fields. Erbium yttria also has been widely studied over the last few years as a upconverting phosphor. Given the above results regarding effect of concentration on emission from erbium-doped yttria, further work needs be done in order to conclusively prove the upconversion pathways in the ceramic material.

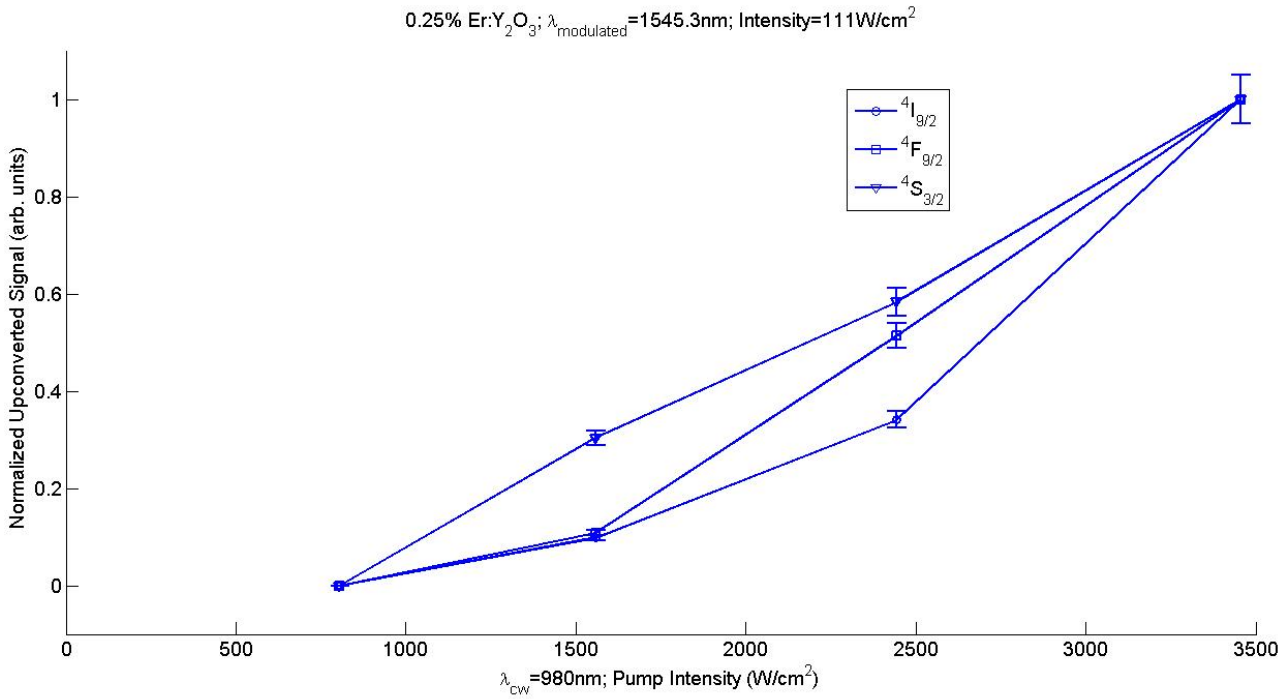

Figure 9.4: Power dependence of upconverted luminescence from ${}^4S_{3/2}$, ${}^4F_{9/2}$ and ${}^4I_{9/2}$ energy levels for $0.25\% Er^{3+}$ doped Y_2O_3. The data presented corresponds to the effect of a modulated 1550nm pump as the population in the ${}^4I_{11/2}$ energy level is increased.

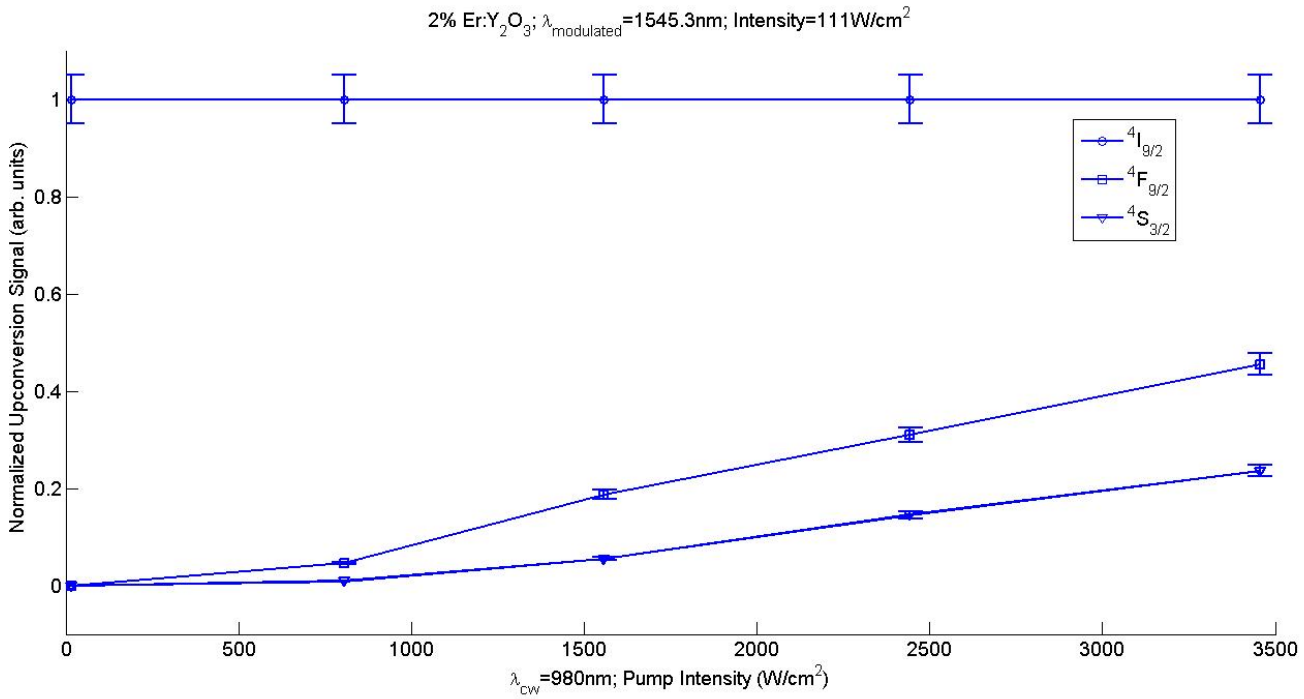

Figure 9.5: Power dependence of upconverted luminescence from ${}^4S_{3/2}$, ${}^4F_{9/2}$ and ${}^4I_{9/2}$ energy levels for $2\% Er^{3+}$ doped Y_2O_3. The data presented corresponds to the effect of a modulated 1550nm pump as the population in the ${}^4I_{11/2}$ energy level is increased.

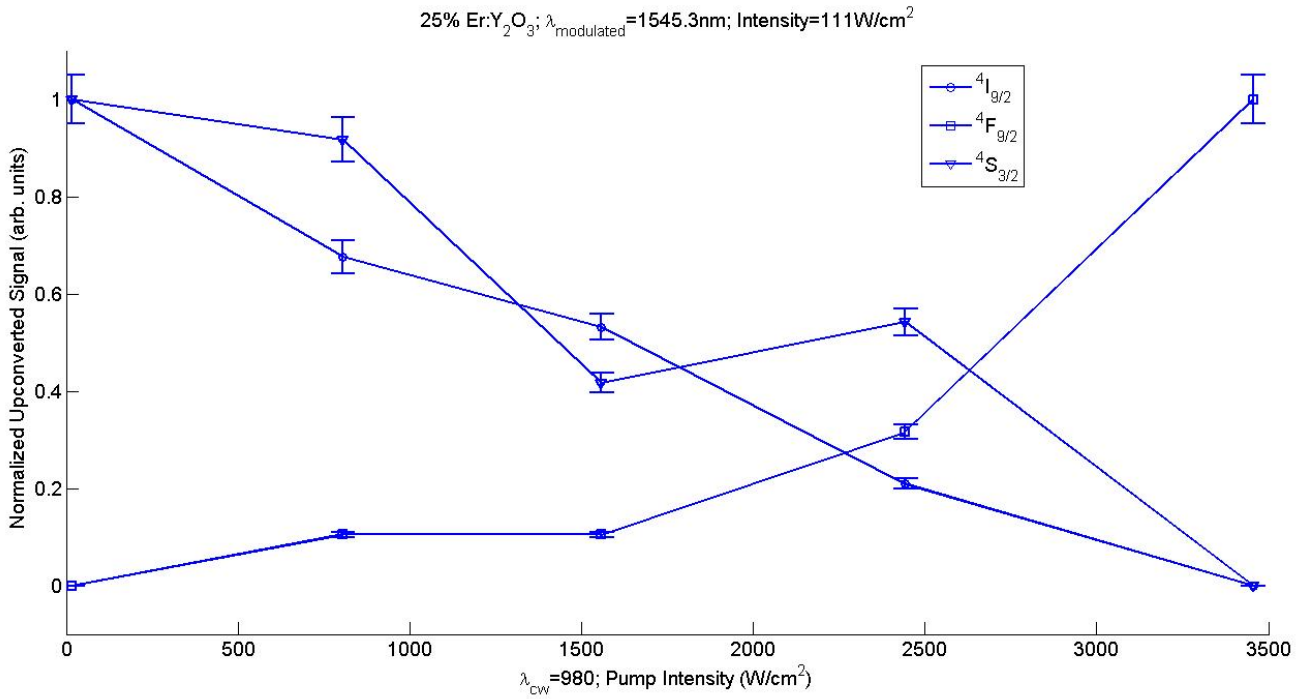

Figure 9.6: Power dependence of upconverted luminescence from ${}^4S_{3/2}$, ${}^4F_{9/2}$ and ${}^4I_{9/2}$ energy levels for $25\%Er^{3+}$ doped Y_2O_3. The data presented corresponds to the effect of a modulated 1550nm pump as the population in the ${}^4I_{11/2}$ energy level is increased.

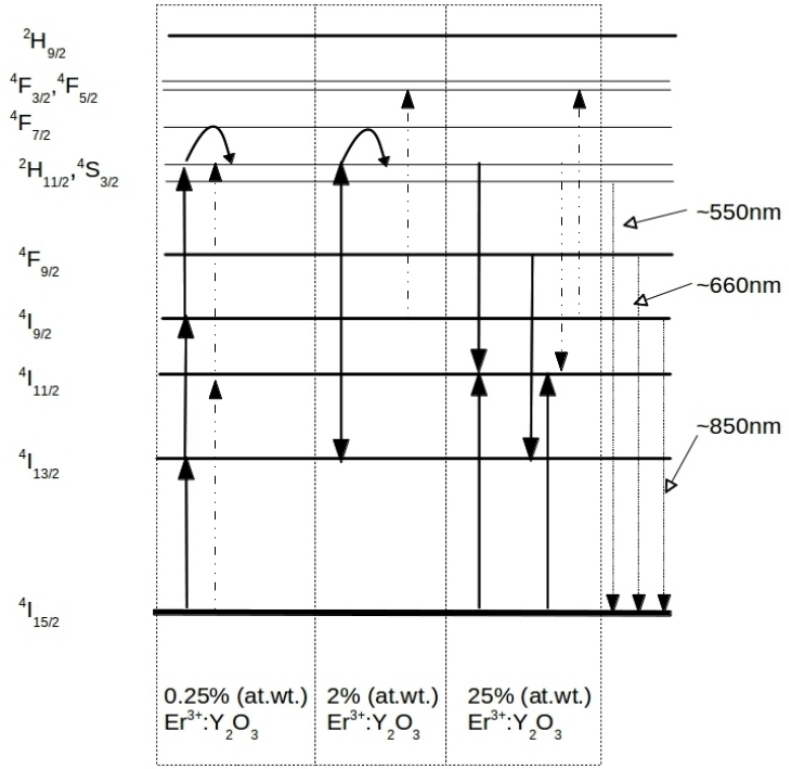

Figure 9.7: Laser absorption pathways. The pathways maybe deduced by considering both the dual-pump experiments and the simple probabilistic model (see Section on Quantitative Analysis). The solid paths refer to absorption pathways corresponding to the 980 pump. The dashed paths correspond to the 1550nm laser radiation.

References

[1] *Intermolecular energy transference and fluorescence*(In German), Th. Förster, Ann. Physik. Vol. 2, Issue 1-2, pgs: 55-75 (1948).

[2] *Transfer Mechanisms of Electronic Exitation Energy*, Th. Förster, Radiation Research Supplement, vol. 2, pgs: 326-339, (1960).

[3] *A theory of sensitized luminescence in solids*,D. L. Dexter,The Journal of Chemical Physics, Vol. 21 Issue 5 pg: 836 (1953).

[4] *Ion-Pair Resonance Mechanism of Energy Transfer in Rare Earth Crystal Fluorescence*, F. Varsanyi and G. H. Dieke, Physical Review Letters,Vol. 7, pgs: 442443 (1961).

[5] *Fluorescence in Mixed Crystals of Ce:$PrCl_3$*, J. S. Margolis, O. M. Stafsudd and E. Y. Wong, Journal of Chemical Physics, Vol. 38, pgs: 2045-2046 (1962).

[6] *Cooperative Optical Absorption in Solids*,D. L. Dexter,Physical Review, vol. 126, Issue 6, pp. 1962-1967.

[7] *Materials and devices using double-pumped-phosphors with energy transfer* , F. Auzel, Proc. IEEE, vol. 61, pg 758, 1973.

[8] *Upconversion and Anti-Stokes Processes with f and d Ions in Solids*, F. Auzel, Chemical Reviews, Vol. 104, No.1, 2004.

[9] *Power Dependence of upconversion luminescence in lanthanide and transition-metal-ion systems*, M. Pollnau, D. R. Gamelin, S. R. Lüthi, H. U. Güdel and M. P. Hehlen, Physical Review B, Vol. 61, no. 5, Feb 2000.

[10] *Near-Infrared (NIR) to Red and Green Up-Conversion Emission from Silica SolGel Thin Films Made with $La_{0.45}Yb_{0.50}Er_{0.05}F_3$ Nanoparticles, Hetero-Looping-Enhanced Energy Transfer (Hetero-LEET): A New Up-Conversion Process*

[11] *The rare earth ion distribution in mixed rare earth-yttrium sesquioxides*, D. Rodic, B. Antic and M. Mitric, Journal of Magnetism and Magentic Materials vol 140-144, pgs: 1181-1182 (1995).

[12] *Determining the site preference of trivalent dopants in bixbyte sesquioxides by atomic-scale simulations*, C. R. Stanek, K. J. McClellan, B. P. Uberuaga, K. E. Sickafus, M. R. Levy and R. W. Grimes, Physical Review B, vol. 75, 134101, (2007).

[13] *Optical spectra, energy levels, and crystal-field analysis of tripositive rare-earth ions in Y_2O_3. IV. C_{3i} sites*, J. B. Gruber, R. P. Leavitt, C. A. Morrison and, N. C. Chang, J. Chemical Physics, vol 82, pg: 5373, (1985).

[14] *Correlation between luminescent properties and local coordination environment for erbium dopant in yttrium oxide nanotubes*, Y. Mao, J. Bargar, M. Toney, J. P. Chang, Journal of Applied Physics, vol. 103, 094316, (2008).

[15] *Synthesis, Morphology, and Optical Chracterization of Nanocrystalline $Er^{3+}:Y_2O_3$*, S. Chandra, F. L. Deepak, J. B. Gruber, and D. Sardar, Journal of Physical Chemistry C, vol 114 (2), pgs: 874-880, (2010).

[16] *Chapter 'Concentration dependent spectroscopic properties of bulk ceramic $Er^{3+}:Y_2O_3$'*, A. Joshi, Part of this PhD Dissertation, UCLA, 2012.

CHAPTER 10

Conclusion

This thesis is a compilation of some of the many pieces of research that need to be considered together to provide a complete picture to a researcher evaluating the suitability of a new candidate optical material. Herein we have provided the newest results in the study of ceramic hosts for solid-state laser engineering purposes.

The refractive index was measured for varying concentrations of the active ion in the host along with first results on the refractive index of the pure ceramic. The Sellemeier formulae provided, should be of significant use to the laser engineer constructing this system, for dispersion affects the Fresnel diffraction losses significantly at the face of the laser rod. Knowledge of the amount of dispersion also will aid cavity designers with critical beam path alignment information. Since it is evident that the substitutional erbium ion causes a linear increase in the dielectric constant (by the effective medium theory), one may easily estimate with some accuracy the index of any doping concentration. We provide this information at various wavelengths in the range extending from the visible to the mid-IR.

The stress-optic coefficients provided will be of value to engineers calculating the effect of high thermal loads on this material during high-power laser operation.

Another critical piece of information are the transmission and emission spec-

tra in the near-IR region. This is the region of pumping for the mid-IR transition at the H_2O molecule vibrational resonance. Multiple spectra have been provided for the near-IR transition as well, showing the effects of concentration on the transmission and emission spectra. An increase in concentration most certainly broadens the absorption lines, but can ruin emission at high enough doping levels in the ceramic host material. Due to the nature of the production of the ceramic hosts, we expect a homogeneous distribution of the dopant in the host this concentration dependent data allows us to conjecture an increase in cross-relaxation between the erbium ions, simply due to an increase in yttrium substitution by erbium in the bixbyte unit cell.

The mid-IR spectra is of importance due to the possibility of lasing some of these lines. We see evidence of emission at the $Er : YAG$ wavelength of $2.936\mu m$ implying we may have an important laser gain media at hand suitable for high-power operation. The absorption and emission cross-sections provided will be of value to researchers working on improving the materials system from the materials stand point. Newer, more accurate Judd-Ofelt parameters are also provided, these add to the extensive literature base for solid state laser materials based on rare-earth elements.

Some temperature dependent studies have also been conducted. Multi-phonon studies provide a good way to evaluate the temperature dependence of laser gain media. The theory outlined above provides a simple evaluation methodology to a metric to gauge how much energy has been converted from optical photons to optical phonons. Some of the results of the multi-phonon study have been slated as being slightly deviant from expectation, and clearly more experimental and theoretical work needs to be done in this area.

Upconversion and energy-transfer was another topic studied. This data and

analysis is of value to scientists who study the intricacies of improving performance by carefully controlling doping levels or adding other dopants to improve absorption at particular wavelengths. Also controlling energy distribution amongst the many lasing levels that erbium provides is important to enhance the generation of certain wavelengths over others. The analysis provided should be useful in that we provide some pathways for transferring energy from one energy level to another.

This thesis concludes a four year-long series of experiments and analysis and is part of an effort to try to characterize ceramic hosts for solid-state lasers.

CHAPTER 11

Future Work

The work presented in this thesis not only reached the conclusion signified by the quantification of particular fundamental values such as absorption and emission wavelengths and spectra, stress-optic behavior, refractive index, multiphonon behavior, up-conversion behavior from certain energy-levels in erbium and to a certain extent energy-transfer, but also opened avenues of further study. And also the possibility of developing newer more sophisticated devices based around particular phenomena that is observed not only in erbium-doped yttria ceramics, but also other oxide hosts.

Chapter #9 details the pursuit of intra-ion energy-transfer pathways in a concentration dependent study of up-converted luminescence from erbium's $^4S_{3/2}$, $^4F_{9/2}$ and $^4I_{9/2}$ energy levels. Trends were noticed with the change in concentration of the active-ion in energy-levels not hitherto reported - $^4F_{9/2}$ and $^4I_{9/2}$.

But what we showed most prominently is that we could manipulate the emission signals dramatically from particular energy-levels by changing minutely (comparative power of the pump) the number of photons in one of the energy-levels in the *energy-transfer pathway* using the dual-pump scheme.

This discovery could potentially revolutionize our ability to enhance or diminish the emission signal of particular - technologically important - wavelengths using multiple pump wavelengths targeting different energy-levels in the path.

Consider for instance the generation of green ($^4S_{3/2} \rightarrow^4 I_{15/2}$) from the sample doped at 2% at. wt. The near-IR emission hardly changes - it is independent of the $\sim 980nm$ pump. Red emission from the $^4F_{9/2}$ energy-level also moves in concert with the emission from the $^4S_{3/2}$ level under direct, continuous pumping of the 980nm pump and modulation of the $^4I_{13/2}$ energy-level by the second pump at 1550nm. (See figure 11.1). Or the relative increase in emission from the $^4F_{9/2}$ when the doping is higher and the supresssion of emission from $^4I_{9/2}$ and $^4S_{3/2}$, under the same conditions.(See 11.2). This proves that pathways, when modulated by modulating populations in particular energy-levels, affect the *feedback mechanisms* that drive the intra-ion energy transfer mechanisms.

Apart from upconverting lasers, erbium doped hosts can be used to make phosphors for multiple uses. The results of the experiment show that, the efficiency of upconversion changes for different emission wavelengths as the concentration changes. This by itself in not however a novel deduction, Pollnau, Huber, Hehlen, etc. have shown such dependence before. We have shown that the emission of certain wavelengths seem to move in concert as concentration changes. We believe this shows that some of the paths to upconverting low energy photons to higher energy ones in erbium are linked. These results may be further used to explain upconversion dynamics in erbium doped materials. The results help shed light on some of the more curious behavior of the erbium ion, such as why certain wavelengths should have a higher intensities of emission than other, perhaps preferred, ones.

11.1 *"..we've now opened the can"-OMS*

We've now proved a method to probe the intricacies of intra and inter-ion energy transfer in erbium doped materials. The crux of the matter is the modulation of

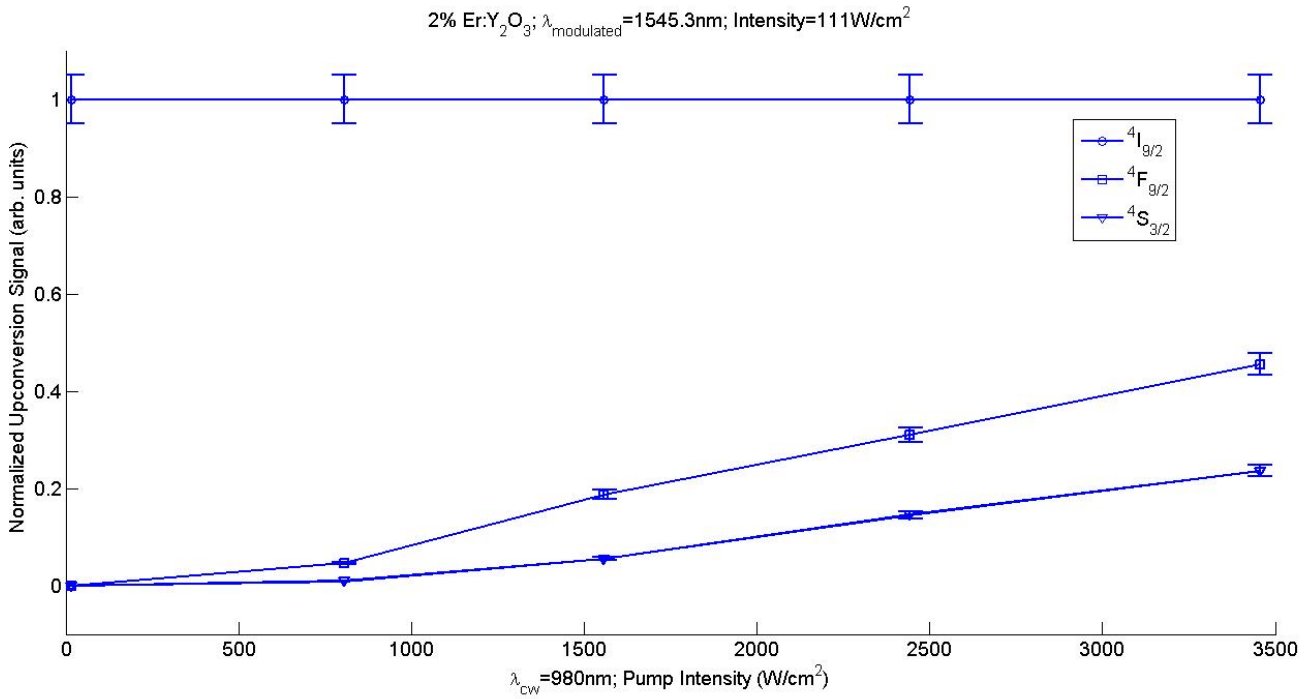

Figure 11.1: Power dependence of up-converted luminescence from $^4S_{3/2}$, $^4F_{9/2}$ and $^4I_{9/2}$ energy levels for $2\% Er^{3+}$ doped Y_2O_3. The data presented corresponds to the effect of a modulated 1550nm pump as the population in the $^4I_{11/2}$ energy level is increased.

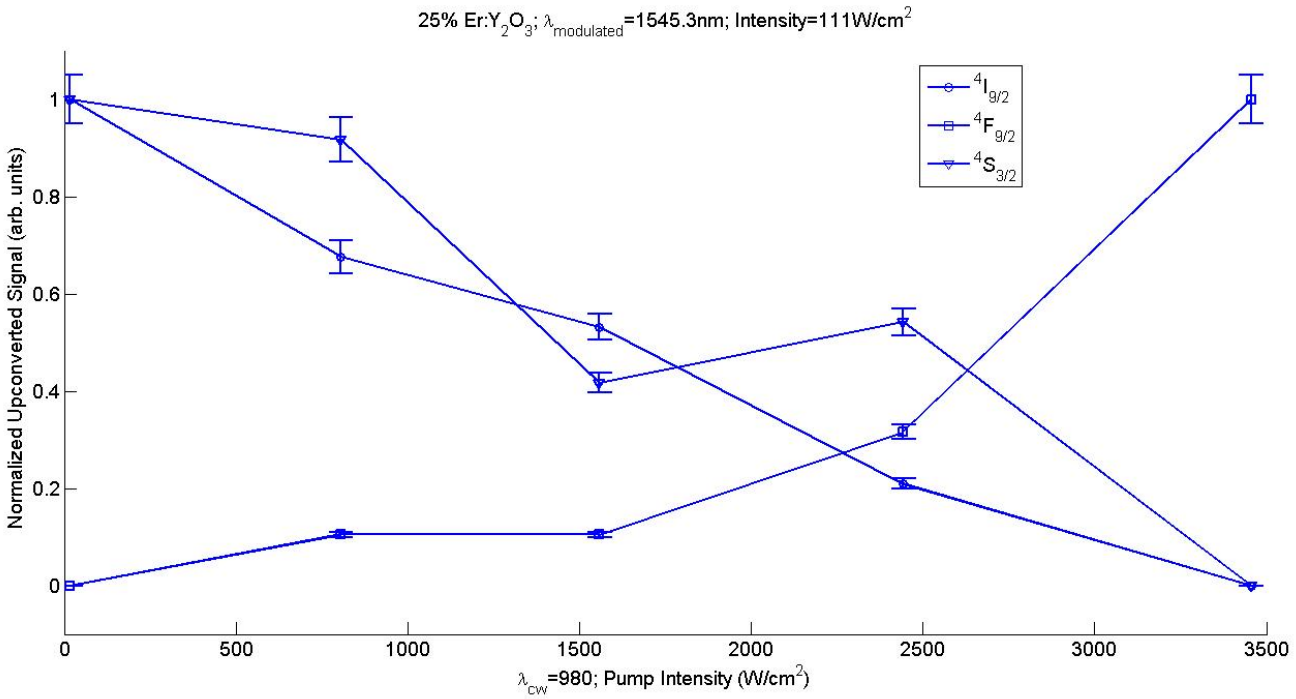

Figure 11.2: Power dependence of up-converted luminescence from ${}^4S_{3/2}$, ${}^4F_{9/2}$ and ${}^4I_{9/2}$ energy levels for $25\%Er^{3+}$ doped Y_2O_3. The data presented corresponds to the effect of a modulated 1550nm pump as the population in the ${}^4I_{11/2}$ energy level is increased.

the feedback *engine* by using multiple pumps.

The method is just a applicable to the generation of technologically important wavelengths such as the mid-IR emission around $\sim 3\mu m$ or the telecommunication bands of $\sim 1.3\mu m$ and $\sim 1.6\mu m$, along with the industrially utilized $\sim 1\mu m$ wavelength.

Consider the following scenario (See Figure 11.3) where the rare-earth ion system is at the heart of a feedback pump scheme involving two pump wavelengths.

The external feedback loop can easily enhance or diminish the emission of the desired wavelength - here λ_A by changing the amplitude of pump #2. The schematic also attempts to show the in-built feedback energy-transfer mechanisms. Here we consider only two inter-twined transitions - transitions A & B, such that pump #1 causes inversion in both but transition B also feeds back into transition A. The application of pump #2 would either enhance or diminish the emission from transition A.

It is needless to point out that real-world systems are many times more complicated than the above thought experiment, and that the above system could be greater enhanced by multiple pump wavelengths affecting an equal or more number of transitions. These transitions may then in turn feedback into desired transitions providing the emission of wavelengths that are useful.

The engineering significance of such a system would parallel the existing and well-studied methods of co-doping to enhance the inverted populations in transitions of technological importance. It is infinitely easier to precisely modulate laser-pump diode bars separately affecting precise transitions to leverage this discovery.

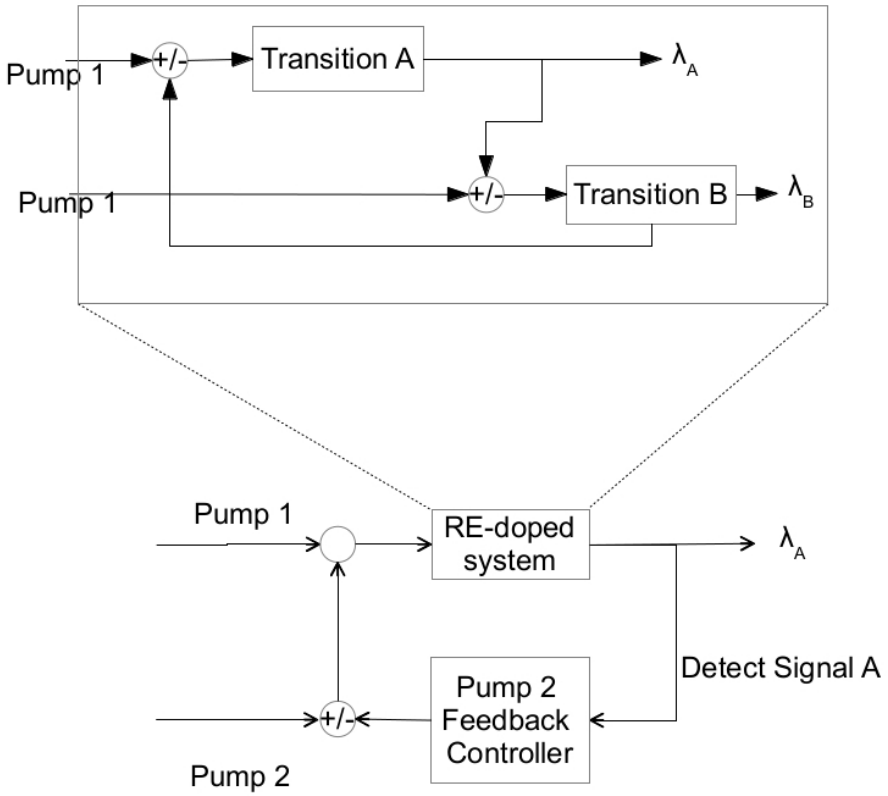

Figure 11.3: Leveraging the modification of energy-transfer pathways using an external feedback system.